Title	ARTIFICIAL CONSTRUCTION OF HIGH T CUPRATES BY LASER MOLECULAR BEAM EPITAXY AND THEIR TWO-DIMENSIONAL SUPERCONDUCTIVITY
Author(s)	金井, 真樹
Citation	大阪大学, 1992, 博士論文
Version Type	VoR
URL	https://doi.org/10.11501/3060117
rights	
Note	

ARTIFICIAL CONSTRUCTION OF HIGH T_c CUPRATES

BY LASER MOLECULAR BEAM EPITAXY AND

THEIR TWO-DIMENSIONAL SUPERCONDUCTIVITY

BY   MASAKI KANAI

ARTIFICIAL CONSTRUCTION OF HIGH T_c CUPRATES
BY LASER MOLECULAR BEAM EPITAXY AND
THEIR TWO-DIMENSIONAL SUPERCONDUCTIVITY

BY   MASAKI KANAI

Contents

4

Construction of a artificial structure which we desire is an attractive work for many material scientists. The first work of this area was be the construction of superlattices based on GaAs by atomic layer epitaxy.[1] Moreover, manipulation of one atom was performed by application of the technique of scanning electron microscopy.[2] These techniques, however, have been applied to a few materials. Recently, the materials which are suitable to the construction of two-dimensional superlattices were discovered. They are cuprate superconductors with layer-type crystal structures.

High temperature superconductivity of the cuprate system was discovered in $La_{2-x}Ba_xCuO_4$ at first by Bednorz and Müller in 1986.[3] Since the first discovery, basic study of cuprate superconductors has been performed powerfully from the various viewpoints of materials, properties and mechanisms. Nowadays, the cuprate superconductors, more than 30 kinds have been found out[4], and the critical temperature (T_c) above 90K has been observed in $Y-Ba-Cu-O$[5], $Bi-Sr-Ca-Cu-O$[6] and $Tl-Ba-Ca-Cu-O$[7] systems.

The characteristic feature of this superconducting family is that these materials have layer-type crystal structures, namely the crystal structures will be constructed by the stacking of some two-dimensional layers. (The crystal structure of $Bi_2Sr_2CaCu_2O_8$ is shown in Fig.1 as an example.) Even though the system includes many elements,[8-11], the structure of each two-dimensional layer is very simple. Therefore, it will be

Construction of a material with an arbitrary structure which we desire is an attractive work for many material scientists. The first work of this area may be the construction of superlattice based on GaAs by atomic layer epitaxy.[1] Nowadays, manipulation of one atom was performed by application of the technique of scanning electron microscopy.[2] These techniques, however, have been applied to a few materials. Recently, the materials which are suitable to the construction of two-dimensional superlattice were discovered. They are cuprate superconductors with layer-type crystal structures.

High temperature superconductivity of the cuprate system was discovered in $La_{2-x}Ba_xCuO_4$ at first by Bednorz and Muller in 1986.[3] Since the first discovery, basic study of cuprate superconductor has been performed powerfully from the various viewpoints of materials, properties and mechanisms. Nowadays, the cuprate superconductors more than 30 kinds have been found out[4], and the critical temperature (T_c) above 90K has been observed in Y-Ba-Cu-O[5], Bi-Sr-Ca-Cu-O[6] and Tl-Ba-Ca-Cu-O[7] systems.

The characteristic feature of this superconducting family is that these materials have layer-type crystal structures, namely the crystal structures will be constructed by the stacking of some two-dimensional layers. (The crystal structure of $Bi_2Sr_2CaCu_2O_8$ is shown in Fig.1 as an example.) Even though the system includes many elements.[8-11], the structure of each two-dimensional layer is very simple. Therefore, it will be

reasonable to synthesize these structures by layer-by-layer stacking of such simple layers. One of the main purposes of the present study is control of the crystal structures of the cuprate superconductors using the layer-by-layer construction. "Structure control" in this study means not only the preparation of a single-phase sample but also the artificial construction of the materials with the structures which we desire.

All the cuprate superconductors have two-dimensional CuO_2 plane, which is the fundamental component of the high-T_c superconductivity, in their crystal structures. So these materials are constructed by the periodical stacking of CuO_2 planes and other various layers. Furthermore, by the variation of the combination of such layers, it may become possible to synthesize a new material or a superlattice structure. The properties of the new materials give us new informations about the cuprate superconductors.

The metastable structures such as superlattice cannot be obtained in bulk samples, because the preparation of bulk samples are usually accompanied with heat-treatment at high temperature, and only thermodynamically stable structures can be prepared. Therefore, the technique of thin film preparation is essential for such artificial construction. In the present study, the thin films were formed by laser ablation method or laser molecular beam epitaxy method. Laser ablation is a phenomenon in which a solid surface is decomposed into atoms or ions by the irradiation of laser pulses with high energy density. The solid decomposed by the irradiation is called "target". The

7

emitted atoms and ions from the targets are accumulated on the substrate to form a thin film. This is an outline of the laser ablation method. "Laser molecular beam epitaxy" means the laser ablation under molecular beam epitaxial condition, where the particles emitted from the targets arrive at the substrate without a collision with molecules of ambient gas. It should be mentioned that thermal evaporation method by infrared- laser irradiation, which has been used from earlier stage, is quite different from the laser ablation method. Laser ablation using a strong pulse-laser is a new method of film preparation and the formation process is very different from that of the other methods such as infrared laser method. The details of the formation process in laser ablation method was still unknown. The study of formation process of "laser ablation method" is one of the purposes of this work.

The contents of this paper are roughly described below.

In Chapter 1, chemical species generated by the excimer-laser ablation are investigated using mass and emission spectroscopies in order to clarify the process of the film formation.

In Chapter 2, the formation of superconducting thin films by laser ablation method is reviewed, and the characteristics of laser ablation method are discussed. Furthermore, the effect of oxidation gas is studied, which is very important factor to form a film of oxide superconductor.

In Chapter 3, superconducting films were prepared by heat-treatment. The effect of lanthanide ion (Ln) in $LnBa_2Cu_3O_y$ system is studied in Chapter 3-1. In Chapter 3-2, the phase

8

control of $Bi_2Sr_2Ca_{n-1}Cu_nO_{2n+4}$ by choosing the heat-treatment condition is tried.

In Chapter 4, the artificial construction by layer-by-layer stacking is attempted. $Bi_2Sr_2Ca_{n-1}Cu_nO_{2n+4}$ structure is constructed by the insertion of Bi_2O_2/Sr_2O_2 layer into the parent structure of $(Ca,Sr)CuO_2$. Furthermore, the growth mechanism is investigated by in-situ spectroscopy.

Finally, the properties of metastable phases synthesized by the layer-by-layer construction are studied in Chapter 5. Furthermore, the charge distribution in this system is determined by the calculation of Madelung energies. From these results, the intrinsic feature of $Bi_2Sr_2Ca_{n-1}Cu_nO_{2n+4}$ is discussed and the origin of the feature is considered.

References

(1) T.Sakamoto, F.Funabashi, K.Ohta, T.Nakagawa, N.J.Kawai and T.Kojima, Jpn.J.Appl.Phys., 23, L657 (1984).

(2) D.M.Eigler and E.K.Schweizer, Nature, 344, 524 (1990).

(3) J.G.Bednorz and K.A.Mullaer, Z.Phys.B, 64, 189 (1986).

(4) H.Nobumasa,K.Shimizu and T.Kawai, Z.Phys.B, 88, 7 (1991).

(5) M.K.Wu, J.R.Ashburn, C.J.Torng, P.H.Hor, R.J.Meng, L.Gao, Z.J.Huang, Y.Q.Wang and C.W.Chu, Phys.Rev.Lett., 58, 908 (1987).

(6) H.Maeda, Y.Tanaka, M.Fukutomi And T.Asano, Jpn.J.Appl.Phys., 27, L209 (1988).

(7) Z.Z.Sheng, A.M.Hermann, A.El Ali, C.Almasan, J.Estrada, T.Datta and R.J.Matson, Phys.Rev.Lett., 60, 937 (1988).

(8)   H.Takagi,   S.Uchida,   K.Kitazawa   and   S.Tanaka, Jpn.J.Appl.Phys., 26, L123 (1987).

(9) M.A.Beno, L.Sonderholm, B.W.Capone, B.G.Hinks, J.D.Jorgensen, I.K.Schuller, C.U.Segre, K.Zuang and J.D.Grace, Appl.Phys.Lett., 51, 57 (1987).

(10)   M.A.Subramanian,   C.C.Torardi,   J.C.Carabrese, J.Gopalakrishnan,   K.J.Morrissey,   T.R.Askew,   R.B.Flippen, V.Chowdahri and A.W.Sleight, Science, 239, 1015 (1988).

(11) E.Takayame-Muromachi, Y.Uchida, A.Ono, F.Izumi, M.Onoda, Y.Matsui, K.Kosuda, S.Takekawa and K.Kata, Jpn.J.Appl.Phys., 27, L365 (1988).

(a)

Sr · CuO₃

Ca

Sr · CuO₃

Bi₂O₂

(b)

(BiO)₂
SrO

Ca

SrO
(BiO)₂

● Cu ○ O ⊕ Sr, Ca
⊘ Bi
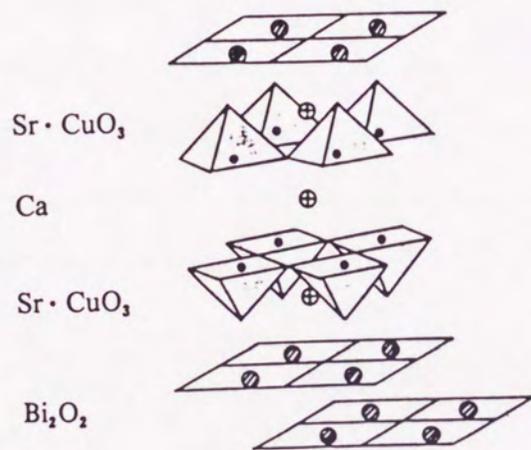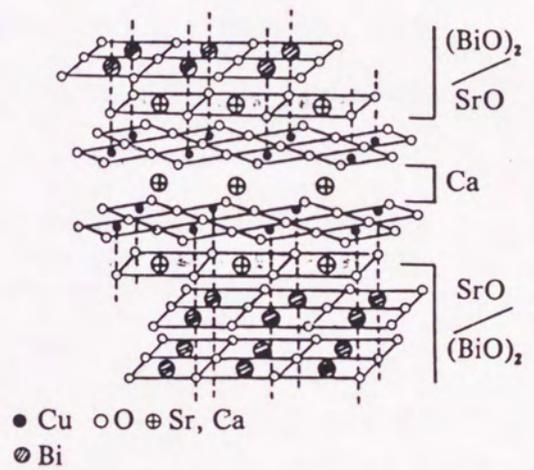
Fig.1 (a) Conventional representation of the crystal structure of $Bi_2Sr_2CaCu_2O_8$, and (b) that represented by the stacking of atomic layers.

Chapter 1

Ablation Phenomenon Induced by Laser Irradiation

11

Abstract

The ablation phenomenon induced by the irradiation of xcimer-laser pulse is studied by mass spectroscopy and emission spectroscopy. When the laser pulse with high energy density irradiates a solid, the solid surface is decomposed into atoms and ions, while clusters or molecules are not produced. A part of the species are in electronically excited state. The velocity distribution of the species does not obey Maxwell-Boltzmann distribution and suggests that the ablation includes non-thermal process. Compared with thermal evaporation method, the species produced by the laser ablation have very fast velocity.

12

Introduction

When strong laser pulses irradiate a solid, the solid surface is decomposed and some kinds of species are generated. This phenomenon is called "laser ablation". The solid irradiated by laser is called target. In this paper, thin films of cuprate superconductors have been prepared by application of laser ablation phenomenon [see Fig.1]. This method is new way to prepare thin films, so the process of the film formation has been unknown.

In my experiment, the film formation is carried out by irradiation of ArF excimer laser into the target placed in a vacuum chamber. This experimental setup is similar to the apparatus for the study of the dynamics of photo-induced surface reaction on semiconductors.[1] Thus, the similar analyzing technique may be possible to study the laser-ablation process. In this section, time-resolved measurement using mass spectrometer was attempted to the investigation.

Furthermore, the laser ablation process is accompanied with the emission of visible-light, whose color is dependent on the elements included in the target solid. This suggests that excited species are generated by the laser ablation process. By the emission spectroscopy, the excited state of the ablated species was studied.

13

Experimental

The experimental apparatus is shown in Fig.2. The light source was ArF excimer laser (Lambda-Physik EMG-103) and the wavelength was 193nm. The laser pulses were focused by a lens on a target placed in the vacuum chamber, and emitted species were detected emission spectrometer and quadrupole mass spectrometer. Some metal or oxide targets were used for this experiment, which were also used for the formation of thin films. The detail of the preparation of the targets will be described in Chapters 3 and 4.

The emission was detected by a streak camera (Hamamatsu C2830) through a slit of polychrometer, and analyzed by a multichannel analyzer (Hamamatsu C2491).

The mass number and the velocity distribution[1] of the emitted species from the target were obtained using mass spectrometer (VG SXP-300). To obtain the velocity distribution, the output signal of mass spectrometer was sent to a transient memory (Kawasaki MR-50E) and time-resolved mass spectra was obtained at first. These data were collected by micro-computer (NEC PC-9801ES) and transferred to intensity-energy curve using following relations. The kinetic energy of a flying particle (E) is given by

$$E=mv^2/2=m(1/t)^2/2 \qquad (1)$$

where m and v indicate mass and velocity of particle, respectively. "l" is the distance between the target and mass spectrometer (l=344mm in this system). "t" is the time when the signal is detected, and t=0 is the time of laser firing.

14

[The laser reaches the target within 20 nanoseconds and the width of one laser pulse is 15ns. These time are enough short, so they can be neglected. Namely, the ablation occurs only at t=0 (delta function approximation).] From eq.(1), following equation is derived.

$$dE=-ml^2/t^3 \cdot dt \qquad (2)$$

This equation leads to

$$dN/dE=t^3/(ml^2) \cdot dN/dt \qquad (3)$$

where N is number of particle, and dN/dt and dN/dE are proportional to the signal intensity in intensity-time curve and intensity-energy curve. If the particles come to thermal equilibrium in the ablation process, next relation should be satisfied from Maxwell-Boltzmann distribution[2,3],

$$\ln\{(dN/dE)/E^{0.5}\}=-E/kT + constant \qquad (4)$$

where k is Boltzmann constant and T is temperature.
In this case, $\ln\{(dN/dE)/E^{0.5}\}$ - E plot should indicate a linear line.

These experiments were performed under the base pressure of 1×10^{-6}Pa. The energy density of laser was calibrated by power-meter (Gentec ED-200).

Results and Discussion

When the energy density of laser was much lower than $100mJ/cm^2$, the emission of visible-light could not be detected. Under this condition, a large part of the generated species from $YBa_2Cu_3O_y$ target has a mass number of 44, which is corresponding to CO_2. The origin of CO_2 will be one adsorbed on the surface, because the x-ray diffraction pattern of the target did not include peaks due to carbonates. The metal elements detected were Y, Ba and CuO, and the signal of Y_2 and Ba_2 cluster could not be observed by mass spectroscopy. These signals disappeared with cut-off of the filament in ionization chamber, so these were neutral atoms and molecules. The intensity of mass signal for Ba had the laser-energy dependence in second order, and that for Y had higher order dependence than second order. The signal intensity is proportional to the amount of the species coming into the mass spectrometer, so these data show the energy dependence of the amount of the products. The intensity did not show the exponential-type dependence, so the formation process of these species should include non-thermal process.[4] Since $YBa_2Cu_3O_y$ is essentially an ionic crystal, the following processes should occur in the formation of the neutral atoms.

$$Ba^{2+} + 2e^- \rightarrow Ba$$
$$Y^{3+} + 3e^- \rightarrow Y$$
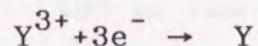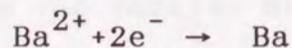
The energy dependences suggest the photo-chemical process with multiphoton excitation[4] where absorption of one photon supplies one electron to cation from anion. In this experiment, Cu was not observed and only CuO was observed. This result suggests that

16

the Cu-O bond in $YBa_2Cu_3O_y$ includes covalence compared with Ba-O or Y-O.[5]

When the energy density exceeded 100 mJ/cm^2, laser ablation process occurred at the target surface. Fig.3 shows the time-resolved emission spectra for the ablation of $BiSrCaCu_2O_y$ target. Just after the irradiation of laser, the very broad continuum emission due to plasma state was observed[6] [see Fig.3(a)]. The plasma emission decayed with half-life period of about 70ns, followed by strong absorption by Ca, Ca^+, Sr and Sr^+ [see Fig.3(b)]. Interestingly, these absorption lines are corresponding to the excitation from the ground states of the species, and the absorptions by excited atoms and ions are not detected at this stage. In Fig.5(a), the energy diagram of Ca is shown. For Ca, only the line at 423nm corresponding to the excitation from the ground state could be observed, and the absorptions at 430, 432, 444 and 445nm due to the excited atoms are not observed in this early step. In the next stage, the plasma emission disappeared, and the emission peaks appeared, which were corresponding to the absorption observed in the earlier stage [Fig.3(c)]. These peaks show the inactivation of excite species which are produced by the absorption of energy of plasma in the earlier stage. The emission showed the relatively long life-time of the excited species, which was longer than 1 microsecond [Fig.3(d)].

Time-integrated emission spectra is shown in Fig.4. The targets were Ca, Sr, Cu metals and Bi_2O_3. The assignments of these emission peaks are shown in energy diagrams in Fig.5.[7]

17

The difference between Fig.3 and Fig.4 is the existence of the emission due to the inactivation to first excited states, which was not observed in Fig.3. But, this will be due to the different time-scale between Fig.3 and Fig.4. Such species will be formed at later stage. A large part of the emission peaks in Fig.4 is also observed in Fig.3, so I consider that the essential difference does not exist between oxide targets and metal targets. In the emission spectra, only neutral atoms and monovalent cations of the metal elements were observed. The emission also shows that a part of the species generated by the laser ablation are in electronically excited states and have excess energy of 2eV or 4eV.

Under the same condition, mass spectra were obtained. Used targets were Ca, Sr, Cu, $CaCuO_2$ and Bi_2O_3. The detected mass numbers were 40, 63, 88 and 209 corresponding to Ca^+, Cu^+, Sr^+ and Bi^+ respectively. Clusters, molecules or divalent ions could not be detected. Fig.6 shows the laser-energy dependence of mass signal intensity. The broken lines were obtained when the filament in ionization chamber was turned off, so these lines show the amounts of cations. The full lines show the data with turned-on filament, so these show the total amounts of neutral atoms and cations. The result shows that a large amount of ion is produced. This behavior is so different from that observed with low laser-energy density. The generation of a large amount of ions is one of the characteristics of laser ablation method. Fig.6 also shows that each element has a threshold intensity where the signal intensity increases steeply. The threshold of Ca for Ca metal target and that for $CaCuO_2$ are different, thus

18

the threshold intensity is dependent on not only kinds of element but also states in the target solid.

When the target includes some metal elements and the laser intensity is near the threshold of one of the elements, the chemical composition of the film may be drastically changed by the slight fluctuation of laser intensity. Therefore, when the target includes some kinds of metal elements, it is important for the film formation that the laser energy should be higher than the threshold intensities of the all metal elements. Above the threshold intensity, any element shows similar behavior, where the signal increased linearly with increase of the laser energy. Therefore the composition of the film will not be sensitive to the fluctuation of laser intensity in the region with high laser-energy.

The distribution of the velocity of Ca, Cu and Bi with enough high laser-energy are shown in Fig.7. The used targets were $CaCuO_2$ for Ca and Cu, and Bi_2O_3 for Bi. The spectra had a large tailing in high energy side. Fig.8 shows $\ln\{(dN/dE)/E^{0.5}\}$-E curve for Cu which is obtained by transformation of the data in Fig.7.[2,3] In the low energy region where the velocity of the particle is slow, the reliability of the data is slightly poor, because the signal intensity may become larger by the saturation of the particles in ionization chamber of mass spectrometer. However, even in the high energy region, the slope could not be fitted by liner line perfectly. This result shows that Maxwell-Boltzmann distribution is not realized in laser ablation process, and suggests that the ablation process includes non-thermal

process. From the data in high energy region in Fig.8, temperature was roughly estimated to be 5×10^5K. This temperature is very high and corresponding to the energy of 40eV or the velocity of 1.1×10^4m/s for Cu.

The emission spectra showed that life-time of the excited species is in order of 1μs. Based on the velocity of 1×10^4m/s, a part of excited species may arrive at the substrate without inactivation, if the distance between the target and the substrate is around 10mm. If the distance becomes larger than 100mm, a large amount of the excited species is inactivated before reaching the substrate.

The profile of the laser ablation process suggested by mass and emission spectra is shown in Fig.9. By the irradiation of strong ArF excimer laser, the solid surface is decomposed and a plasma state is produced at first. With decay of the plasma, atoms and ions in ground state is formed, and the species are excited electronically by absorption of the plasma emission. The excited atoms and ions have excess internal energy of 2eV or 4eV. The neutral atoms and monovalent ions including such excited species reach the substrate surface to form a thin film. The species have relatively high kinetic energy which is in order of 10eV.

Conclusion

The ablation phenomena induced by excimer-laser irradiation was investigated using mass and emission spectroscopies. Just after the irradiation, a plasma state is produced and after that, atoms and monovalent ions are formed. A part of the species is in the electronically excited state. Clusters, molecules or divalent ions are not produced. Each species has threshold laser-intensity, and the threshold depends on kinds of element and states in the target solid. The distribution of the velocity of the particles is not consistent with Maxwell-Boltzmann distribution. This result suggests that the laser ablation includes non-thermal process. The velocity of the species is very fast. The rough estimation shows the velocity is in order of 10^4m/s.

References

(1) T.Kawai and T.Sakata, Chem.Phys.Lett., 69, 33 (1980)

(2) G.M.Barrow, Physical Chemistry 4th Edition, Chapter 2, (McGrow-Hill, New York, 1979).

(3) T.Nakayama and N.Itoh, Radiation Effet Lett., 67, 129 (1982).

(4) D.van Linde, Topics Appl.Phys., 18, 204 (1977).

(5) J.E.Rothenberg, J.Koren and JJ.Ritsko, J.Appl.Phys., 57, 5072 (1985).

(6) J.F.Ready, Effects on High-Power Laser Radiation, (Academic Press, New York, 1971).

(7) T.A.Anderson, A.R.Forester and M.L.Parsons, Appl.Spectrosc., 36, 504 (1982).
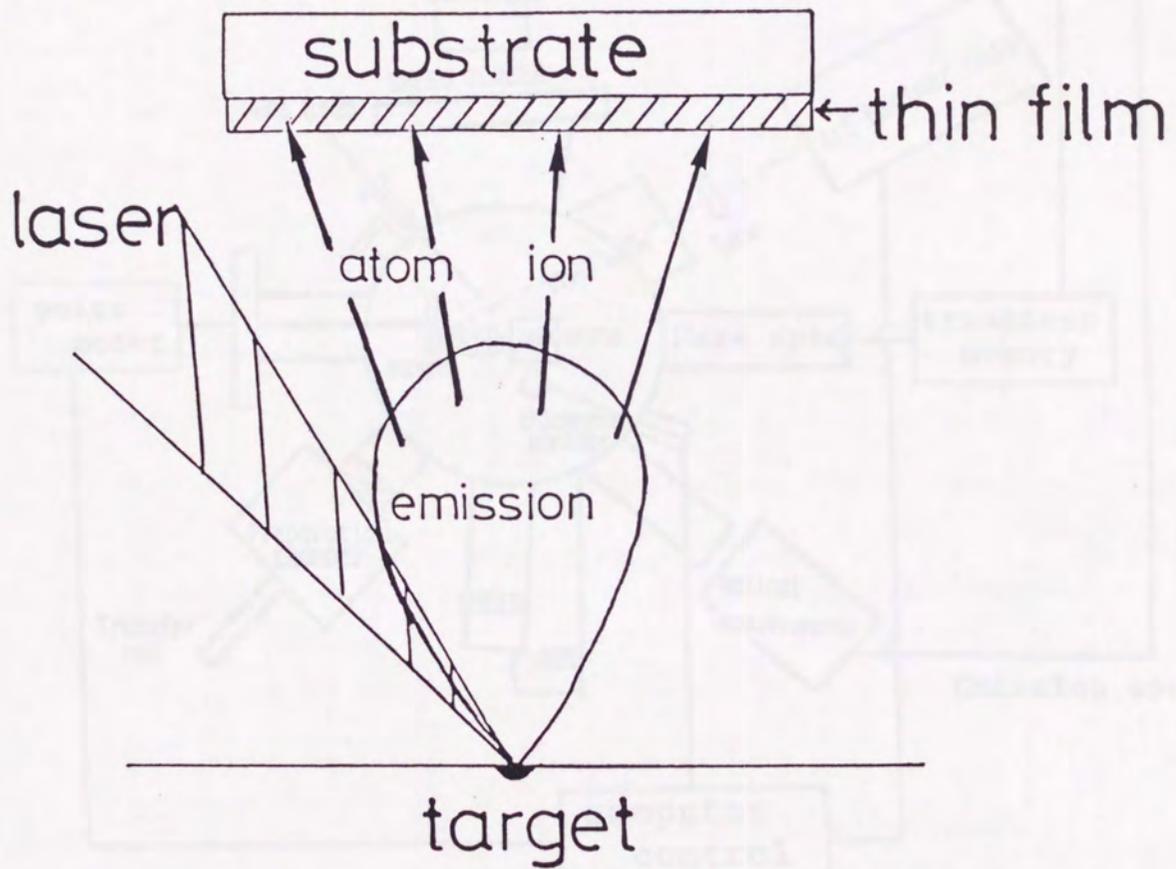
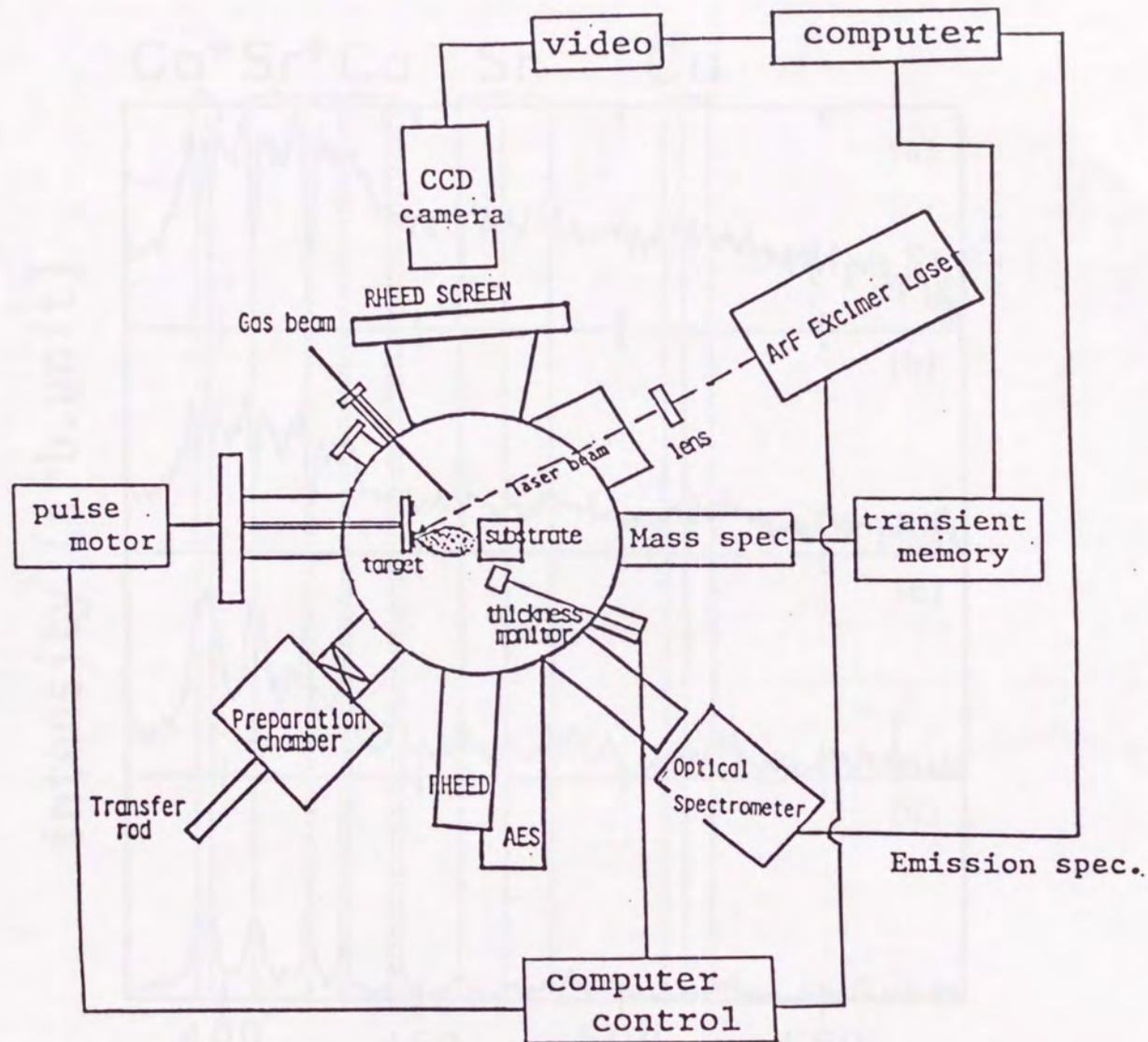Fig.1 The profile of film formation in laser ablation method.

Fig.2 The experimental apparatus for ArF excimer-laser ablation.
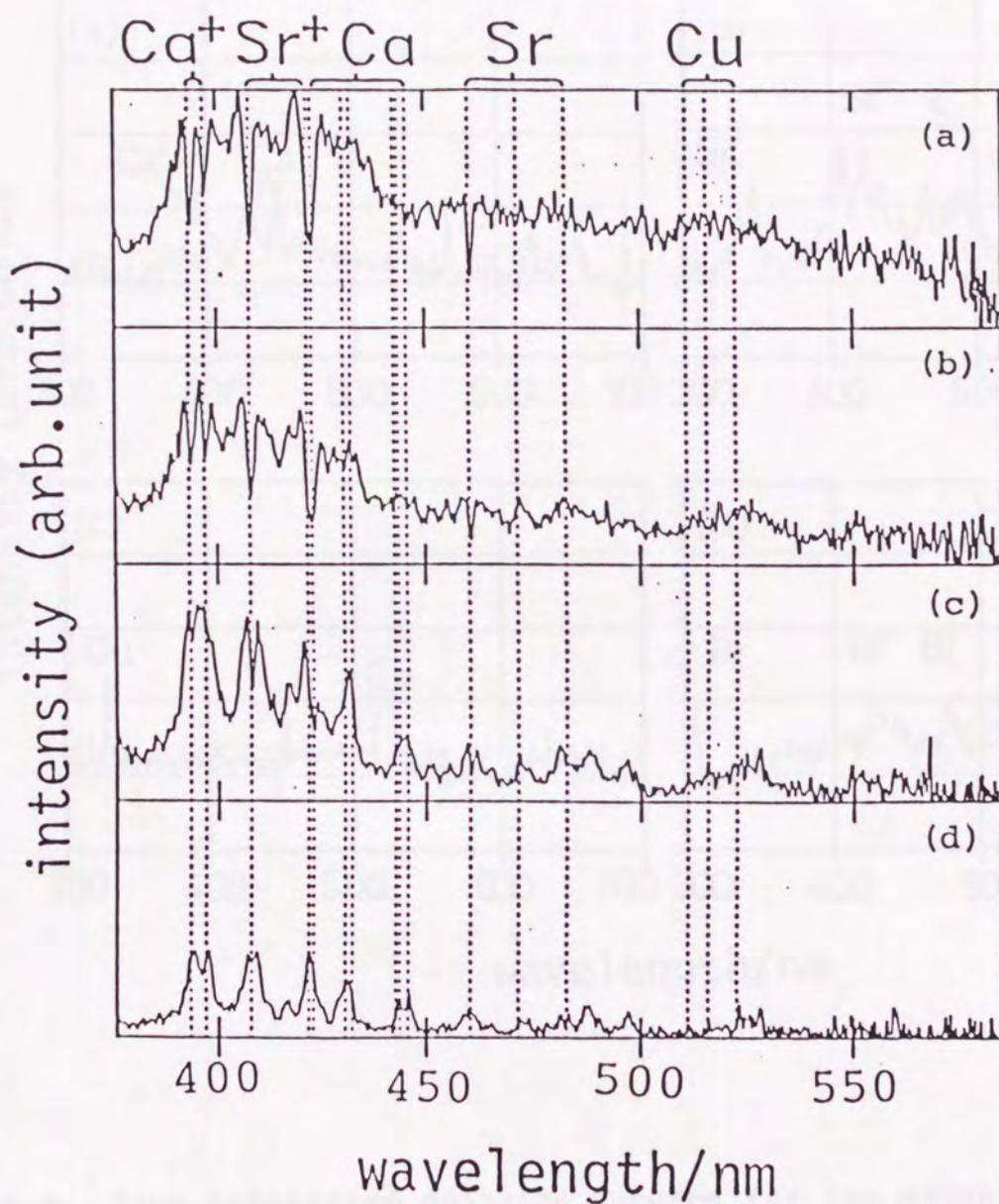The species were detected by quadrupole mass spectrometer and
emission spectrometer.

Fig.3   Time-resolved emission spectra obtained upon the ablation of $BiSrCaCu_2O_y$. (a) 54-142ns, (b) 104-192ns, (c) 204-292ns   and (d) 454-542ns.
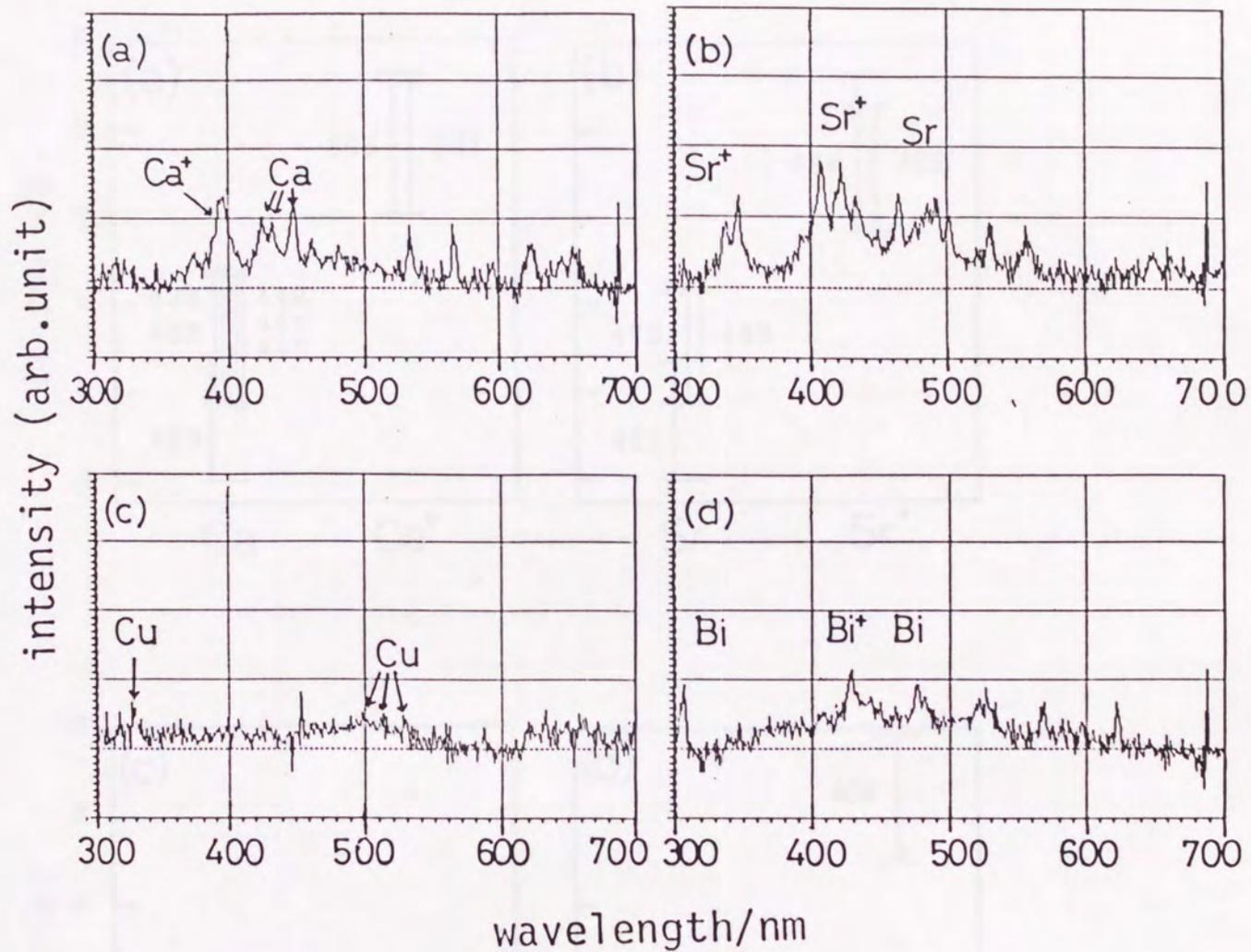
Fig.4   Time-integrated emission spectra for the ablation of   (a) Ca, (b) Sr, (c) Cu metals and (d) Bi_2O_3.
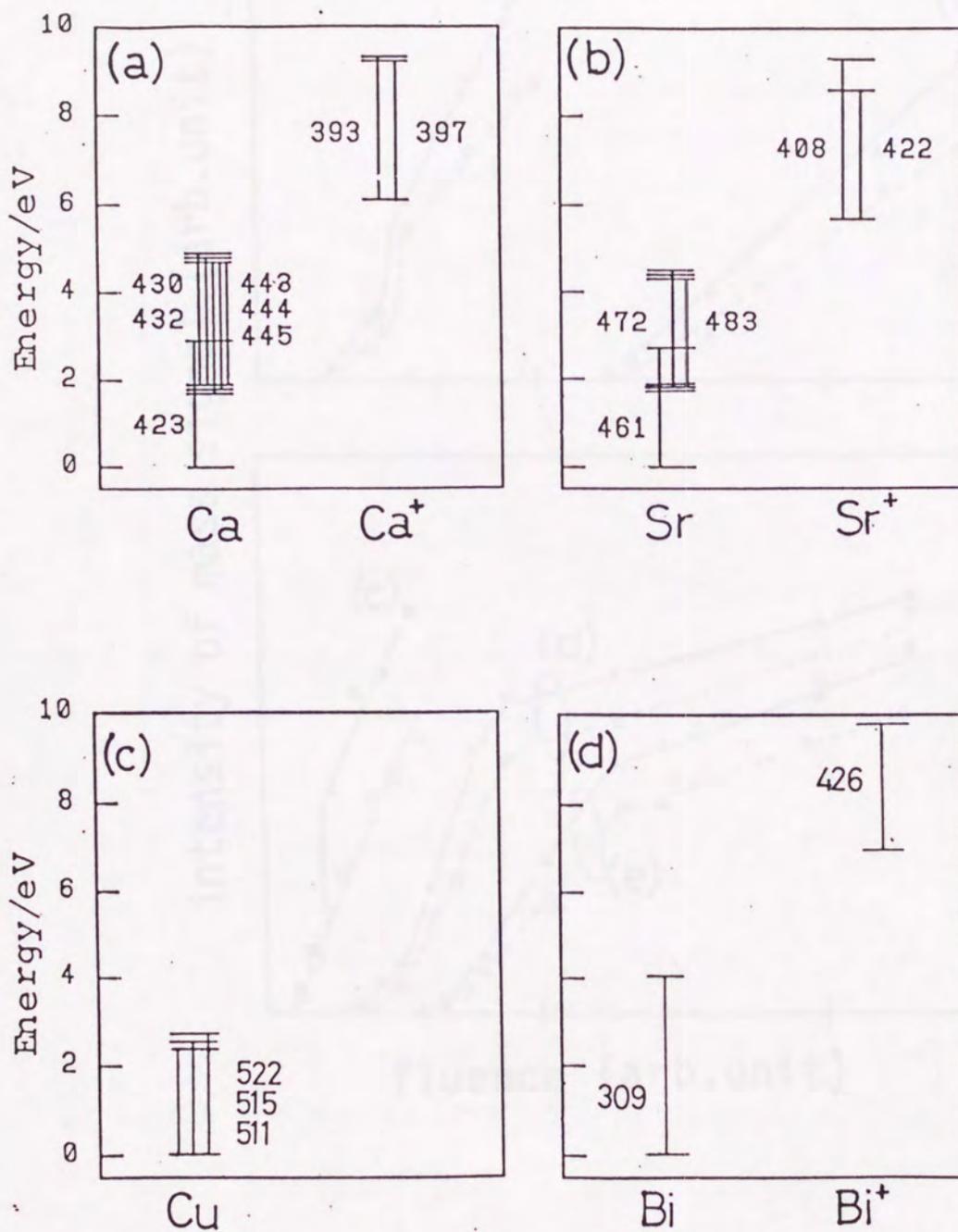
Fig.5   Energy diagrams of the electronic states and observed transition observed in emission spectra. The numbers in the figure indicate the wavelengthes corresponding to the energies in unit of nm.
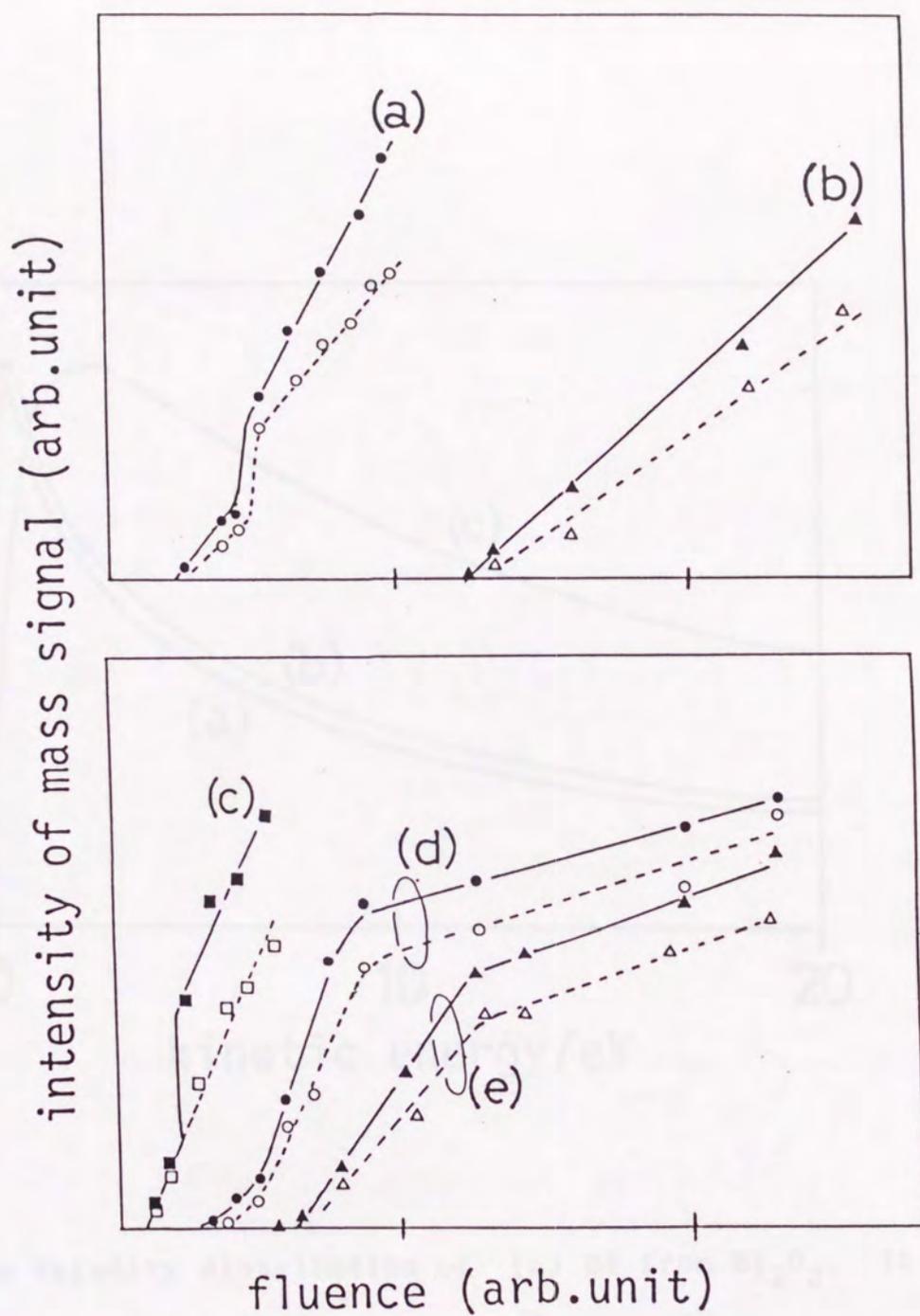
Fig.6 The laser energy dependence of signal intensity of mass spetra for (a) Ca$^+$ from Ca target, (b) Cu$^+$ from Cu target, (c) Bi$^+$ from Bi$_2$O$_3$, (d) Ca$^+$ from CaCuO$_2$ and (e) Cu$^+$ from CaCuO$_2$. The broken line shows the intensity of only ion, and the full line for total amount of atom and ion.

Fig.7   The velocity distribution of (a) Bi from Bi_2O_3, (b) Cu

From Cu target and (c) Ca from Ca target.

Fig.8 The plot of $\ln\{(dN/dE)/E^{0.5}\}$ - E for Cu, which is obtained by the transformation of the velocity distribution in Fig.8.
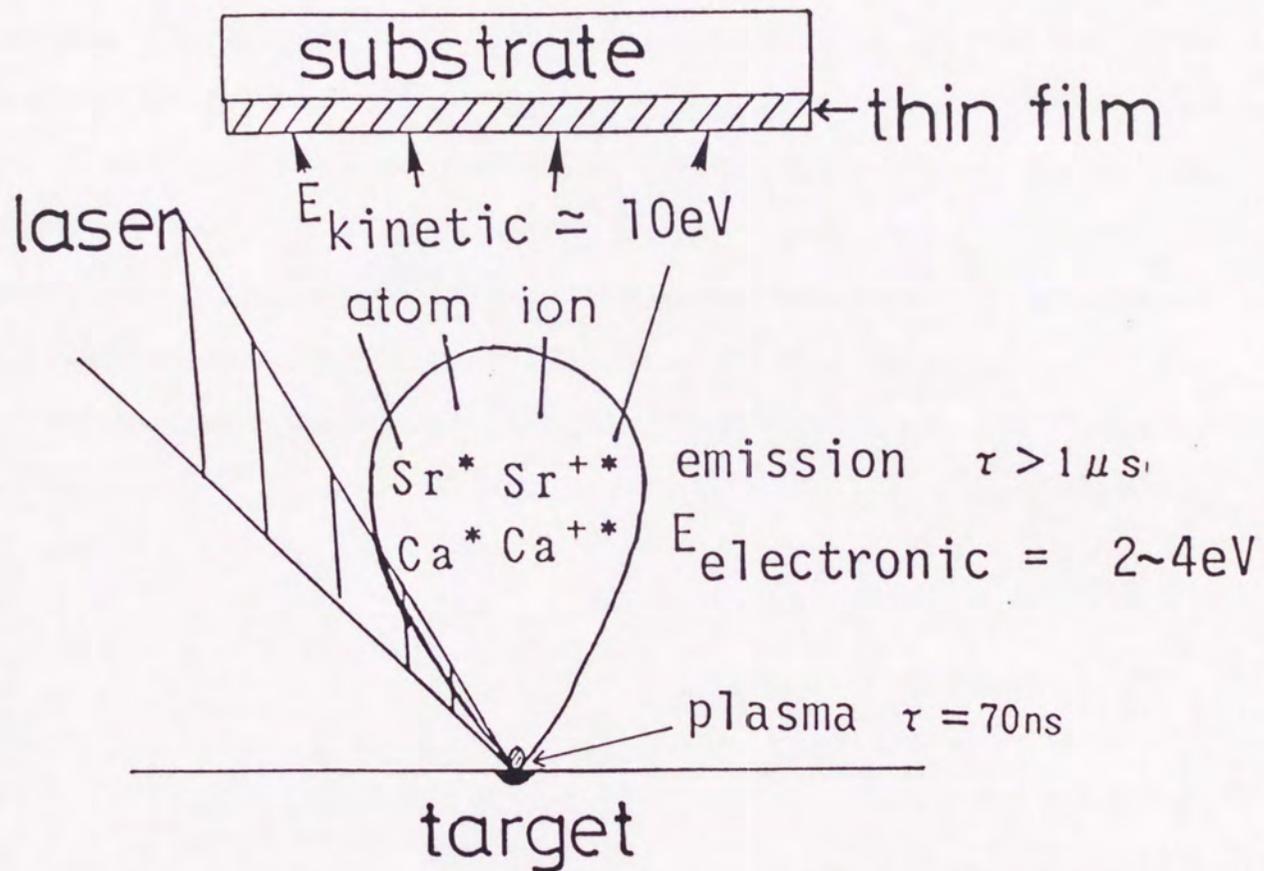
Fig.9   The profile of laser ablation process suggested by mass and emission spectra.

Chapter 2

Laser Ablation and Thin Film Crystal Growth

Abstract

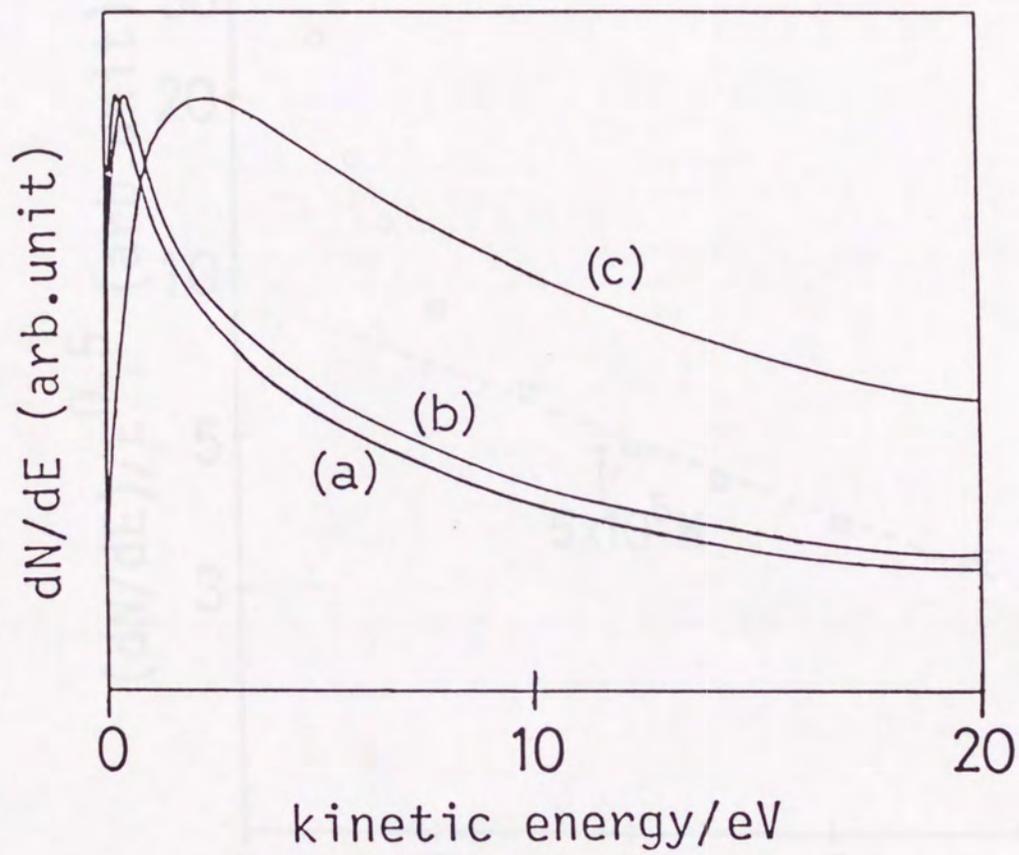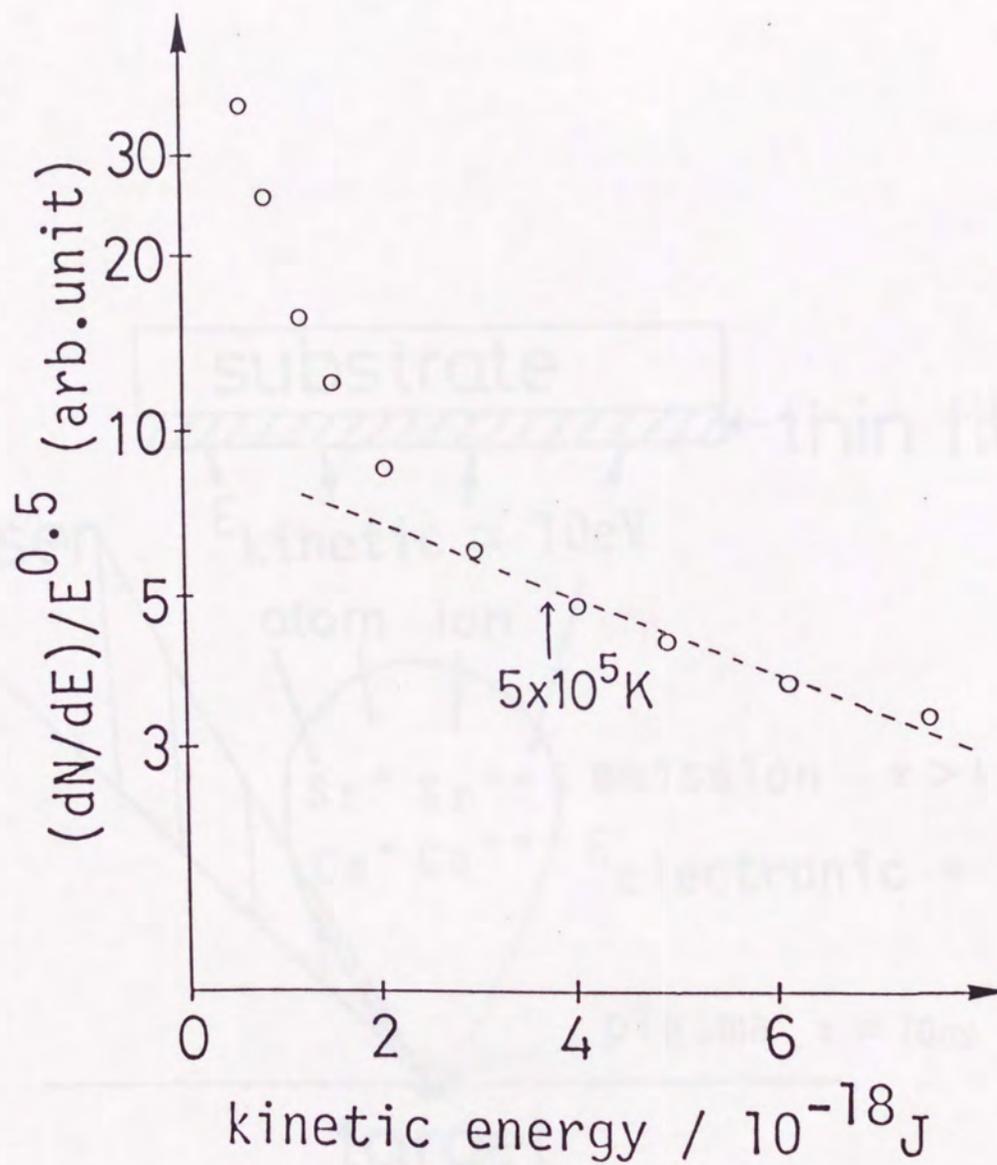Thin films of cuprate superconductors and the related materials are grown by laser ablation method, and characteristics of this method are investigated. One of the advantages of this method is that the chemical composition of the targets is transferred to that in the film. Therefore, this way is very suitable for the film preparation of the system including many elements. The effect of the excited species generated by the laser ablation is also discussed. Furthermore, three kinds of oxidation gas, O_2, N_2O and NO_2, are used during the film deposition, and the effects of the gases are studied. Compared with conventional O_2, N_2O is effective for the preparation under low-temperature condition, and NO_2 is useful under low-pressure condition.

24

Introduction

Thin films of oxides have been grown by various methods, such as sputtering[1,2] and evaporation methods[3,4]. In my experiment, the ablation phenomenon induced by ArF excimer-laser irradiation is applied for the film formation of cuprate superconductors or the related materials. The laser ablation method has some characteristics which are not observed in other methods. Thus, the features of this method are clarified in this section.

There are two ways to form a oxide thin film. One is the formation through two steps. In this way, the amorphous film is deposited in vacuum at room temperature at first, and after the deposition, the film is sintered for oxidation and crystallization. This is a way similar to the formation of powder samples. The other is a film-formation with one step, where the deposition, oxidation and crystallization of the films occur simultaneously. In this way, the films are deposited on a heated substrate under an oxidation gas. The films formed by this way are called "as-grown films". In this section, the films have been formed by these two ways, and the properties of the prepared films have been investigated to study the characteristics of laser ablation method.

For the preparation of as-grown films of cuprate superconductors, oxidation gases must be introduced into the formation chamber during the film growth, because copper is hard to be oxidized. The properties of the cuprate superconductors are very sensitive to the slight difference of oxygen

content[5,6], so the effect of the oxidation gas is very important. I have been used N_2O and NO_2 with strong oxidation power[7] as oxidation gases. The film prepared under N_2O or NO_2 gas was compared with that formed under conventional O_2 gas, and the effects of the gases were studied.

Experimental

Thin films were prepared by laser ablation method. The experimental setup is shown in Fig.1. The distance between the target and the substrate was 20mm in this apparatus. Pulses of ArF excimer-laser were focused on the target placed in the vacuum chamber, and emitted atoms and ions were accumulated on the substrate placed at the opposite side of the target. The preparation of the targets is described in Chapters.3 and 4 in detail.

Thin films of $YBa_2Cu_3O_y$ were prepared by the ablation of $YBa_2Cu_3O_y$ target. The films were deposited on cubic-ZrO_2 (100) substrates at room temperature, and the obtained amorphous films were sintered in a furnace after the deposition to form Y-Ba-Cu-O films [see Chapter 3-1]. On the other hand, as-grown films of Bi-Sr-Ca-Cu-O were prepared on MgO (100) substrate by successive supply of BiO_x, $SrCuO_x$, $CaCuO_x$ and SrO_x. Details of this method is shown in Chapter4-1.

During the film formation, the substrate was heated and oxidation gas was dosed into the formation chamber. Three kinds of oxidation gases were used, which were O_2, N_2O and NO_2. The laser beam was split into two direction. One beam was for ablation, and the other was for substrate irradiation [see Fig.1].

X-ray diffraction patterns of the prepared films were obtained using Rigaku RAD-RC system with CuK_α line. the measurement method was a conventional θ-2θ scanning. From the diffraction patterns, the features of laser ablation method were

27

investigated. Furthermore, the effect of oxidation gas and
substrate irradiation were also studied.

Results and Discussion

A Y-Ba-Cu-O thin film was prepared by the deposition with laser ablation followed by heat-treatment. Fig.2 shows the x-ray diffraction pattern of the film prepared by heating at 1193K for 1 minute. All diffraction peaks can be assigned to these of $YBa_2Cu_3O_y$ except the peak of the substrate, so this film was consist of the single-phase of $YBa_2Cu_3O_y$. The indices of the reflections are also presented in Fig.2. This $YBa_2Cu_3O_y$ system is very sensitive to the deviation of chemical composition of the metal elements and the slight deviation of the chemical composition results in the formation of a second-phase.[8] Thus Fig.2 indicates that the chemical composition in the target and that in the film are almost same, since the chemical composition of the target was also $YBa_2Cu_3O_y$. Namely, in laser ablation method, the composition in the target is transferred into the film without a large deviation. This behavior, which is so different from that in other method[1-4], is the characteristic feature of laser ablation method. For this reason, this method is very suitable for the film formation of the system including many elements. The films of such system will be obtained by the ablation of the bulk material which we want to prepare.

In the formation of as-grown films, a slight deviation of the chemical composition occurs, because high temperature of the substrate leads to the reevaporation of the elements.[9] Thus, a correction of the target composition may be necessary in this way. In general, however, the deviation is very small, so the advantage of laser ablation method does not disappear.

This result should be compared with the data obtained by mass spectroscopy, which have been shown in Chapter 1. The mass spectroscopy showed that each metal element in a target has different threshold laser-intensity [see Chapter 1, Fig.7]. This result suggests that the energy density of the laser should be higher than the threshold of any element in the target to take advantage of laser ablation method. If not so, the element with higher threshold intensity than the laser energy can not be ablated resulting in the drastic deviation of chemical composition.

The formation of as-grown Bi-Sr-Ca-Cu-O films indicated that the laser intensity had another effect on the film growth. Figs.3(a) and 3(b) show the x-ray diffraction patterns of the as-grown Bi-Sr-Ca-Cu-O thin films. The film in Fig.3(b) was prepared with weaker laser power than that in Fig.3(a). Other condition was same, where the substrate temperature was 873K, and 10Pa of N_2O gas was dosed as an oxidation gas. Furthermore, the deposition rates of the two films were controlled to be same by the change of repetition rate of the laser pulse. Even though the almost same condition, the x-ray diffraction patterns were so different, and the film prepared with stronger laser power had better crystallinity. This difference, however, is not due to the deviation of chemical compositions of these two films, because the laser energies for both experiments were stronger than the threshold intensities of all elements. I consider that it is due to the difference of excess energy included in the particles emitted from the target by the laser ablation. Since

the result of mass spectroscopy showed the velocity distribution was not sensitive to the laser energy, the excess energy in the electronically exited state will be possible for the cause of the difference. In practice, it was detected by my eyes that the emission of the excited species reached the substrate surface in the film formation for Fig.3(a), and it did not reach for Fig.3(b). In order to clarify this problem, I should compare the emission spectra between these two conditions. The spectrum with weaker laser power, however, could not obtained, because the emission in such condition is too weak to be detected by our apparatus.

In next step, the gas effect and substrate irradiation effect on the formation of as-grown $Bi_2Sr_2CuO_6$ films were studied. Figs.4(a)-4(c) show x-ray diffraction patterns of as-grown films prepared at 873K in 6Pa of (a) N_2O without substrate irradiation, (b) N_2O with irradiation and (c) O_2 with irradiation. Although both films formed in N_2O showed the diffraction peaks of $Bi_2Sr_2CuO_6$, the peaks of the film formed without the substrate irradiation [Fig.4(a)] were much weaker and broader than those with the irradiation [Fig.4(b)]. This behavior shows that substrate irradiation is effective for the formation of $Bi_2Sr_2CuO_6$ structure in N_2O ambient. In contrast, the as-grown film formed in O_2 at the same substrate temperature of 873K gave only some weak peaks, and even the irradiation in O_2 gave no changes on the film formation [Fig.4(c)]. Thus N_2O is effective when combined with substrate excitation by ArF excimer laser. The reason for this result seems to be the increase of active oxygen radicals generated by the decomposition of N_2O by the

31

irradiation.[10] The variation of the diffraction patterns versus the substrate temperature indicated that the crystal structure of $Bi_2Sr_2CuO_6$ was formed above 873K in 6Pa of N_2O, and above 923K in O_2.

Although as-grown crystallized films could be prepared above 923K in either gas, there were some differences in the properties between the films formed in N_2O and O_2. Figs.5(a) and 5(b) show x-ray diffraction patterns of the as-grown films formed at 953K in 6Pa of (a) N_2O and (b) O_2 with substrate irradiation. Though the diffraction pattern showed that the film formed in N_2O was the single phase of $Bi_2Sr_2CuO_6$ [Fig.5(a)], in spite of that, the film had a high resistivity of over 10^2 ohm·cm. On the other hand, the film formed in O_2 included the impurity of CuO [see Fig.5(b)], but this film has a low resistivity of 1×10^{-3} ohm·cm. The disadvantages of high resistivity and CuO impurity for each gas could be eliminated by using the mixture of N_2O and O_2. Fig.5 (c) shows the diffraction pattern of the film prepared in the mixture of 5Pa of N_2O and 1Pa of O_2 (which is called "mixed gas"). The film formed in the mixed gas gave a diffraction pattern of single-phase of $Bi_2Sr_2CuO_6$, including no impurity peak such as CuO, and had a low resistivity of 1×10^{-3} ohm·cm. Thus, the mixed gas of N_2O and O_2 is useful to form a single-phase film with low resistivity.

In addition to the difference of impurity and resistivity, the lattice constant c was also varied with the change of the ambient gas. The lattice constant c calculated from the diffraction peaks in Figs.5(a), 5(b) and 5(c) are 2.460, 2.455 and 2.455nm,

respectively. The film formed in N_2O, which had a high resistivity, had a longer c-axis than those of the other two films. These changes can be explained as follows. The Bi-Sr-Ca-Cu-O system has an oxygen nonstoichiometry[11], and the sample with longer c-axis has a smaller oxygen content according to the correlation reported by Takeuchi et al.[12] Since the carrier in this system is mainly supplied by the excess oxygen in Bi_2O_2 layer[12-14], the film with smaller excess oxygen has a lower carrier concentration resulting in higher resistivity. Thus, the differences in the lattice constant and also the resistivity are due to the differences of the content of excess oxygen in the $Bi_2Sr_2CuO_6$ structure. The results in this experiment show that the sample formed in N_2O has a lower oxygen content than the one formed in O_2 or the mixed gas. This is due to that the concentration of the oxygen radical produced from N_2O would not be so high in this experimental condition. Even if the concentration is low, the oxidation and crystallization of the films are promoted by the high chemical activity of oxygen radical, and the substrate temperature to form a crystallized as-grown film is lowered in N_2O. However, the low oxygen concentration leads to the low content of excess oxygen in the structure, so the oxygen content of the film formed in NO_2 is lower than that formed in O_2 or the mixed gas.

Concerning the CuO impurity in the film formed in O_2 [Fig.5(b)], this impurity did not come from the deviation of chemical composition, because it appeared even in the film prepared from Cu-poor targets in O_2 ambient. The disappearance of the CuO peak in the film formed in the mixed gas [Fig.5(c)]

suggests that CuO is formed only in a relatively high O_2 pressure, such as 6Pa. In the mixed gas, the partial pressure of O_2 is lower, which is 1/6 of that of the pure O_2 ambient we used, so CuO would not be formed in the mixed gas.

Figs.6(a) and 6(b) show x-ray diffraction patterns of the as-grown films formed at 923K in (a) 1×10^{-2}Pa of NO_2 and (b) 4×10^{-2} Pa of O_2 with substrate irradiation. While the film formed in O_2 was amorphous [Fig.6(b)], crystallized film could be formed in NO_2 at such low pressure of 1×10^{-2}Pa [Fig.6(a)]. Since the film formed in 1×10^{-2}Pa of N_2O was also amorphous, NO_2 was found to be very effective for the film growth under low-pressure conditions compared with O_2 or N_2O.

The changes of the free energy were calculated for the production of 1mol of oxygen atom from O_2, N_2O and NO_2 at 1×10^{-2}Pa and 1000K.[15] The calculated values are shown as

$$(1/2)O_2 \rightarrow O \qquad \Delta G= 121.9kJ,$$
$$N_2O \rightarrow N_2+O \qquad \Delta G= -99.8kJ,$$
$$NO_2 \rightarrow NO+O \qquad \Delta G= 38.6kJ.$$
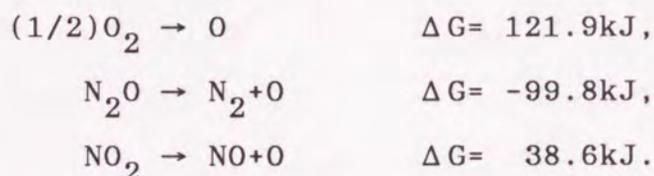
These result indicate that the release of oxygen atoms from N_2O is the easiest among the three reactions. The result, however, indicated that NO_2 is the most effective for the oxidation under low-pressure condition. This discrepancy suggests the difference of the oxidation mechanism in each gas. For example, from the analogy with metal nitrates, adsorption of NO_2 on metal element may readily occur and a stable intermediate chemical species may be formed. If the oxidation in NO_2 proceeds through the formation of the intermediate metal nitrate, the activation

34

energy of the reaction must be low. In this case, the oxidation
rate in NO_2 must be more rapid than that in N_2O.

Conclusion

Thin films of the cuprate superconductors were prepared by laser ablation method. The characteristic feature of this method is that the chemical composition of the film is almost same with that in the target solid. The crystallinity of the films is dependent on the laser intensity in the laser ablation method. This will be due to the effect of excess energy of the electronically excited species, which is not formed in sputtering or evaporation methods. Though N_2O gas with substrate excitation is effective for the formation of a single-phase $Bi_2Sr_2CuO_6$ film at lower temperature, the film had a high resistivity because of a low oxygen content. For the formation of a single-phase film with low resistivity, the mixture of N_2O and O_2 was effective. On the other hand, NO_2 was very effective for the formation under low-pressure condition.

References

(1)   D.K.Lathrop, S.E.Russek and R.A.Buhrmann,   Appl.Phys.Lett.,
51, 1554 (1987).

(2)   T.Terashima,   K.Iijima, K.Yamamoto, Y.Bando and T.Mazaki,
Jpn.J.Appl.Phys., 27, L91 (1988).

(3)   Y.Enomoto,   T.murakami,   M.Suzuki   and   K.Moriwaki,
Jpn.J.Appl.Phys., 26, L1248 (1987).

(4)   H.Adachi,   K.Setsune   and   K.Wasa,   Phys.Rev.B,   35,   8824
(1987).

(5)   T.Tamegai, k.koga, K.Suzuki, M.Ichihara, F.Sakai and Y.Iye,
Jpn.J.Appl.Phys., 28, L112 (1989).

(6) E.Sonder, B.C.Chakoumakos and B.C.Sales, Phys.Rev.B, 40, 6872
(1989).

(7) K.Jones, Comprehensive Inorganic chemistry Vol.2,   (pergamon,
Oxford, 1973).

(8)   R.A.Laudise, L.F.Schneemeyer and R.L.Barns,   J.Cryst.Growth,
85, 569 (1987).

(9)   O.Michigami,   H.Asano,   Y.Katoh,   S.Kubo   and   K.Tanabe,
Jpn.J.Appl.Phys., 26, L1199, (1987).

(10)   H.Okabe, Photochemistry of Small Molecules,   (Willey,   New
York, 1978).

(11)   T.Ishida, Jpn.J.Appl.Phys., 27, L2327 (1988).

(12)   K.Takeuchi, M.Kawasaki, M.Yoshimoto, Y.Saito and H.Koinuma,
Jpn.J.Appl.Phys., 29, L70 (1990).

(13) H.Hattori, K.Nakamura and K.Ogawa, Jpn.J.Appl.Phys., 29, L36
(1990).

(14)   C.C.Torardi, J.B.Parise, M.A.Sabramanian,   J.Gopalakrishnan

and A.W.Sleight, Physica C, 157, 115 (1989).

(15)   K.S.Pitzer and L.Brewer, Thermodynamics, (McGraw-Hill,   New
York, 1961).
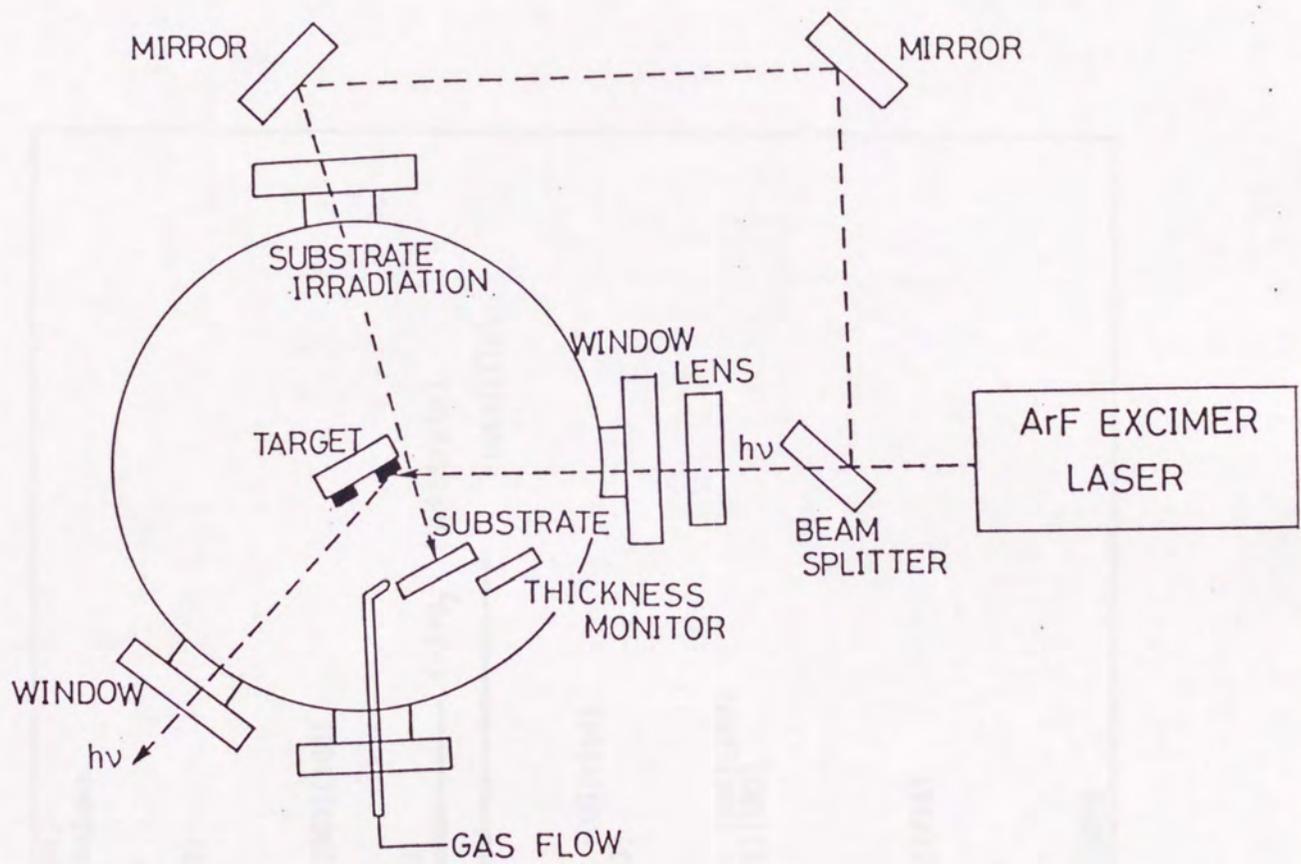
Fig-1   Apparatus used in this section. The laser beam is split
into two directions. One is used for the ablation and the other
for substrate irradiation.

38

Fig.1   Apparatus used in this section.   The laser beam is   spl

into   two directions. One is used for the ablation and the   oth

for substrate irradiation.
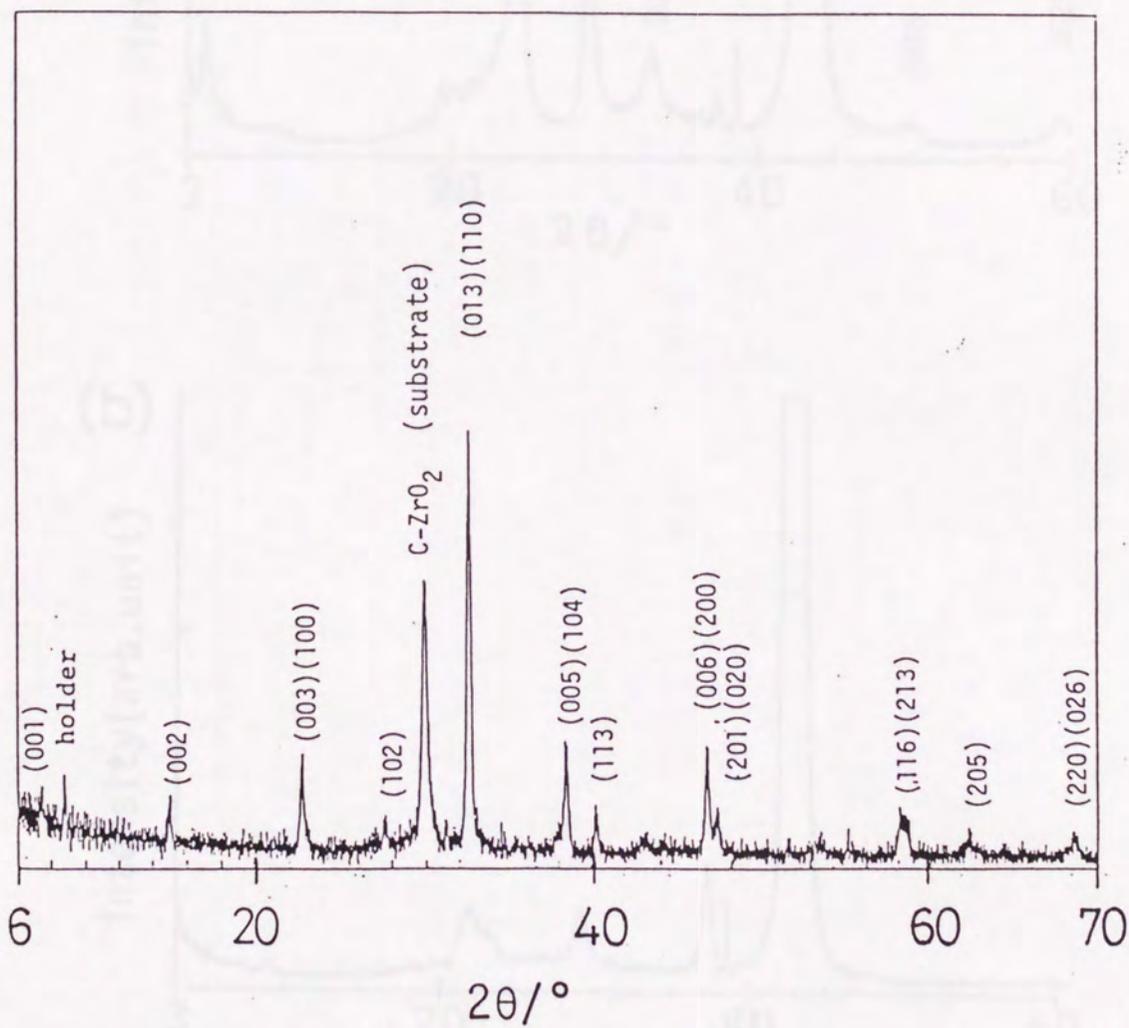
Fig.2 A x-ray diffraction pattern of Y-Ba-Cu-O film prepared by
the ablation of $YBa_2Cu_3O_y$ target.
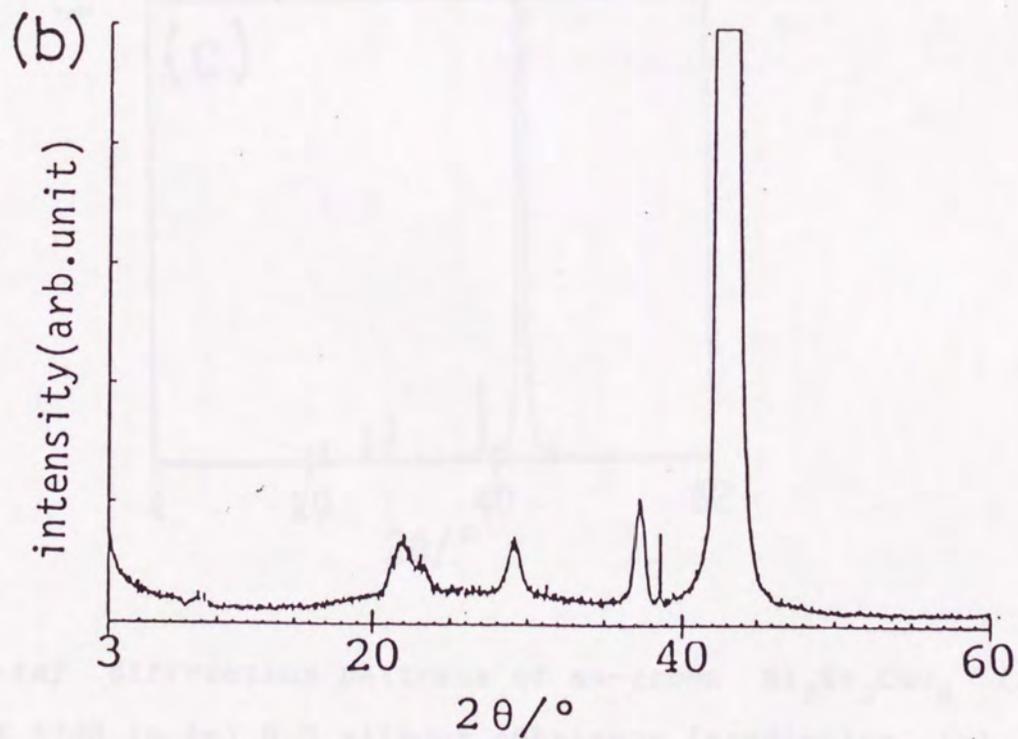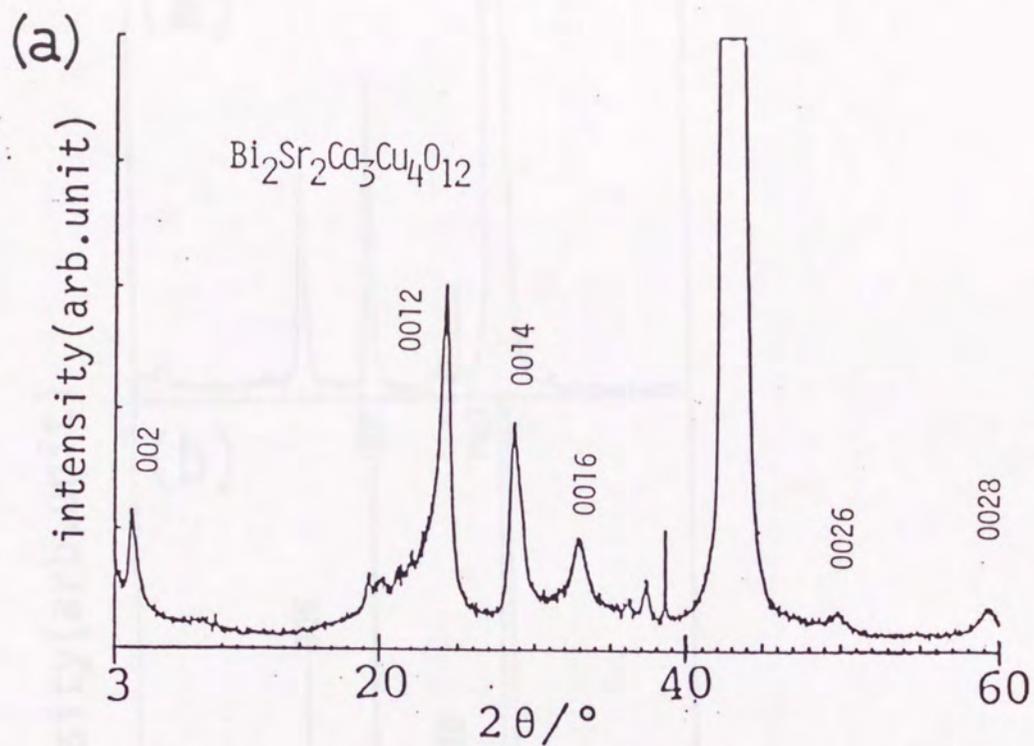
Fig.3 X-ray diffraction patterns of as-grown Bi-Sr-Ca-Cu-O thin films prepared with (a) higher laser intensity and (b) lower intensity.   The   pattern of (a) shows the   structure of $Bi_2Sr_2Ca_3Cu_4O_{12}$ [refer Chapter 4].
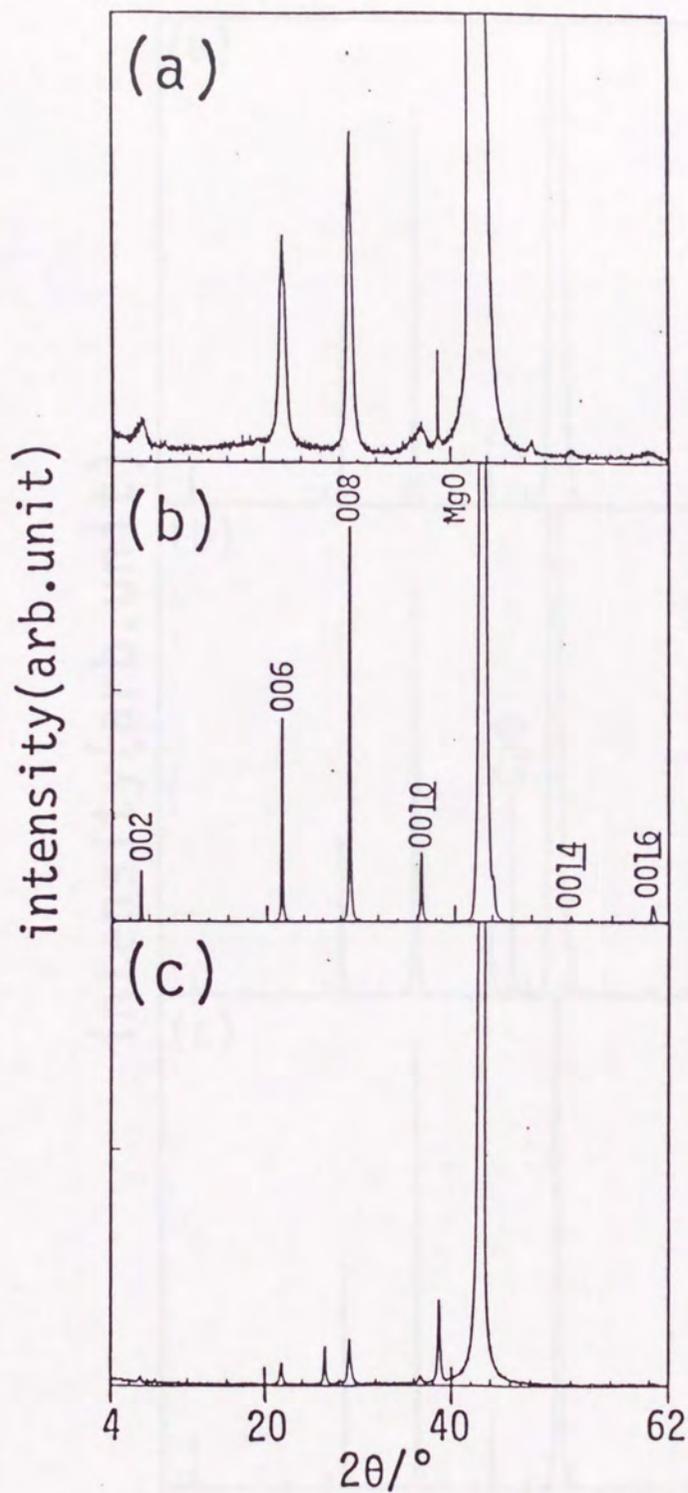
Fig.4 X-ray diffraction patterns of as-grown $Bi_2Sr_2CuO_6$ films formed at 873K in (a) N_2O without substrate irradiation, (b) N_2O with irradiation and (c) O_2 with irradiation.
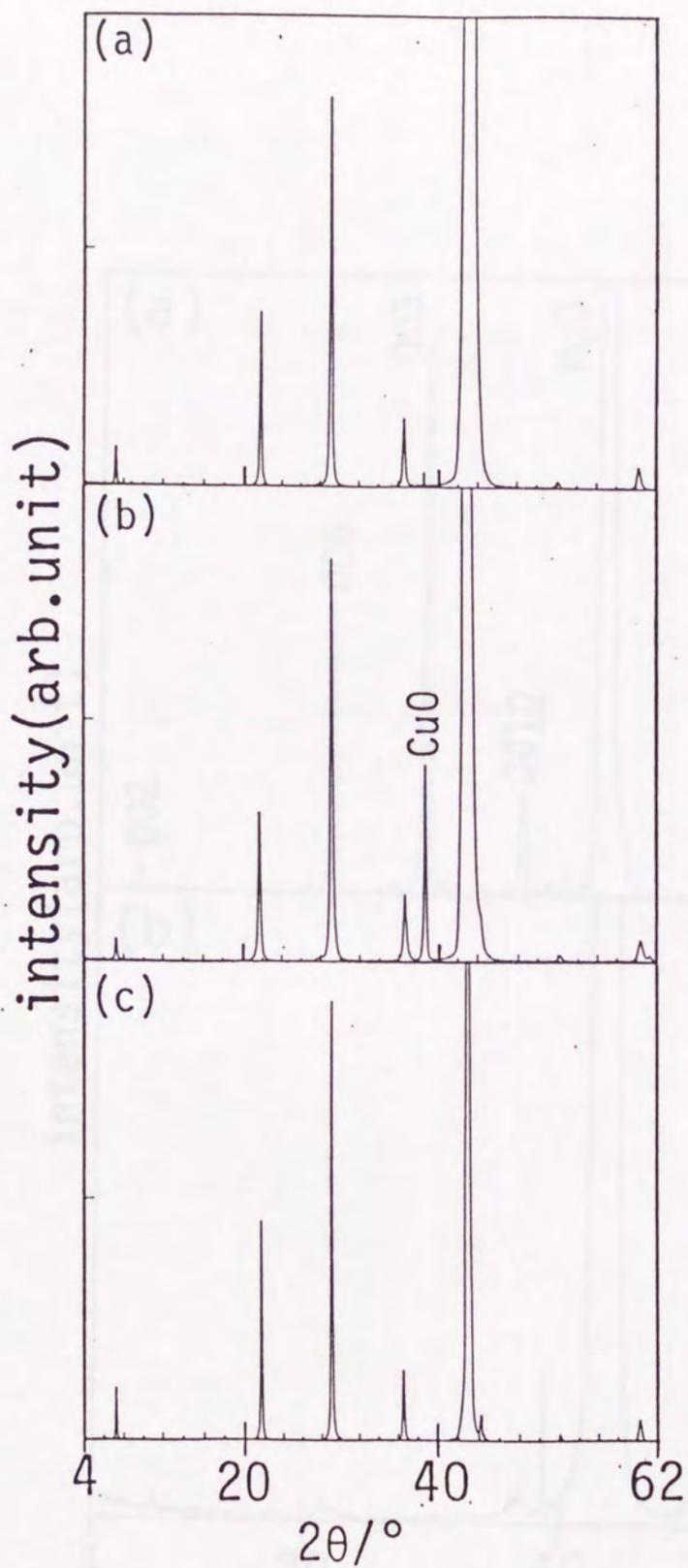
Fig.5   X-ray diffraction patterns of as-grown $Bi_2Sr_2CuO_6$ films formed at 953K in (a) N_2O,   (b) O_2 and (c) a mixture of N_2O and O_2.
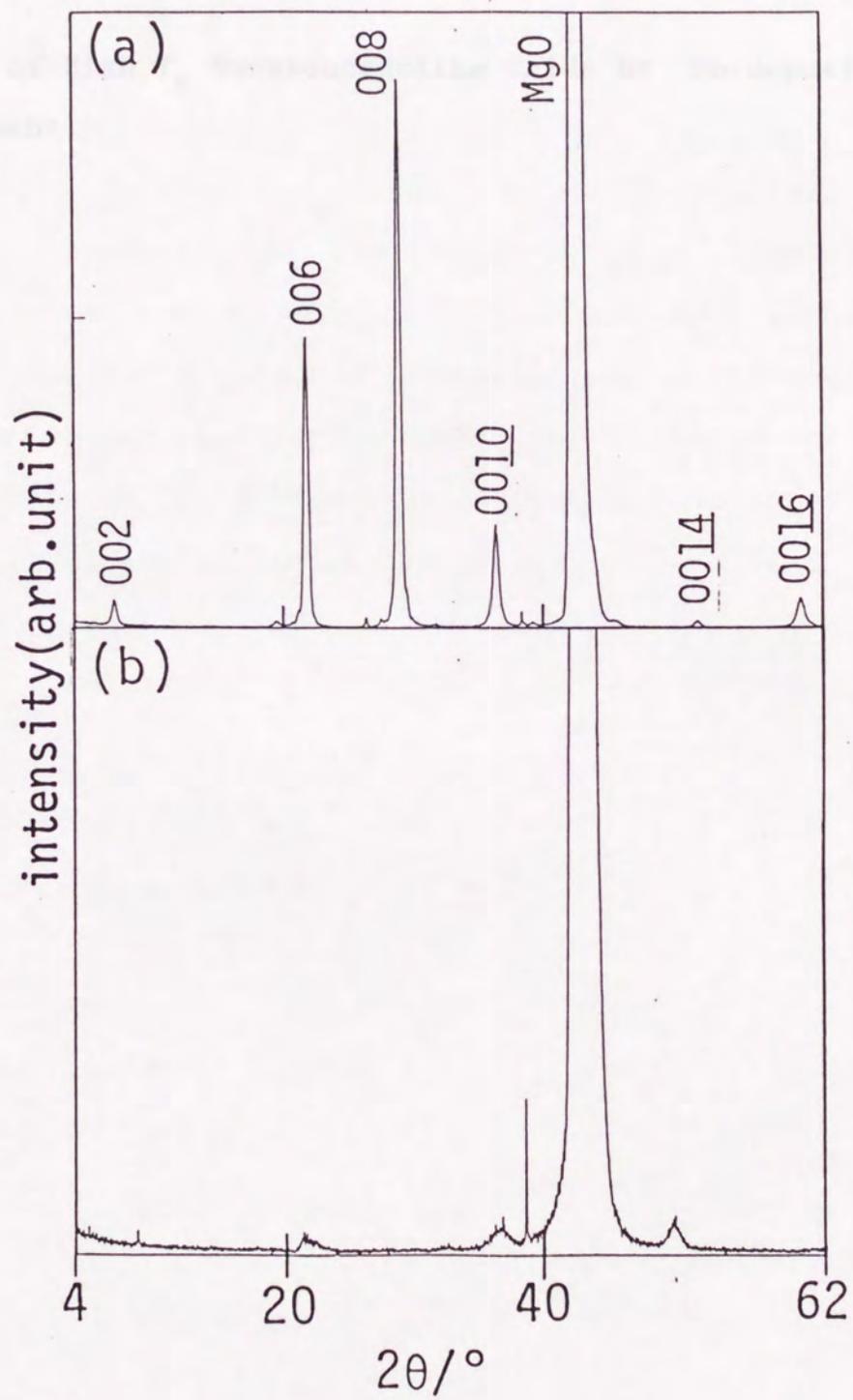
Fig.6   X-ray diffraction patterns of as-grown $Bi_2Sr_2CuO_6$ films formed at 923K in (a) $1 \times 10^{-2} Pa$ of NO_2 and (b) $4 \times 10^{-2} Pa$ of O_2.

Chapter 3

Crystal Growth of High T$_c$ Superconducting Oxide by Co-deposition
and Heat treatment

LnBa$_2$Cu$_3$O$_7$ thin films with nine different lanthanide ions have
been prepared by co-deposition of metal elements of lanthanum,
barium and copper at room temperature, followed by heat treatment
at high temperature. Systematic changes of the structure and
superconducting properties are compared with the change of the
lanthanide element. It becomes clear that the changes are
related to the radii of the lanthanide ions.

Chapter 3-1:

Effect of Lanthanide Ions on the Properties of $LnBa_2Cu_3O_y$ Thin Films

Abstract

$LnBa_2Cu_3O_y$ thin films with nine different lanthanide ions have been prepared by co-deposition of metal elements of lanthanide, barium and copper at room temperature, followed by heat treatment at high temperature. Systematic changes of the structure and superconducting properties are observed with the change of the lanthanide element. It becomes clear that the changes are related to the radii of the lanthanide ion.

Introduction

The superconductivity in $YBa_2Cu_3O_y$ was reported by Chu et al in 1987 at first.[1] This superconductor has a oxygen deficient type triple layered perovskite structure[2]. The crystal structure of this system is shown in Fig.1. Since the lanthanide ion has small ionic radius, the oxygen site beside the lanthanide ion is usually deficient. The oxygen content (y) in this system can be varied from 6.0 to 7.0 and the structure and properties are drastically changed with the variation of the oxygen content.[3] This oxygen nonstoichiometry is due to the variation of occupancy of O(1) oxygen site [see Fig.1(a)].[4] With the oxygen content (y) above 6.7, oxygen site beside Cu(1) is perfectly deficient along a-axis and only that along b-axis is occupied to form Cu(1)-O(1) chain structure. In this region, the system has an orthorhombic crystal structure and becomes superconductor below 90K. The occupancy of O(1) decreases with the decrease of oxygen content. The transition temperature is about 60K with oxygen content (y) between 6.4 and 6.7. With y below 6.4, the system changes to a semiconductor having a tetragonal crystal structure [see Fig.1 (b)]. It is well known that the change of the electric properties is due to the change of carrier concentration accompanied with the change of oxygen content.[5]

One of the characteristic feature of $YBa_2Cu_3O_y$ system is that the substitution of lanthanide ions, such as Er, Ho and Dy, for Y site does not decrease the superconducting transition temperature (T_c).[6] However, the systematic changes in the

properties as a result of the different lanthanide ions have   not

been studied yet.

In   thin films, the oxygen content will quickly come to   the

equilibrium value compared with bulk samples.   Therefore, it   is

easier   to obtain the samples with homogenous oxygen   content   in

the thin films.   In this section, the variation of the properties

of $LnBa_2Cu_3O_y$ thin films against nine kinds of lanthanide   ions

are   described.   The lanthanide ions represented by "Ln" are   Er,

Ho, Dy, Y, Gd, Eu, Sm, Nd and La.

Experimental

Since a slight deviation of chemical composition leads to the formation of second phase in Ln-Ba-Cu-O system[7], the strict control of the composition is needed for the film formation. In laser ablation method, the chemical composition of the films does not change significantly from that of the target materials as described in Chapter 2, so this method is suitable for this experiment. In order to take the advantage of this way, the films were deposited on substrates at room temperature in order to prevent the deviation of the chemical composition by the reevaporation at high temperature. The deposited films are amorphous-like, so the films were sintered at high temperature after the deposition to prepare $LnBa_2Cu_3O_y$ samples. In this way, the films including the different lanthanide elements can be synthesized by the same procedure without the significant deviation of the chemical composition.

Nine kinds of $LnBa_2Cu_3O_y$ targets for the ablation were prepared by sintering the mixture of Ln_2O_3 (Seimi, purity 99.9%), $BaCO_3$ (Wako, 99%) and CuO (Wako 99.9%) with the molar ratio of Ln:Ba:Cu=1:2:3 at 1123K for 10 hours under O_2 atmosphere. The lanthanide ions represented by "Ln" are Er, Ho, Dy, Y, Gd, Eu, Sm, Nd and La. The experimental setup has been shown in Chapter 2. Cubic ZrO_2 (100) (Tateho Chemical) were used as a substrate. Typical film thickness is about 2μm. All the films were treated in a furnace under the same condition, where the films were heated at 1193K for 1 minutes to crystallize and oxidize the sample, followed by annealing at 823K for 5 hours under O_2

43

atmosphere. The annealing process at 823K was needed to supply enough oxygen into the $LnBa_2Cu_3O_y$ system, because the semiconducting tetragonal phase with poor oxygen content is more stable above 873K and below this temperature the orthorhombic phase becomes stable.[4]

Resistivity-temperature (R-T) curves of the films were obtained with a standard four-probe technique. In this method, four electrode are attached to the sample, and outside two electrodes are used for supply of the current and inside two for voltage measurement. The resistivity can be obtained from the supplied current and measured voltage. By this method, sample resistivity can be measured without the effect of the contact resistance between the films and the electrodes. The samples were cooled in a glass Dewar with liquid He, and the temperature was measured using a calibrated semiconductor sensor. Gold wire leads were attached to the films through indium electrodes. The lowest resistivity we could measure in this system was 10^{-6} ohm·cm. The typical current density in the measurement of resistance was $1A/cm^2$.

X-ray diffraction (XRD) patterns were measured using CuK_α with conventional θ-2θ scanning.

Results and Discussion

Typical resistivity-temperature curve of $YBaCu_3O_y$ is shown in Fig.2. The decrease of resistivity due to superconductivity can be observed around 90K.

Fig.3 shows the (001) and (200),(020) peaks in the XRD patterns for the series of $LnBa_2Cu_3O_y$ films. In this figure, we see that the films with smaller lanthanide ions, such as Er, Ho, Dy and Y, show clear separation between (200) and (020) peaks, indicating the formation of orthorhombic structures. Furthermore, the intensities of the (001) peak, which is due to the triple layered perovskite structure, are strong in these compounds. These films exhibited superconductivity below 90K. Contrary to the above, the films with the larger lanthanide ions, such as Gd and Eu, exhibited unclear separation between (200) and (020) peaks, finally overlapping to form single peak in the $SmBa_2Cu_3O_y$ and $NdBa_2Cu_3O_y$ films. The $LaBa_2Cu_3O_y$ film showed the narrowest single peak. The (001) peak tended to become weaker for the larger lanthanide ions and (001) peak disappeared in $NdBa_2Cu_3O_y$ and $LaBa_2Cu_3O_y$. The films with larger lanthanide ions exhibited semiconducting resistance-temperature behaviors.

The changes in separation between the (200) and the (020) peaks can be explained as follows. When smaller lanthanide element was exchanged for a larger one, it was observed that the elongation of the lattice constant c of $LnBa_2Cu_3O_y$ was smaller than the increase of the ionic radius of lanthanide.[8] Namely, Ba-Ba length is compressed by larger lanthanide ions [see Fig.4]. Therefore, oxygen in the Cu(1)-O(1) chain cannot be

45

easily incorporated between Ba-Ba and oxygen content y in LnBa$_2$Cu$_3$O$_y$ approaches 6.0 when the lanthanide becomes larger [see Fig.4]. In these case, it is difficult to obtain a superconductor with orthorhombic structure including enough oxygen content. For this reason, the structure comes close to tetragonal symmetry with poor oxygen content when the lanthanide ionic radii become larger.

In terms of the changes in the (001) peak intensity, three different explanations will be possible. The first is that the film with the smaller lanthanide ion may have been oriented to the direction with its c-axis perpendicular to the substrate surface, thus giving a stronger (001) peak. The XRD patterns of all the films, however, resemble those of the powdered samples and the intensity of (003) peak was not particularly strong in the film with smaller lanthanide. Therefore, these films were not oriented as above, making this explanation invalid.

The second explanation is that the structural factor of the (001) peak may be smaller for larger lanthanide systems, because the scattering factor of a larger lanthanide ion is close to that of the Ba^{2+} ion, and the scatterings by Ln^{3+} and Ba^{2+} are compensated each other in (001) diffraction. Actually the scattering factor of La^{3+} is nearly equal to that of Ba^{2+}. In order to check this assumption, the peak intensities of (001) and (113) were calculated for orthorhombic ErBa$_2$Cu$_3$O$_y$ and tetragonal LaBa$_2$Cu$_3$O$_y$ using the following equation.[9]

$$I = L \cdot p \cdot [\Sigma f_i \exp\{-2\pi i(hx+ky+lz)\}\exp(-B_i \sin^2\theta/\lambda^2)]^2 \qquad (1)$$

where I is intensity, L is Lorentz factor, p is polarization

factor, f_i is atomic scattering factor[10], h,k,l are Miller indices, x,y,z are atomic positions[11,12] and B_i is temperature factor[11,12] The calculation shows that the intensities of (001) and (113) for $LaBa_2Cu_3O_y$ should be about 50% and 70% of those for $ErBa_2Cu_3O_y$, respectively. Since the (113) peaks were clearly seen in both the La-Ba-Cu-O and Er-Ba-Cu-O systems, the (001) peak of $LaBa_2Cu_3O_y$ should appear if the film really has the triple perovskite structure.

Thus the third explanation, being the most plausible explanation for the disappearance of the (001) peak in larger Ln systems, is that the oxygen deficient type triple layered perovskite structure was not formed under our experimental condition and instead a structure like a normal perovskite is favored. The larger lanthanide ions have a larger coordination number, such as 12 for oxygen anion, so that the oxygen deficient layer will not be formed around the larger lanthanide ions. (see Fig.1) Furthermore, large lanthanide ions are readily exchanged for Ba^{2+} ion.[13] For these reasons, the profile of the XRD pattern of $LnBa_2Cu_3O_y$ with larger lanthanide may come close to that of normal perovskite structure, thus the (001) peak becomes weaker.

Conclusion

In conclusion, the incorporation of the smaller lanthanide ion in $LnBa_2Cu_3O_y$ film results in easier formation not only of the orthorhombic structure but also of the oxygen deficient type triple layered perovskite structure. Larger lanthanide elements, such as La, Nd and Sm, prevent the incorporation of oxygen which is necessary for the formation of Cu-O chain structure. These behaviors strongly affect the superconducting properties of $LnBa_2Cu_3O_y$ thin films. Thus the superconducting films with T_c around 90K can be easily formed in the systems with smaller lanthanide ions such as $ErBa_2Cu_3O_y$, $HoBa_2Cu_3O_y$, $YBa_2Cu_3O_y$, $DyBa_2Cu_3O_y$ and $GdBa_2Cu_3O_y$, whereas orthorhombic $LaBa_2Cu_3O_y$, $NdBa_2Cu_3O_y$, $SmBa_2Cu_3O_y$ and $EuBa_2Cu_3O_y$ are not readily formed. Finally, in $LaBa_2Cu_3O_y$ system, a triple layered perovskite structure itself is not easily formed.

References

(1) M.K.Wu, J.R.Ashburn, C.J.Torng, P.H.Hor, R.L.Meng, L.Gao, Z.J.Huang, Y.Q.Wang and C.W.Chu, Phys.Rev.Lett., 58, 908 (1987).

(2) M.A.Beno, L.Sonderholm, B.W.Capone, B.G.Hinks, J.D.Jorgensen, I.K.Schuller, C.U.Segre, K.Zuang and J.D.Grace, Appl.Phys.Lett., 51, 57 (1987).

(3) M.Ishikawa, T.Takabatake and Y.Nakazawa, Physica B, 148, 322 (1987).

(4) Y.Nakazawa, M.Ishikawa, T.Takabatake, K.Koga and K.Terakuma, Jpn.J.Appl.Phys., 26, L796 (1987).

(5) Z.Z.Wang, J.Clayhold, N.P.Ong, J.M.Tarascon, L.H.Greene, W.R.McKinnon and G.W.Hull, Phy.Rev.B, 36, 7222 (1987).

(6) P.H.Hor, R.L.Meng, Y.Q.Wang, L.Gao, Z.J.Huang, J.Bechtold, K.Forester and C.W.Chu, Phys.Rev.Lett., 58, 1891 (1987).

(7) R.A.Laudise, L.F.Schneemeyer, and R.L.Barns, J.Cryst.Growth, 85, 569 (1987).

(8) H.Asano, K.Takita, H.Katoh, H.Ashinaga, T.Ishigaki, M.Nishino, M.Imai and K.Masuda, Jpn.J.Appl.Phys., 26, L1410 (1987).

(9) I.Nitta, X-ray Crystallography, (Maruzen, Tokyo, 1959).

(10) J.A.Ibers and W.C.Hamilton, International Tables for X-ray Crystallography Vol.4, (The Kynoch Press, Birmingham 1974).

(11) T.Ishigaki, H.Asano and K.Takita, Jpn.J.Appl.Phys., 26, L987 (1987).

(12) R.Yoshizaki, H.Sawada, T.Iwazumi, Y.Saito, Y.Abe, H.Ikeda, K.Imai and I.Nakai, Jpn.J.Appl.Phys., 26, L1703 (1987).

(13) S.Tsurumi, T.Iwata, Y.Tajima and M.Hikita, Jpn.J.Appl.Phys., 26, L1865 (1987)
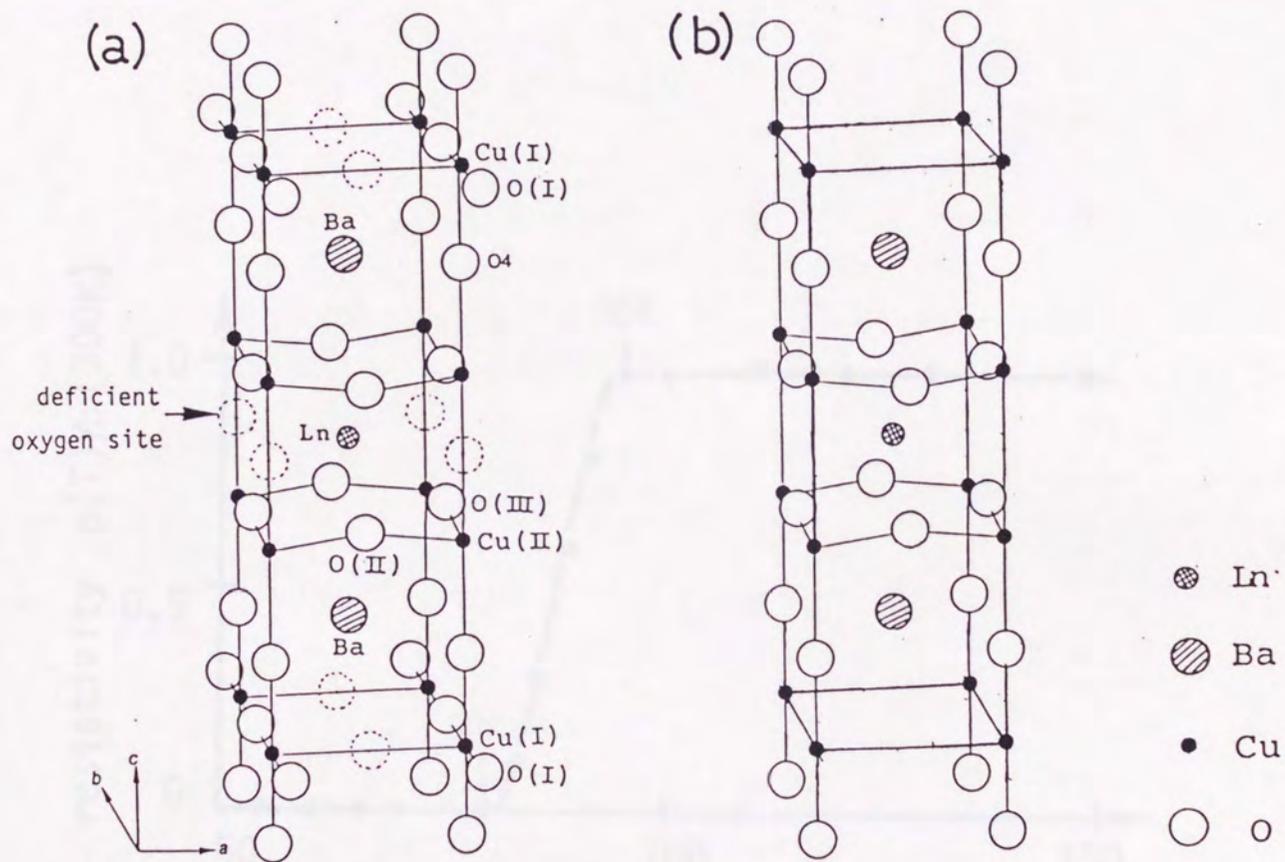
Fig.1 The crystal structure of (a) $LnBa_2Cu_3O_7$ and (b) $LnBa_2Cu_3O_6$, where Ln shows yttrium or lanthonide ion.
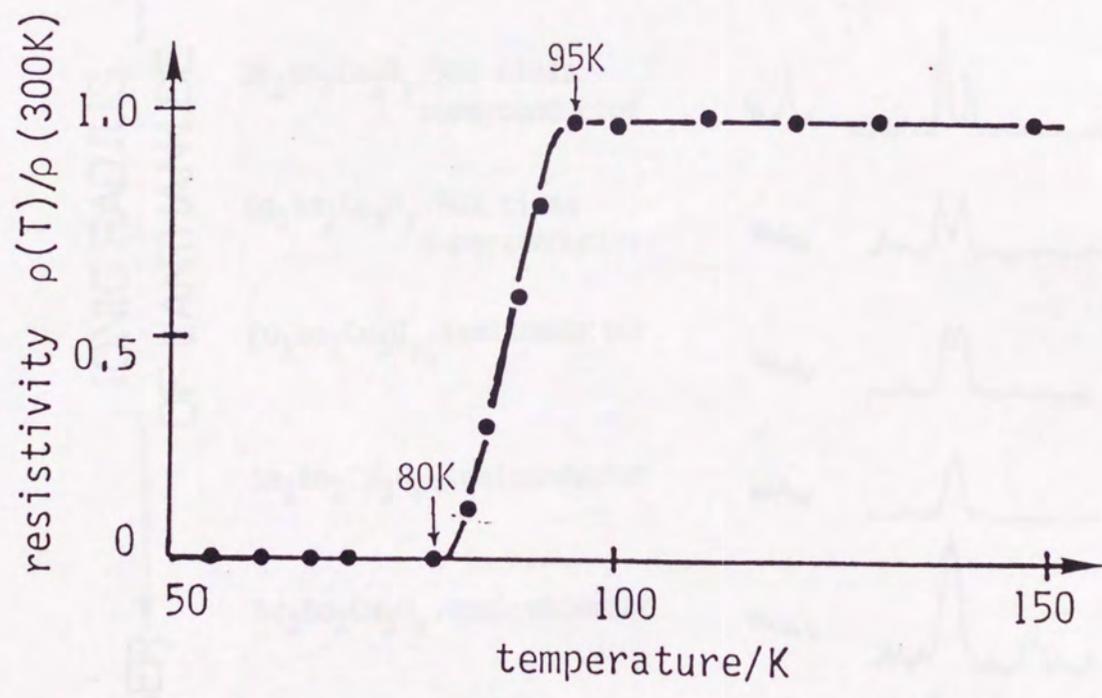
Fig.2 Resistivity-temperature curve of $YBa_2Cu_3O_y$ thin film.
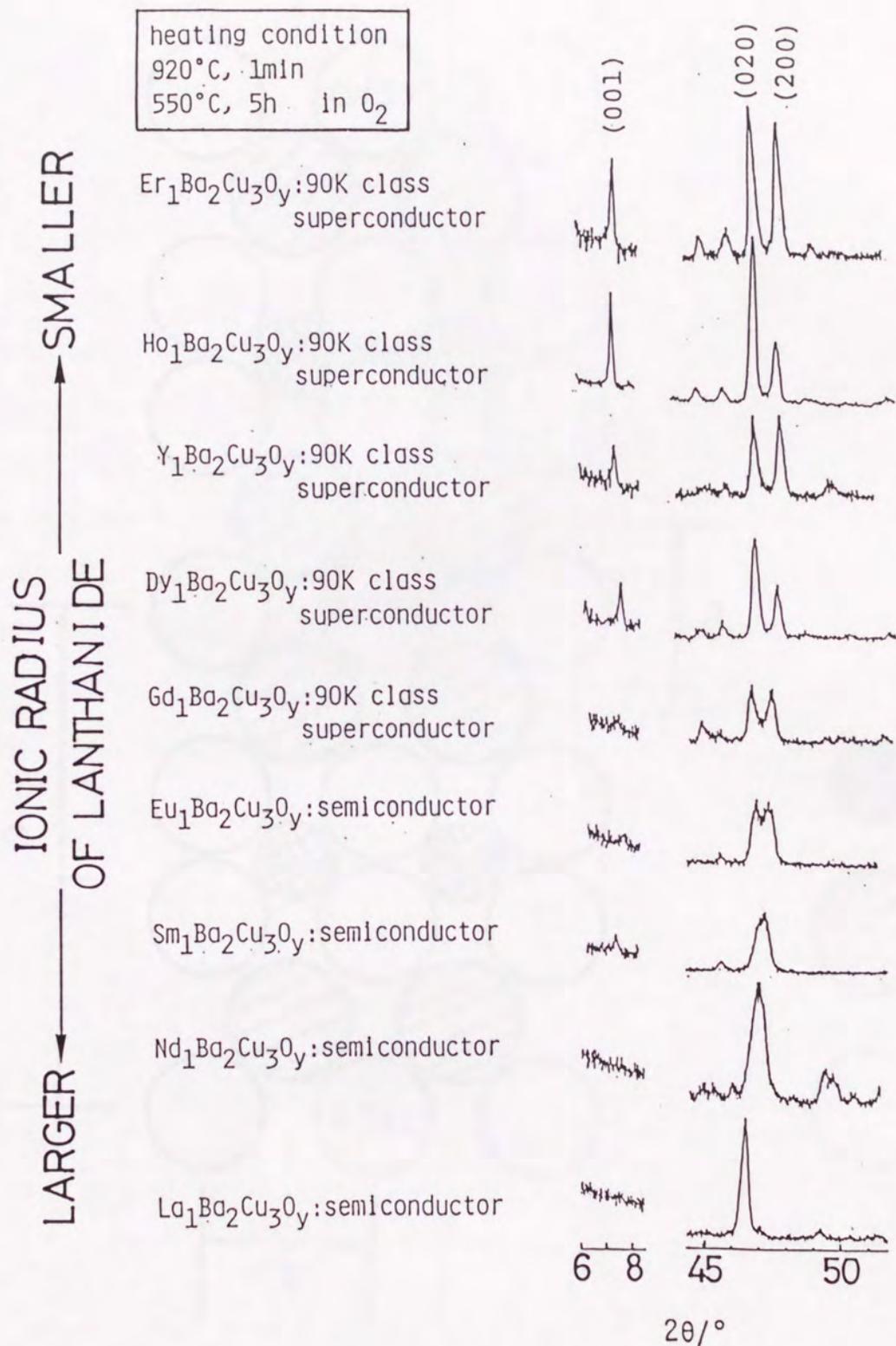
Fig.3 Diffraction-peak profiles of the series of $LnBa_2Cu_3O_y$ films for nine lanthanide ions. All films were treated in the same condition.
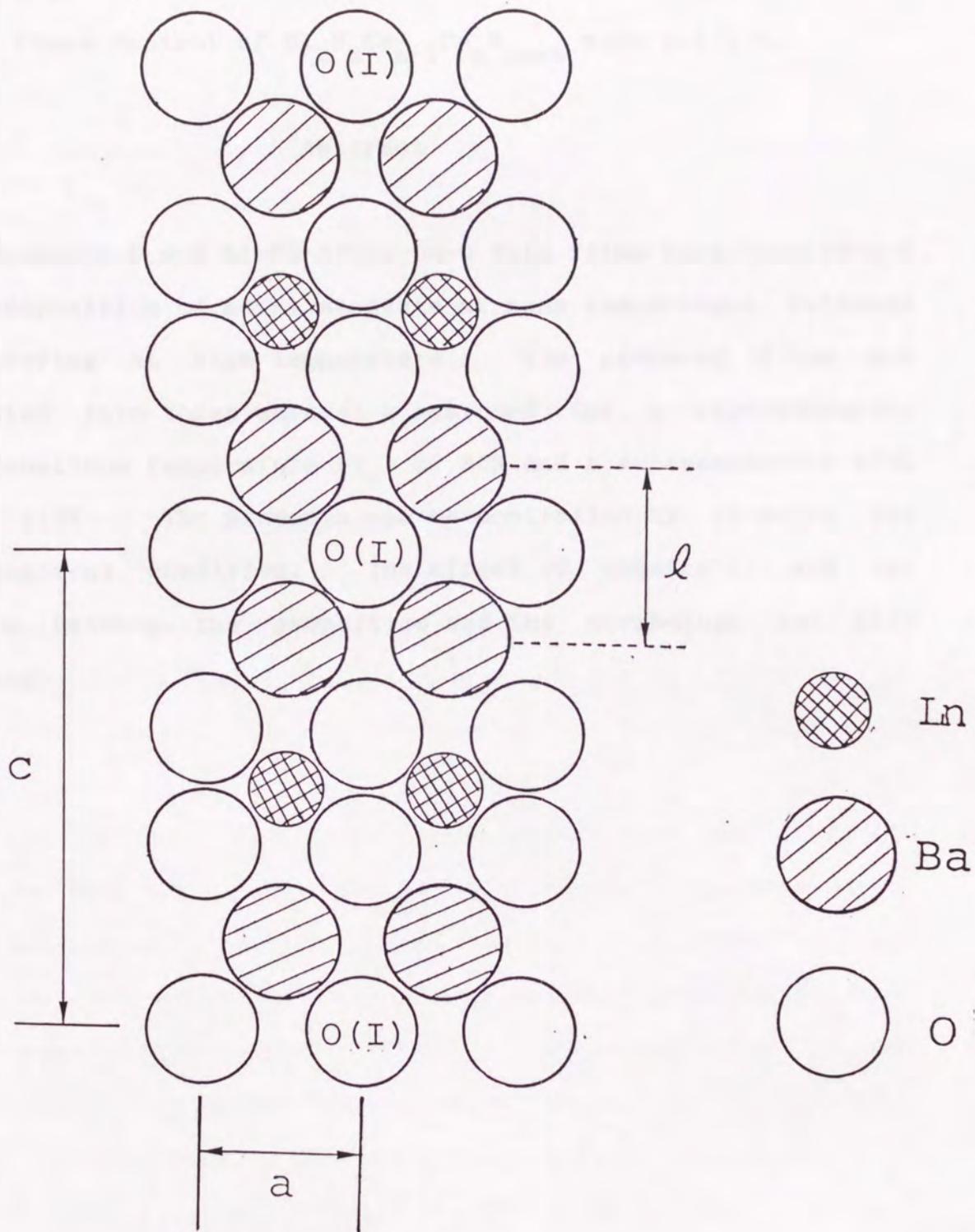
Fig.4 The arrangement of ions in (020) plane of $LnBa_2Cu_3O_y$. With decrease of l in the figure, the incorporation of oxygen at O(1) site becomes difficult.

Chapter 3-2:

Phase Control of $Bi_2S_2Ca_{n-1}Cu_nO_{2n+4}$ with n=1,2,3.

Abstract

Bi-Sr-Ca-Cu-O and Bi-Pb-Sr-Ca-Cu-O thin films have been formed by co-deposition of metal elements at room temperature followed by sintering at high temperature. The prepared films are classified into three phases: a semiconductor, a superconductor with transition temperature (T_c) of 80K and a superconductor with Tc of 110K. The products can be controlled by choosing the heat-treatment condition. The effect of substrate, and the relation between the properties and the morphology are also discussed.

50

Introduction

The superconductivity in Bi-Sr-Ca-Cu-O system above liquid-nitrogen temperature was observed by Maeda and co-workers in 1988.[1] In this system, three phases have been found, which can be represented by $Bi_2Sr_2Ca_{n-1}Cu_nO_{2n+4}$ with n=1,2 and 3.[2-4] The crystal structures of the phases are shown in Fig.1. These three phases have similar crystal structures and only the numbers of CuO_2 planes between adjacent Bi_2O_2 layers are different. Therefore, the three phases have the almost same lattice constants a and b, and different lattice constant c. $Bi_2Sr_2CuO_6$ phase including single CuO_2 layer, $Bi_2Sr_2CaCu_2O_8$ phase with double CuO_2 layers and $Bi_2Sr_2Ca_2Cu_3O_{10}$ phase with triple CuO_2 layers are called "2201", "2212" and "2223" phase, respectively. Each phase has the lattice constant c of 2.44nm, 3.08nm or 3.68nm.

It is very interesting that these phases have so different properties even though they have similar crystal structure except the number of CuO_2 planes. 2201 phase is a semiconductor, and 2212 phase is a superconductor with Tc of 80K. 2223 phase shows the superconductivity above 100K. Detailed investigation of the properties of each phases will be effective for the clarification of the superconducting mechanism in cuprate superconductors. For such study, it is necessary to form a single-phase sample of each phase, but these are often obtained in mixed-phase sample.

In this section, thin films of Bi-Sr-Ca-Cu-O and Pb-doped Bi-Pb-Sr-Ca-Cu-O were prepared by the co-deposition of metal elements at room temperature followed by sintering at high

51

temperature. The changes of the structure and property of the Bi-Sr-Ca-Cu-O films accompanied with the variation of heat-treatment condition were investigated. The phase control by heat treatment is the most conventional and basic way of phase control. Furthermore, the films were prepared on MgO, cubic ZrO_2 and $SrTiO_3$ substrates, and the effect of the substrate was investigated.

Experimental

Bi-Sr-Ca-Cu-O system is not sensitive to the deviation of the chemical composition of starting materials from the ideal composition. In this experiment, the chemical composition of the target is fixed at Bi:Sr:Ca:Cu = 1:1:1:2 for Bi-Sr-Ca-Cu-O or Bi:Pb:Sr:Ca:Cu = 0.8:0.2:1:1:2 for Bi-Pb-Sr-Ca-Cu-O system in molar ratio.[1] The targets for the ablation were synthesized by calcining mixture of Bi_2O_3 (Wako, purity=99.9%), PbO (Wako, 99%), $SrCO_3$ (Wako, 99.9%), $CaCO_3$ (Mitsuwa, 99.9%) and CuO (Wako, 99.9%) at 1153K for 10 hours. The films were deposited by ArF laser ablation of the targets at room temperature and after that, the films are oxidized and crystallized by heating in a furnace. The furnace temperature was raised to 1073 or 1173K. The typical thickness of the film was $2\mu m$. MgO(100), cubic-ZrO_2(100) or $SrTiO_3$(100) (Tateho Chemical) was used as a substrate.

Resistivity-temperature (R-T) curve of the film was obtained using standard four probe technique. X-ray diffraction (XRD) pattern was measured using CuK_α with θ-2θ scanning. The surface morphology of the film was obtained by scanning electron microscopy (SEM) using JOEL JSM-25S system with acceleration voltage of 25kV.

53

Results and Discussion

Figs.2(a) and 2(b) shows a resistivity-temperature curve and an x-ray diffraction pattern of a Bi-Sr-Ca-Cu-O film on MgO (100) substrate prepared by heating at 1163K for 1 minute in air. The film exhibited semiconducting resistance-temperature behavior in which the resistivity increased with decrease of temperature. The x-ray diffraction pattern showed a series of strong peaks at $2\theta = 7.2°$, $21.9°$, $29.2°$, $36.8°$ and $44.5°$. These peaks are corresponding to (001) diffraction of 2201 phase including single CuO_2 plane.[2] Since the (001) peaks with odd l are disappeared with the disappearance rule of x-ray diffraction, only the (001) with even l can be seen. The strong (001) lines indicate that the film is oriented with its c-axis perpendicular to the substrate surface. The 2201 phase was formed when the film was sintered above the melting point of 1163K for 1 minute or below 1073K for 1 hour.

Annealing the Bi-Sr-Ca-Cu-O film on MgO substrate at a temperature between 1163K and 1073K led to the appearance of x-ray diffraction peaks at $2\theta = 5.7°$, $23.2°$, $29.3°$ and $35.1°$ instead of the 7.2° series peaks. Figs.3(a) and 3(b) show an R-T curve and an XRD pattern of a Bi-Sr-Ca-Cu-O film sintered at 1123K for 15 minutes followed by 1153K sintering for 1 minute in air. The strong peaks were corresponding to the (001) diffraction of 2212 phase including double CuO_2 plane in the crystal structure.[3,4] The diffraction pattern shows that the film is oriented with the c-axis perpendicular to the substrate surface, which is similar to the 2201 film described above. The

54

R-T curve showed a superconducting transition with zero resistance temperature of 80K. The critical current density of this film is about $1\times10^5 A/cm^2$ at 10K.

The films on MgO annealed at 1123K for 1 minute also exhibited a diffraction pattern of 2212 single-phase, but the pattern was similar to the powdered sample indicating a random oriented film without a preferred orientation. In most cases, annealing at the temperature between 1138K and 1158K led to the formation of the oriented 2212 film, whereas sintering above 1163K formed the oriented 2201 film. Thus, I could separately prepare the oriented Bi-Sr-Ca-Cu-O film including single or double CuO_2 planes by choosing proper heating temperature.

The heating temperature around the melting point was really critical for the superconducting property of these films. Figs.4(a) and 4(c) show R-T curves of the films sintered at 1153K for 1 minute and that sintered at 1158K for 1 minute. These films had almost same x-ray diffraction patterns of oriented 2212 films. In spite of that, the resistivity-temperature behaviors were so different. The film heated at 1153K had the tailing of the resistivity below 80K in the R-T curve, while the film heated at 1158K exhibited a sharp superconducting transition without the tailing. The tailing observed in the former film were enlarged by the increase of the measuring current density. The tailing was strongly related to the morphology of the films. Figs. 4(b) and 4(d) show SEM photographs of those films. It revealed that the film annealed at 1153K consisted of small grains whose diameters are about $5\mu m$ [see Fig.4(a)]. The heating at 1158K

just below the melting point changed the morphology of the film dramatically giving continuous film as shown in Fig.4(d). These results suggest that the tailing in R-T curve is due to the weak coupling of the superconducting particles. Bi-Sr-Ca-Cu-O superconductors have very short coherence length, which is discussed in detail at Chapter 5. Due to the short coherence length, the superconductivity in this system is easily disturbed by a little amount of impurity. In the film with the granular morphology as shown in Fig.4(b), the tailing of the superconducting transition arises from the disturbance by the grain boundary. The enlargement of the tailing by the increase of current density can be explained by the presence of many weak couplings with different critical currents in the sample. The heating just below the melting point makes the continuous film as shown in Fig.4(d), and decreases the weak coupling of grain boundary drastically. Thus that film shows a sharp superconducting transition without the tailing.

Concerning 2223 phase, a slight decrease of the resistivity around 110K were observed in the film heated at 1158K in 1 minute [see Fig.5(a)]. The heat treatment just below the melting point is essential to the appearance of the resistivity decrease at 110K, and the film annealed above 1163K or below 1153K did not show the decrease at 110K. The XRD pattern of the films with resistivity decrease at 110K, however, indicated that main product was 2212 phase [see Fig.5(b)]. The peaks due to 2223 phase could not detected in the pattern, thus a very little amount of 2223 phase must be formed in the films. Though Bi-Sr-Ca-Cu-O films were formed under various heating condition

in this experiment, it was very difficult to grow a large amount of 2223 phase. So I performed Pb doping into Bi-Sr-Ca-Cu-O films, which promoted the formation of 2223 phase in bulk sample.[5] The Bi-Pb-Sr-Ca-Cu-O films prepared by the ablation of $Bi_{0.8}Pb_{0.2}SrCaCu_2O_y$ target had lower melting point of 1123K than Pb-undoped Bi-Sr-Ca-Cu-O system, and the decrease of the resistivity around 110K also appeared with the heating just below the melting temperature. Figs.6(a) and 6(b) show the R-T curve and XRD pattern for the Bi-Pb-Sr-Ca-Cu-O film sintered at 1123K for 15 hours followed by annealing at 773K for 15 hours. The diffraction pattern shows that the sample is the mixture of 2212 and 2223 phases, but in Pb-doped Bi-Pb-Sr-Ca-Cu-O, the diffraction peaks at $2\theta = 4.8°$, $23.9°$, $28.8°$ and $33.7°$ corresponding to those of the 2223 phase with triple CuO_2 planes can be clearly observed. The R-T curve shows that the resistivity of this film decreases around 110K and zero-resistance temperature is 95K.

In my experiment, the product of Bi-Sr-Ca-Cu-O and Bi-Pb-Sr-Ca-Cu-O thin films can be controlled by choosing the heating temperature. The relation between the heating temperature and products is summarized in Fig.7.

In this step, the promotion of 2223 formation by Pb doping are explained as follows. Since a large amount of 2223 phase is formed in the temperature range, which is above the melting point of 2212 and below that of 2223. Though the melting point of 2223 is very close to that of 2212 in Bi-Sr-Ca-Cu-O system, the difference between the melting point of 2212 and that of 2223

57

becomes wider with doping of Pb.[6] For this reason, the doping of Pb makes it easier to prepare the 2223 phase.

Finally, the effect of the substrate is described. In the above experiments, MgO (100) was used as a substrate. Cubic-ZrO_2 (100) and $SrTiO_3$ (100) substrates were also examined, and the property of the film on each substrate was compared. The 2212 films on cubic ZrO_2 exhibited a R-T behavior similar to that on MgO, while the films on $SrTiO_3$ showed semiconducting R-T behavior above 100K and a broad superconducting transition with a very low zero-resistance temperature around 15K. Thus MgO and c-ZrO_2 is better candidates as the substrates for Bi-Sr-Ca-cu-O films and $SrTiO_3$ is improper, when the films are formed by annealing at high temperature. Recent result of secondary ion mass spectroscopy[7] suggests that inter-diffusion between $SrTiO_3$ and the film deteriorates the superconductivity, and the diffusion is suppressed in the films on MgO substrate. However, it should be mentioned that $SrTiO_3$ substrate is appropriate from the viewpoint of the crystal structure, because the crystal structure and the lattice constants a and b of the $SrTiO_3$ is similar to those of the cuprate superconductors. If the films can be formed at lower temperature and inter-diffusion can be suppressed, $SrTiO_3$ (100) substrate becomes very useful. In practice, $SrTiO_3$ is used as a substrate in following section in order to obtain epitaxial films. In those experiments, the as-grown films are prepared at relatively low temperature, so the inter-diffusion should be suppressed.

Conclusion

Bi-Sr-Ca-Cu-O and Bi-Pb-Sr-Ca-Cu-O thin films were prepared by co-deposition followed by high-temperature sintering. The three types of the oriented films with its c-axis perpendicular to the substrate surface were formed, and they were classified to 2201, 2212 and 2223 phases. The 2201 and 2212 films can be prepared separately by choosing the heating temperature. The 2223 phase can be formed only in Bi-Pb-Sr-Ca-Cu-O film, but it was difficult to obtain a single-phase sample. The 2201 film shows semiconducting resistivity-temperature behavior, and 2212 and 2223 films exhibit superconductivity below 80K and 110K,respectively. The superconducting properties in these films are strongly dependent upon the morphology of the films reflecting the short coherence length of this system. The tailing of superconducting transition was often observed on the film with granular morphology. To prevent the appearance of the tailing, the heating just below the melting temperature to form a continuous morphology is effective. MgO (100) and c-ZrO_2 (100) substrates are suitable as the substrate in this preparation method. In the film with $SrTiO_3$ (100) substrate, the deterioration of the superconducting property caused by high temperature treatment was often observed.

References

(1) H.Maeda, Y.Tanaka, M.Fukutomi and T.Asano, Jpn.J.Appl.Phy., 27, L209 (1988).

(2) E.Takayama-Muromachi, Y.Uchida, A.Ona, F.Izumi, M.Onada, Y.Matsui, K.Kosuda, S.Takekawa and K.Kato, Jpn.J.Appl.Phys., 27, L365 (1988).

(3)   M.A.Sabramanian,   C.C.Torardi,   J.C.Calabrese, J.Gopalakrishnan,   K.J.Morrissey,   T.R.Askew,   R.B.Flippen, V.Chawdahri and A.W.Sleight, Science, 239, 1015 (1988).

(4)   H.Nobumasa,   K.Shimizu,   Y.Kitano   and   T.Kawai, Jpn.J.Appl.Phys., 27, L846 (1988).

(5) S.A.Sunshine, T.Siegrist, L.F.Schneemeyer, D.W.Murphy, R.J.Cava, B.Batlogg, R.B.van Dover, R.F.Fleming, S.H.Glarum, S.Nakahara, R.Farrow, J.J.Krajewski, S.M.Zahurak, J.V.Waszczak, J.H.Marshall, P.Marsh, L.W.Rupp Jr. and W.F.Peck, Phys.Rev.B, 38, 893 (1988).

(6) T.Hatano, K.Aota, S.Ikeda, K.Nakamura and K.Ogawa, Jpn.J.Appl.Phys., 27, L2055 (1988).

(7) T.Soe, K.Sakamoto, M.Motohashi and K.Homma, Extended Abstracts (The 51st Autumn Meeting); The Japan Society of Applied Physics, (The Japan Society of Applied Physics, Tokyo, 1990).
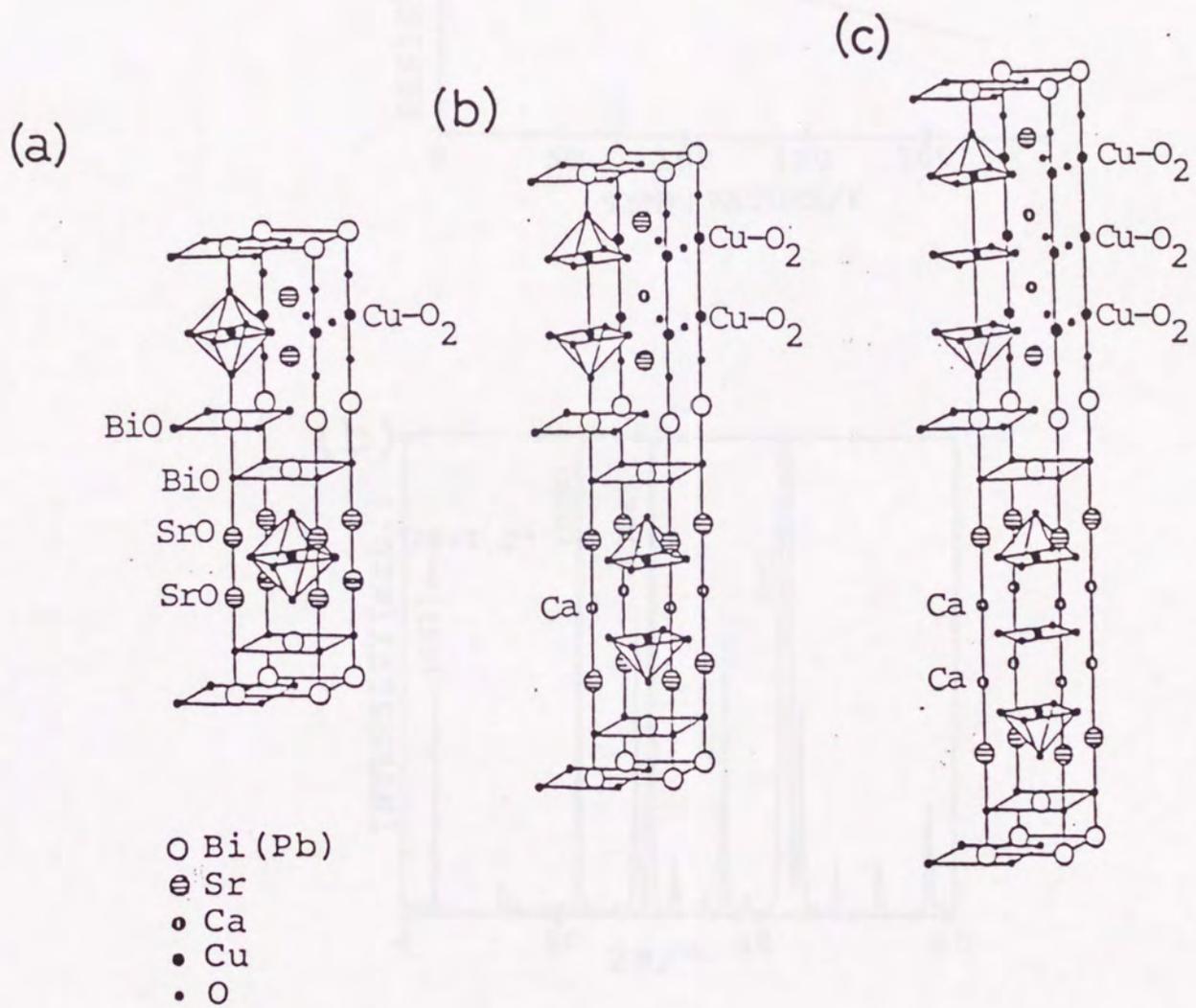
(a)

(b)

(c)

Cu–O_2

Cu–O_2

Cu–O_2

Cu–O_2

Cu–O_2

Cu–O_2

BiO

BiO

SrO

SrO

Ca

Ca

Ca

Ca

O Bi(Pb)
⊖ Sr
o Ca
• Cu
• O

Fig.1 The crystal structures of $Bi_2Sr_2Ca_{n-1}Cu_nO_{2n+4}$ with (a)n=1,
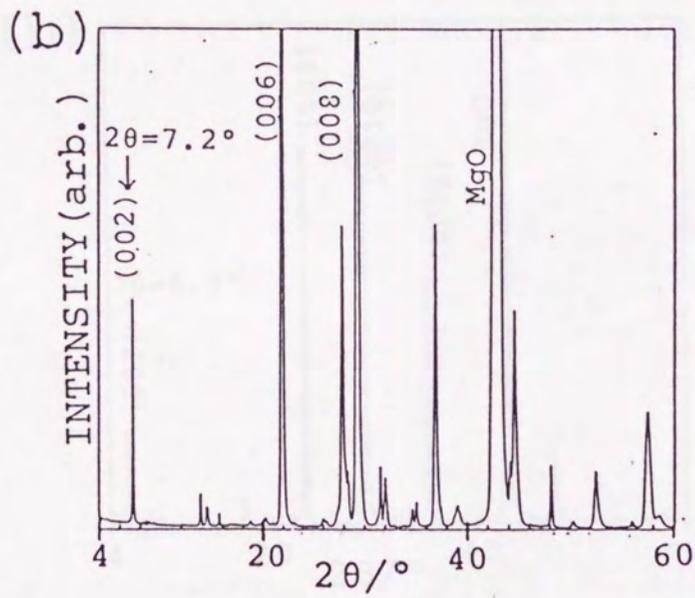(b) n=2 and (c) n=3.

(a)

(b)

Fig.2 (a) R-T curve and (b) X-ray diffraction pattern of a Bi-Sr-Ca-Cu-O film prepared by heating at 1163K for 1 minute in air.

(a)

RESISTIVITY (arb.)

TEMPERATURE/K

0   50   100   150   200

(b)

INTENSITY (arb.)

$2\theta = 5.7°$

(002)

(008)

(0010)

(0012)

MgO

$2\theta/°$

4   20   40   60

Fig.3 (a) R-T curve and (b) x-ray diffraction curve of a Bi-Sr-Ca-Cu-O film prepared by annealing at 1123K for 1 minute followed by heating at 1153K for 1 minute in air.

(a)

(b)

(c)

(d)

10μm

10μm
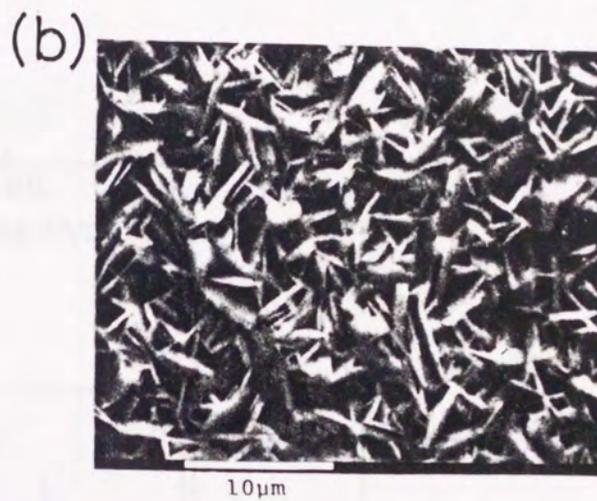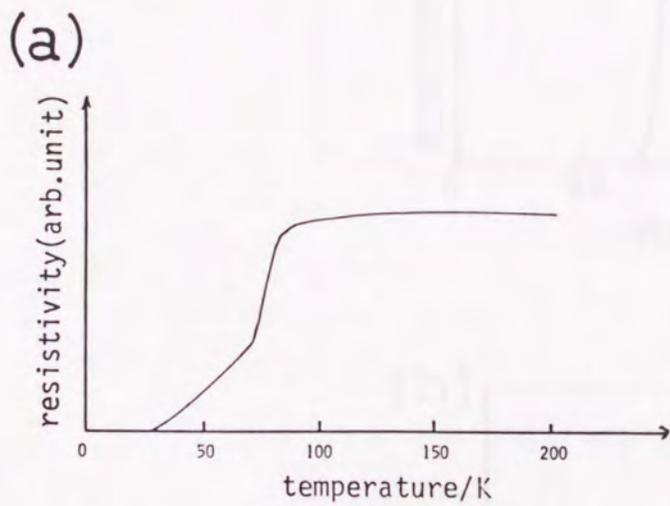
Fig.4 R-T curveas and SEM photographs of the films (a)(b) annealed at 1153K for 1 minute and (c)(d) heated at 1158K for 1 minute.
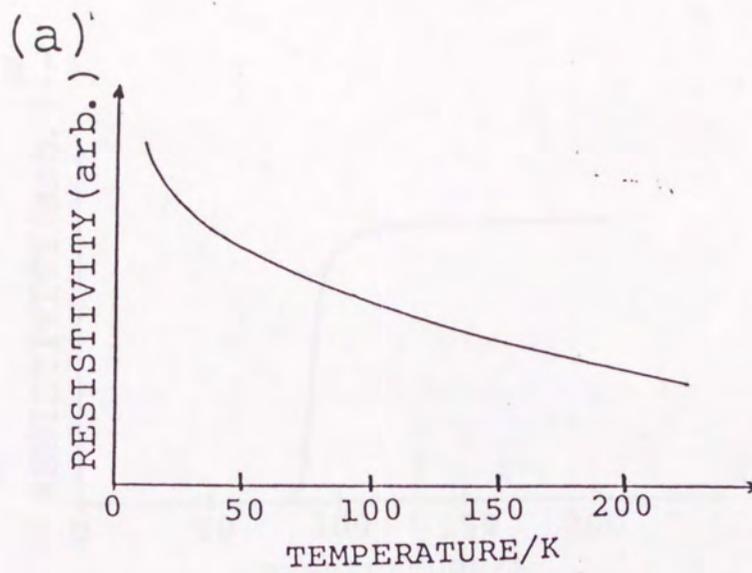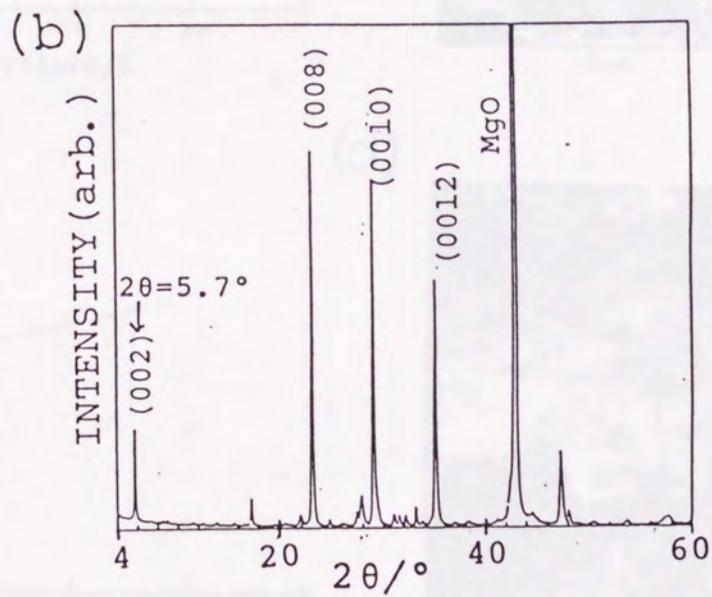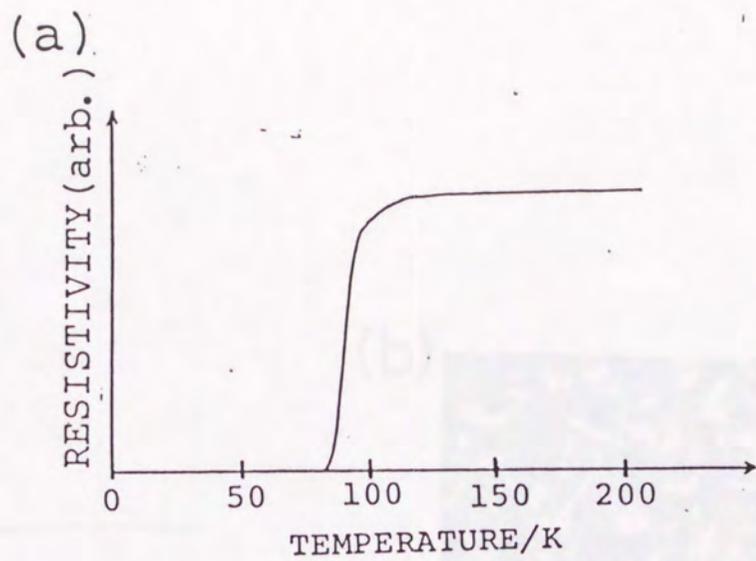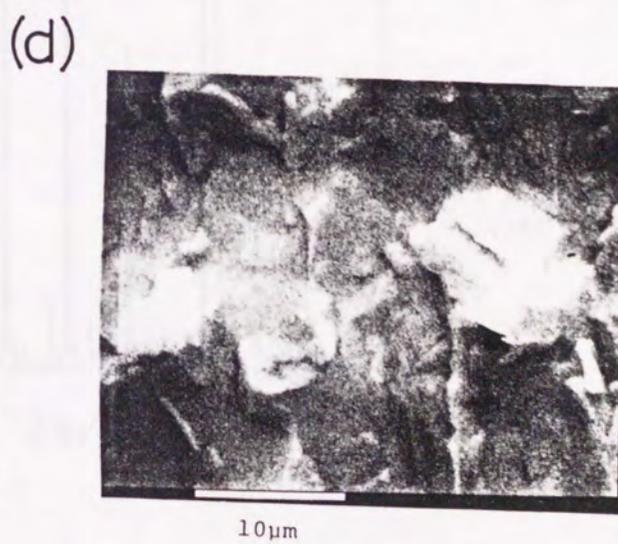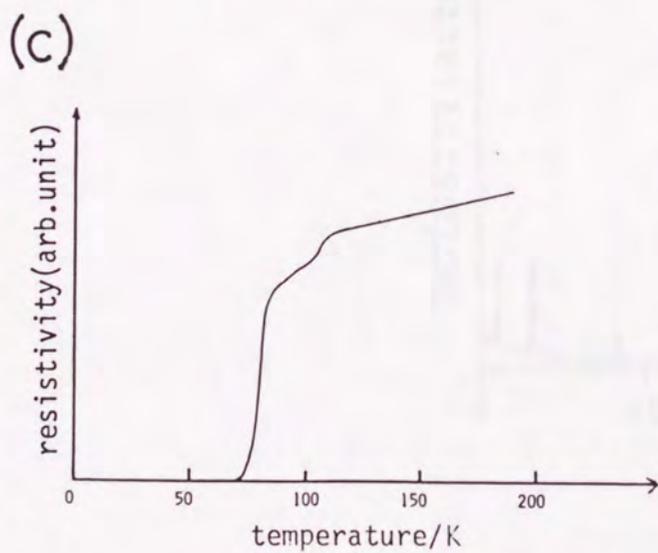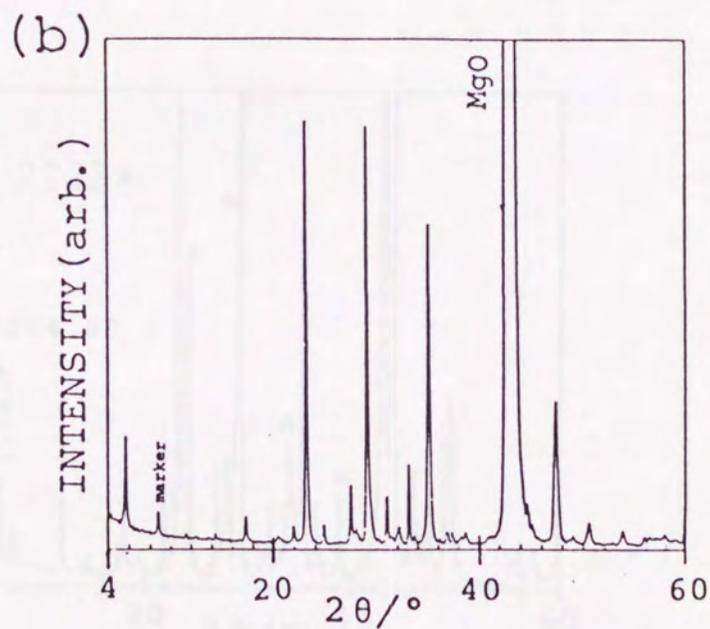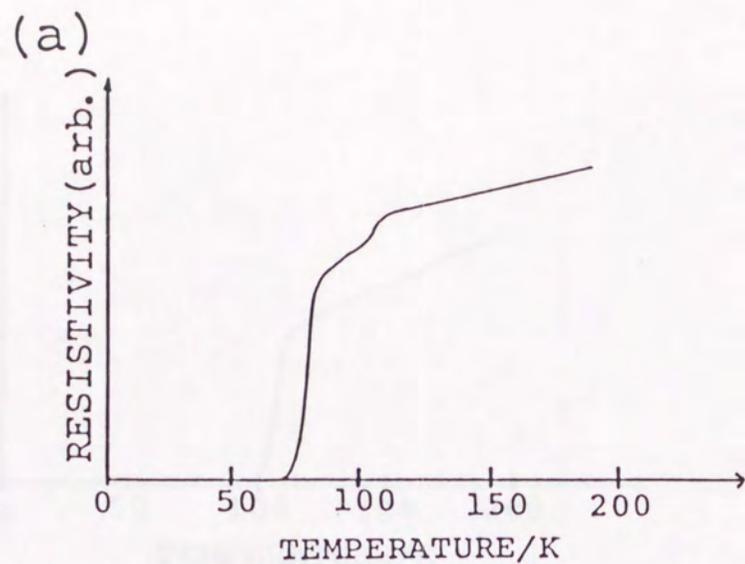
Fig.5   (a) R-T curve and (b) X-ray diffraction pattern of a Bi-
Sr-Ca-Cu-O film prepared by heating at 1158K for 1 minute in air.
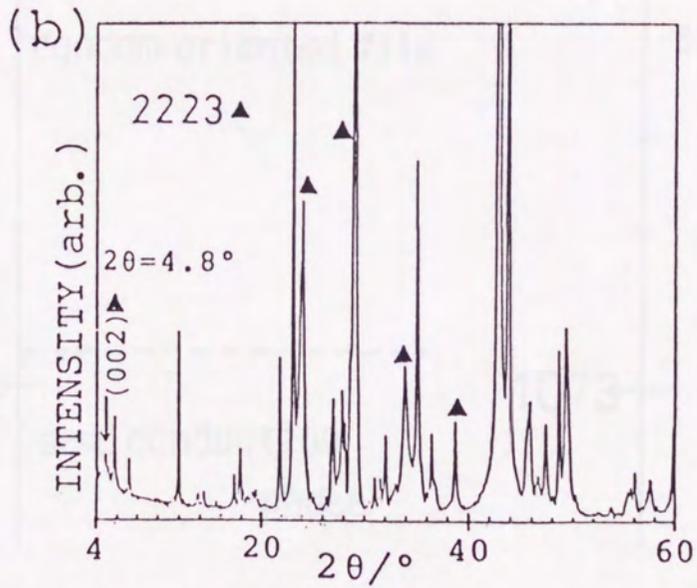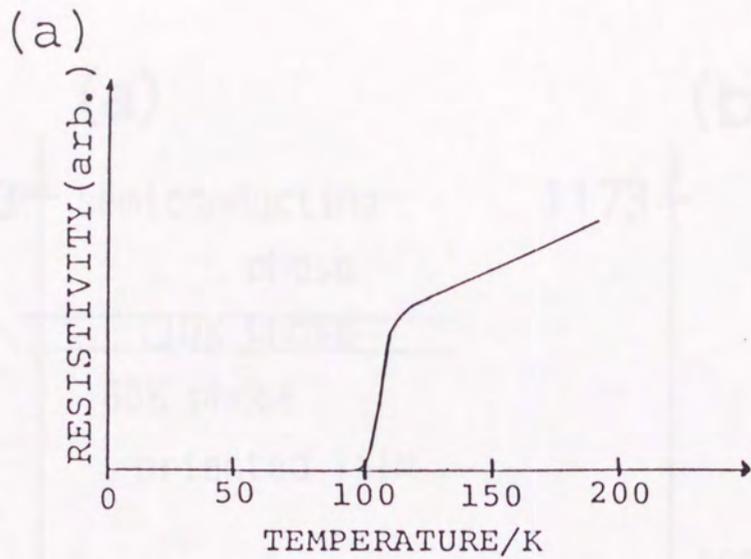
Fig.6 (a) R-T curve and (b) x-ray diffraction pattern of a Bi-Pb-Sr-Ca-Cu-O film prepared by heating at 1123K for 15 hours in air.

(a)

heating temperature/K

1173 — semiconducting phase

m.p. — 110K phase

80K phase

oriented film

- - - - - - - -

1123 — 80K phase

random oriented film

- - - - - - - -

1073 —

semiconducting phase

(b)

1173 —

semiconducting phase

1123 m.p. — 110K phase

80K phase

oriented film

1073 —
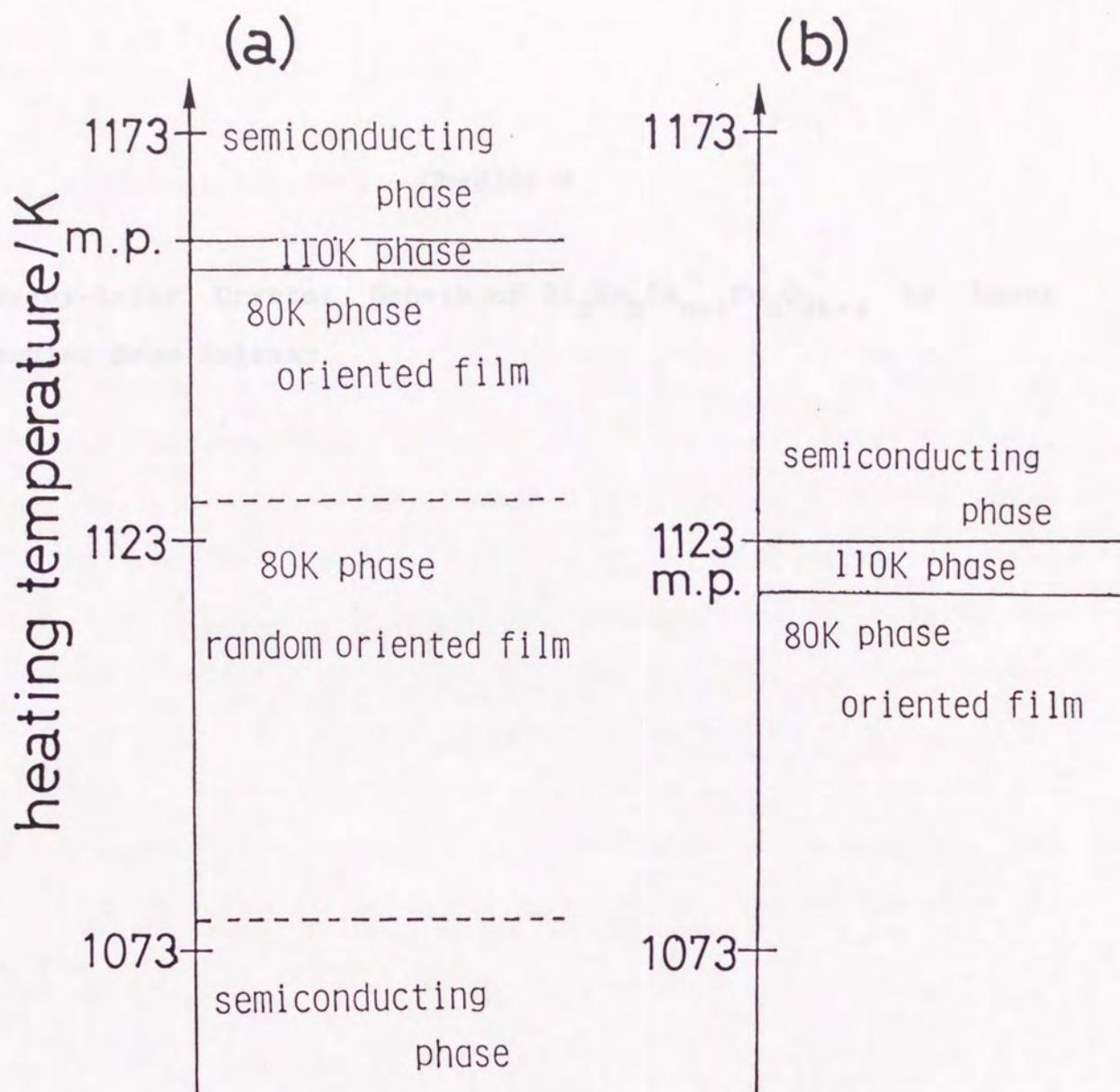
Fig.7 Relation between products and heating temperature for (a) $BiSrCaCuO_y$ and for (b) $Bi_{0.8}Pb_{0.2}SrCaCu_2O_y$.

Chapter 4

Layer-by-layer Crystal Growth of $Bi_2Sr_2Ca_{n-1}Cu_nO_{2n+4}$ by Laser Molecular Beam Epitaxy

Chapter 4-1:

Artificial Construction of $Bi_2Sr_2Ca_{n-1}Cu_nO_{2n+4}$ (n=1 to 10) and the Related Materials

Abstract

The phase control of $Bi_2Sr_2Ca_{n-1}Cu_nO_{2n+4}$ is performed by artificial construction of the structure by layer-by-layer deposition. At first, the epitaxial film of the parent material of the cuprate superconductors, which is $(Ca,Sr)CuO_2$, is formed. In next step, Bi_2O_2/Sr_2O_2 layer and the parent material layer are periodically stacked to form a $Bi_2Sr_2Ca_{n-1}Cu_nO_{2n+4}$ film. The epitaxial film of $(Ca,Sr)CuO_2$ can be grown on $SrTiO_3$ (100) substrate. The layer-by-layer stacking makes it possible not only to prepare the structure with different n separately, but also to grow the phase with n > 3, which can not be obtained in bulk samples.

Introduction

In Chapter 3-1, the phase control of Bi-Sr-Ca-Cu-O films by choosing the heat-treatment condition was described. This method, however, is the same way applied in bulk samples. Here, the phase control by the characteristic way of film samples, namely the control by layer-by-layer deposition is attempted. In this method, an artificial construction of the structure is performed by layer-by-layer stacking of some atomic or molecular layers according to the desired crystal structure.

The phases in Bi-Sr-Ca-Cu-O system can be represented by the chemical formula of $Bi_2Sr_2Ca_{n-1}Cu_nO_{2n+4}$, where n shows the number of CuO_2 planes between adjacent Bi_2O_2 layers. The crystal structures with n=1 to 5 are shown in Fig.1. Among these, only the phases with n=1,2,3 can be prepared in bulk samples. These materials have layer type crystal structures, in which simple metal-oxide layers such as BiO, SrO, CaO and CuO_2 layers are periodically stacked along the direction of c-axis as shown in Fig.1.[1] Thus, the synthesis of $Bi_2Sr_2Ca_{n-1}Cu_nO_{2n+4}$ by layer-by-layer stacking of these layers must be possible, and the film will be prepared with its c-axis oriented in perpendicular direction to the substrate surface.

It is well known that all the cuprate superconductors have two-dimensional CuO_2 planes in their crystal structures. The material with the simplest crystal structure including CuO_2 planes is $Ca_{0.86}Sr_{0.14}CuO_2$ discovered by Siegrist et al in 1988.[2] This has a oxygen-deficient simple perovskite structure which consists of two dimensional CuO_2 planes separated

63

by Ca(Sr) ions as shown in Fig.2. This material is a semiconductor, not a superconductor, and called "parent material" of cuprate superconductors in view of the crystal structure.

The structure of cuprate superconductors can be constructed by the periodic insertion of the layers, such as La_2O_2 and/or Bi_2O_2/Sr_2O_2, into the parent material. The insertion of $(La,Sr)_2O_2$ with rock-salt type structure forms the $La_{2-x}Sr_xCuO_4$ superconductor[3], BaO/CuO-chain makes $YBa_2Cu_3O_y$[4] and Bi_2O_2/Sr_2O_2 makes $Bi_2Sr_2Ca_{n-1}Cu_nO_{2n+4}$[1] [see Fig.3]. This is my guiding principle for layer-by-layer construction of their structures. Based on this concept, the preparation of $(Ca,Sr)CuO_2$ film has been tried at first, which is the most fundamental technique for the film formation of the cuprate superconductors by layer-by-layer construction.

For the construction of $Bi_2Sr_2Ca_{n-1}Cu_nO_{2n+4}$ by layer-by-layer stacking, an epitaxial growth of $(Ca,Sr)CuO_2$ with its c-axis perpendicular to the substrate surface is desirable. Therefore, a $(Ca,Sr)CuO_2$ thin film is prepared, and the orientation of the film is investigated at first. In next step, $Bi_2Sr_2Ca_{n-1}Cu_nO_{2n+4}$ thin films are constructed by the insertion of Bi_2O_2/Sr_2O_2 layer into the parent structure of $(Ca,Sr)CuO_2$. Furthermore, I have tried to control the number of CuO_2 planes (n) in this system by changing the periodicity of Bi_2O_2/Sr_2O_2 insertion.

Experimental

The films prepared by layer-by-layer stacking often have metastable structures. Such phases are decomposed into a thermodynamically stable structure with heat-treatment at high temperature, so the high-temperature annealing after the film deposition should be avoided in this experiment, namely as-grown films should be prepared. In this section, the as-grown films were prepared by laser ablation method under molecular beam epitaxial condition (called "laser MBE"). The molecular beam epitaxial condition means that the mean free paths of particles emitted from a target are much longer than the distance between the target and the substrate, namely the particles reach the substrate without a collision with the molecules of ambient gas. Of course, the pressure of oxidation gas must be low, thus NO_2 was used, which is effective for the preparation under low-pressure condition as described in Chapter 2. In this experiment, $1x10^{-3}$Pa of NO_2 was dosed during the deposition, where the mean free paths of atoms or ions are about $5x10^4$mm. This value is much longer than the distance between the target and the substrate ($1x10^2$mm).

The film growth under MBE condition has some advantages as follows.

1. Side reaction caused by the collision of atoms(ions) and gas molecules can be avoided,

2. Roughening of film surface caused by the oxidizing gas with high pressure can be avoided,

3. The surface of the growing film can be observed by in-situ

65

reflection high energy electron diffraction (RHEED).

For the epitaxial growth, the lattice constants of substrates should be close to those of the film, so $SrTiO_3$ (100) (Earth-Jewery, surface roughness < 0.5nm) was used as a substrate. The symmetry of the crystal structure of $(Ca,Sr)CuO_2$ is tetragonal, and the lattice constants a and c are 0.386nm and 0.320nm, respectively.[2] $SrTiO_3$ has a cubic structure with lattice constant of 0.391nm. The lattice mismatch between a-axis (and b-axis) of $(Ca,Sr)CuO_2$ and that of $SrTiO_3$ is about 1.3%. Furthermore, the $SrTiO_3$ has a perovskite structure, which is similar to that of $(Ca,Sr)CuO_2$, so $SrTiO_3$ must be proper as a substrate, and the epitaxial growth is expected. The apparatus for the laser MBE has been shown in Chapter 1. The film of $(Ca,Sr)CuO_2$ was prepared by the ablation of $Ca_{1-x}Sr_xCuO_y$ (x=0, 0.14, 0.3, 0.5) targets. For the $Bi_2Sr_2Ca_{n-1}Cu_nO_{2n+4}$ film, $Sr_{0.9}CuO_y$, $Ca_{0.86}Sr_{0.14}CuO_2$, Sr metal and Bi_2O_3 targets were used. The targets of Ca-Sr-Cu oxide were prepared by calcining the mixture of $CaCO_3$, $SrCO_3$ and CuO at 1173K for 6 hours. The chemical compositions of the targets represented here are the mixing ratios of the starting materials.

Before the film growth, $SrTiO_3$ substrate was cleaned by heating it in 5×10^{-4} Pa of NO_2 at 923K for 20 minutes to remove the carbon contamination on the surface. On the cleaned surface, the films were prepared by laser MBE method at the substrate temperature of 873K or 923K under 1×10^{-3} Pa of NO_2. $Bi_2Sr_2Ca_{n-1}Cu_nO_{2n+4}$ was prepared by the successive ablation of

four kinds of targets. $Sr_{0.9}CuO_y$ target was used for the formation of SrO/CuO_2 layer, $(Ca,Sr)CuO_2$ target for $Ca(Sr)/CuO_2$ layer, Sr target for SrO layer and Bi_2O_3 target for Bi_2O_2 layer. This was 1 cycle for the layer-by-layer stacking, and it is corresponding to half thickness of the unit-cell of $Bi_2Sr_2Ca_{n1}$-Cu_nO_{2n+4} [see Fig.1 and Fig.4]. The number of CuO_2 plane (n) in this system was controlled by the changing the deposition thickness of $Ca(Sr)/CuO_2$ layer in the one cycle. The cycle of the successive deposition was repeated to form the film. Typical thickness of the film was 60nm. The profile of the layer-by-layer construction by the successive ablation is shown in Fig.4.

During the film growth, the film surface was investigated by in-situ RHEED observation with acceleration voltage of 15kV (Physitec, RHG-1000). The formation process was controlled by a computer system (NEC PC-9801F). In the preparation of $Bi_2Sr_2Ca_{n-1}Cu_nO_{2n+4}$ by the successive ablation, the replacement of the targets was carried out using a pulse motor with feedback from the film thickness monitor with quartz oscillator (Inficon, XTC deposition monitor) and variation of the RHEED signal intensity. The structures of the films were investigated using RHEED and x-ray diffraction (XRD).

67

Results and Discussion

Figs 5(a) and 5(b) show the RHEED pattern of the SrTiO$_3$ (100) and that of the as-grown film formed on the substrate by the ablation of Ca$_{0.86}$Sr$_{0.14}$CuO$_2$ target. The streak pattern of RHEED indicates the epitaxial growth of the film with smooth surface, because random oriented film should have a ring-like pattern or rough surface makes the pattern spotty [refer Appendix A]. The x-ray diffraction pattern of the same film is shown in Fig.6. The pattern has only (001) diffraction peaks of the parent material without peaks attributed to other phases. These patterns show the single-phase film of (Ca,Sr)CuO$_2$ could be grown with the epitaxial direction which I expected.

The XRD patterns of Ca$_{1-x}$Sr$_x$CuO$_2$ with x=0, 0.14, 0.3 and 0.5 are shown in Fig.7. The thicknesses of these films were about 6nm, which is thinner than that of the film in Fig.6 (50nm), so the diffraction peaks in Fig.7 became weaker than those in Fig.6. The patterns indicate that these films had the same crystal structure with the parent material. The RHEED patterns were also similar. Thus, the parent structure can be grown in wider range of Sr concentration from x=0 to 0.5 in the thin films, while the structure can be formed only within the very narrow range of chemical composition near Ca$_{0.86}$Sr$_{0.14}$CuO$_2$ in bulk samples.[2] This result must be the effect of the substrate, namely the epitaxial growth on the SrTiO$_3$ substrate forces to form the structure of the parent material, because the crystal structure of the parent material is so similar to that of SrTiO$_3$.

Though the thin films of Ca$_{1-x}$Sr$_x$CuO$_2$ with x=0 to 0.5 had

68

the same crystal structure, the crystallinity and the morphology of the films were slightly changed with the variation of the Sr concentration. In lower Sr concentration, the streaks in the RHEED pattern had light and shaded parts, and the widths of the streaks were wider. With increase of Sr, the streaks became sharper, and the intensity distribution became homogenous. This variation indicates that crystallinity and smoothness of the films are improved with the increase of Sr concentration. The x-ray diffraction patterns, on the other hand, show that the film with such a high strontium concentration of x=0.5 contains a little amount of other phases [see Fig.7(d)]. These behaviors can be explained by two factors. One is the matching of the lattice constants between the film and the substrate, and the other is the charge balance of the substance during the film growth. According to the investigation in the bulk $Ca_{0.86}Sr_{0.14}CuO_2$, the lattice constant a (a=0.386nm) is slightly smaller than that of the $SrTiO_3$ substrate (a=0.391nm).[2] Thus, the lattice matching should be improved by the substitution of larger Sr ion for smaller Ca. This effect may result in the improvement of crystallinity and smoothness of the films. A high concentration of Sr, however, promotes the inclusion of excess oxygen at the normally deficient oxygen-site, because larger Sr ion occupies a cation site coordinated by 12 oxygens. Since too much oxygen breaks the charge balance in the system, high Sr concentration leads to the instability of the parent structure resulting in the formation of other phases. In this manner, appropriate Sr concentration is determined by the lattice

matching and the charge balance. Under our experimental condition, optimum Sr concentration ranges from 10 to 20% of Ca, that is $Ca_{1-x}Sr_xCuO_2$ with x=0.1 to 0.2.

Based on the technique of $(Ca,Sr)CuO_2$ formation, Bi_2Sr_2-$Ca_{n-1}Cu_nO_{2n+4}$ thin films were grown by successive ablation of $SrCuO_y$, $(Ca,Sr)CuO_2$, Sr metal and Bi_2O_3 targets. Fig.8 shows the x-ray diffraction patterns of the $Bi_2Sr_2Ca_{n-1}Cu_nO_{2n+4}$ films with changing the thickness of $Ca(Sr)/CuO_2$ layer in one cycle of the deposition. When the film was formed from three targets of $SrCuO_y$, Sr and Bi_2O_3 without $(Ca,Sr)CuO_2$, the film had the XRD pattern of $Bi_2Sr_2CuO_6$ structure including single CuO_2 plane (n=1), which is shown in Fig.8(a). The film was oriented with its c-axis perpendicular to the substrate surface and had the lattice constant c of 2.44nm. By the insertion of $(Ca)Sr/CuO_2$ layer using $(Ca,Sr)CuO_2$ target, the structure was changed to $Bi_2Sr_2CaCu_2O_8$ (n=2) with c-axis of 3.06nm [see Fig.8(b)]. Furthermore, the increase of the thickness of $Ca(Sr)/CuO_2$ made the $Bi_2Sr_2Ca_2Cu_3O_{10}$ (n=3) film, whose c-axis was 3.73nm as shown in Fig.8(c). The phases with n > 3 can not be obtained in bulk samples, whereas the layer-by-layer deposition method makes the growth of such phases possible. The diffraction patterns in Figs.8(d) and 8(e) show that the Bi-Sr-Ca-Cu-O films with lattice constants of 4.35nm and 5.00nm were formed. These values correspond to the lattice constants c of the $Bi_2Sr_2Ca_{n-1}Cu_nO_{2n+4}$ structure including four and five CuO_2 layers (n=4 and 5), respectively. In order to make sure that the films have the structures with four and five CuO_2 planes, I have assumed the ideal structures of these phases [see Figs.1(d) and 1(e)] and

70

calculated the x-ray diffraction intensities of (001) peaks of these structures. The equation for the calculation of x-ray diffraction intensities has been described in Chapter 3-1 [see Chapter 3, eq(1)].[5,6] The XRD pattern and calculated result for n=5 are shown in Fig.9. The good agreement indicates that the structures with n=5, which can not be obtained in bulk samples, could be actually grown. Using the layer-by-layer deposition technique, I have succeeded in the formation of $Bi_2Sr_2Ca_{n-1}Cu_nO_{2n+4}$ with n up to 10, and among them, the structures with n > 3 are new materials. The XRD pattern and the calculated diffraction pattern of $Bi_2Sr_2Ca_9Cu_{10}O_{24}$ with n=10 are shown in Fig.10.

Fig.11 shows the RHEED pattern of $Bi_2Sr_2CaCu_2O_8$ film formed by layer-by-layer deposition. This is the pattern of the surface just after the deposition of Bi_2O_2 layer. The streak pattern indicates that the film was epitaxially grown and the surface had a good smoothness. Along (010) direction, which is corresponding to the (110) direction of $(Ca,Sr)CuO_2$ or $SrTiO_3$, a superstructure due to an incommensurate modulation could be observed.[7,8] The period of the modulation is about 4.7 times of b-axis, which is the same value observed in bulk samples. If the film is single crystal, the superstructure appears along only b-axis. In this film, however, the same superstructure appeared when the sample was rotated in 90 degrees. This result shows that the film have a twin structure. The RHEED pattern hardly changed with the variation of number of CuO_2 planes (n) in $Bi_2Sr_2Ca_{n-1}Cu_nO_{2n+4}$.

When the $Bi_2Sr_2Ca_{n-1}Cu_nO_{2n+4}$ films with n > 3 were annealed

71

at temperature above 923K after the growth, the structures decomposed into $Bi_2Sr_2CaCu_2O_8$ with n=2, namely such crystal structures must be unstable at high temperature. In practice, the phases with n > 3 can not be formed in bulk samples at present. The reason for the growth of the metastable phases in the as-grown films would be that the layer-by-layer stacking forced the films to have such crystal structures. In addition, relatively low substrate temperature suppressed the diffusion of elements which make a thermodynamically stable structure. Furthermore, the growth under the condition where the parent material can be formed was also important for the formation of the metastable phases with larger n. The structure of the parent material of $(Ca,Sr)CuO_2$ consists of infinite CuO_2 planes. Thus, if the parent structure can be grown, the structure $Bi_2Sr_2Ca_{n-1}Cu_nO_{2n+4}$ with any n can be prepared in principle. Actually, it was very difficult to form the structure with larger n under the condition where the parent structure was not grown.

For the growth of $Bi_2Sr_2Ca_{n-1}Cu_nO_{2n+4}$ by this method, it is very important to control the deposition thickness of each layer in layer-by-layer stacking strictly. If not so, the other phases were formed instead of the desired structure, and sometimes the film became amorphous. The thickness of each layer, however, was very thin (a few angstrom for one layer), so the control was not so easy. In my experiment, the thickness was controlled using the oscillation of RHEED intensity observed during the growth. Since one oscillation of the intensity is corresponding to the formation of one layer, the thickness can be controlled by this technique strictly (see Appendix A). The variation of the RHEED

72

intensity is strongly related to the growth mechanism of the film, so the details of the intensity oscillation and the thickness control using the oscillation are discussed in following Chapter 4-2, in connection with the growth mechanism of the film.

73

Conclusion

The epitaxial film of the parent material of cuprate superconductors, $Ca_{1-x}Sr_xCuO_2$, was grown on $SrTiO_3$ (100) substrate. The range of Sr concentration where the parent structure could be made was x=0 to 0.5, and it is much larger than that for bulk samples. The variation of the crystallinity and the morphology with the change of Sr concentration can be explained by two factors, which are the lattice matching and the charge balance. Based on the technique of $(Ca,Sr)CuO_2$ formation, $Bi_2Sr_2Ca_{n-1}Cu_nO_{2n+4}$ films were prepared by layer-by-layer stacking. This method makes it possible not only to form the structure with different number of CuO_2 planes (n) separately, but also to grow the structures with n > 3, which can not be obtained in bulk samples.

References

(1)   J.Akimitsu,   A.Yamazaki,   H.Sawa   and   H.Fujiki, Jpn.J.Appl.Phys., 26, L736 (1987).

(2) T.Siegrist, S.M.Zahurak, D.W.Murphy and R.S.Roth, Nature, 334, 231 (1988).

(3)   H.Takagi,   S.Uchida,   K.Kitazawa   and   S.Tanaka, Jpn.J.Appl.Phys., 26, L123 (1987).

(4)   M.A.Beno,   L.Sonderholm,   B.W.Capone,   B.G.Hinks, J.D.Jorgensen, I.K.Schuller, C.U.Segre, K.Zuang and J.D.Grace, Appl.Phys.Lett., 51, 57 (1987).

(5) K.Imai,   I.Nakai,   T.Kawashima,   S.Sueno   and   A.Ono, Jpn.J.Appl.Phys., 27, L1661 (1988).

(6) C.C.Torardi, J.B.Parise, M.A.Subramanian, J.Goparakrishnan and A.W.Sleight, Physica C, 157, 115 (1989).

(7)   T.Onozuka,   T.Kajitani,   M.Hirabayashi,   H.Sato   and T.E.Mitchell, Jpn.J.Appl.Phys., 28, L1775 (1989).

(8) Y.Hirotsu, O.Tomioka, N.Yamamoto, Y.Nakamura, S.Nagakura, Y.Iwai and M.Takata, Jpn.J.Appl.Phys., 28, L1783 (1989).
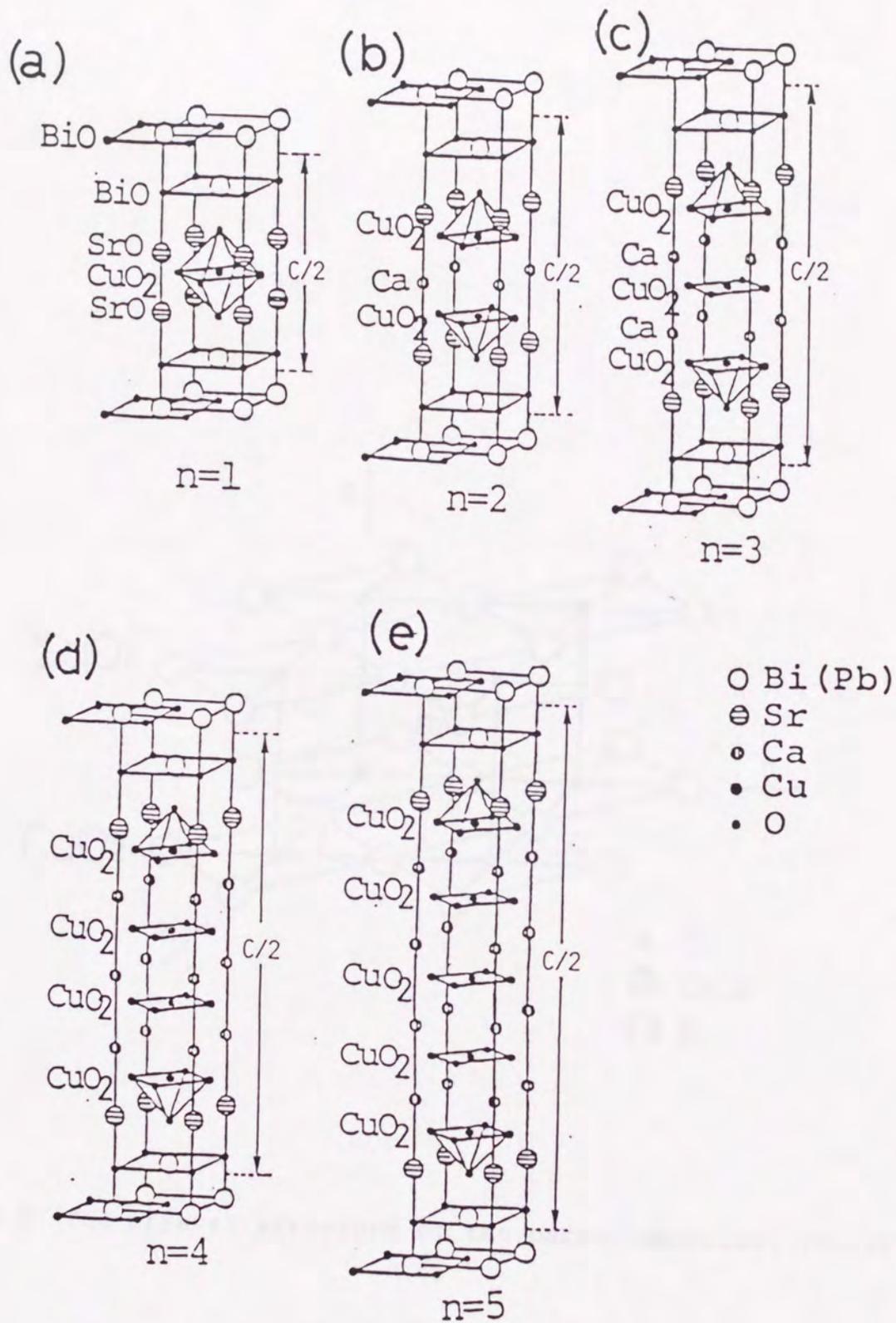
Fig.1 The crystal structures of $Bi_2Sr_2Ca_{n-1}Cu_nO_{2n+4}$ with (a) n=1, (b) n=2, (c) n=3, (d) n=4 and (e) n=5.
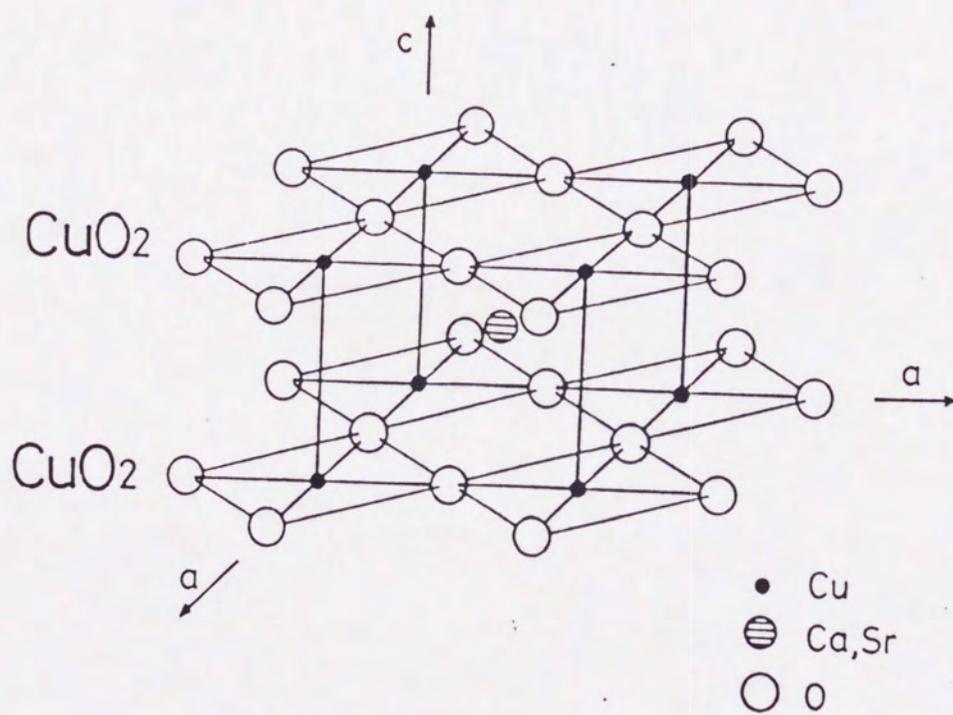
CuO₂

CuO₂

Fig.2   The crystal structure of the parent material, (Ca,Sr)CuO₂.

$(Ca,Sr)CuO_2$

$Bi_2Sr_2Ca_{n-1}Cu_nO_{2n+4}$
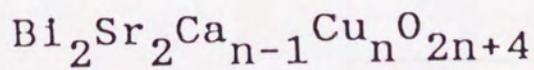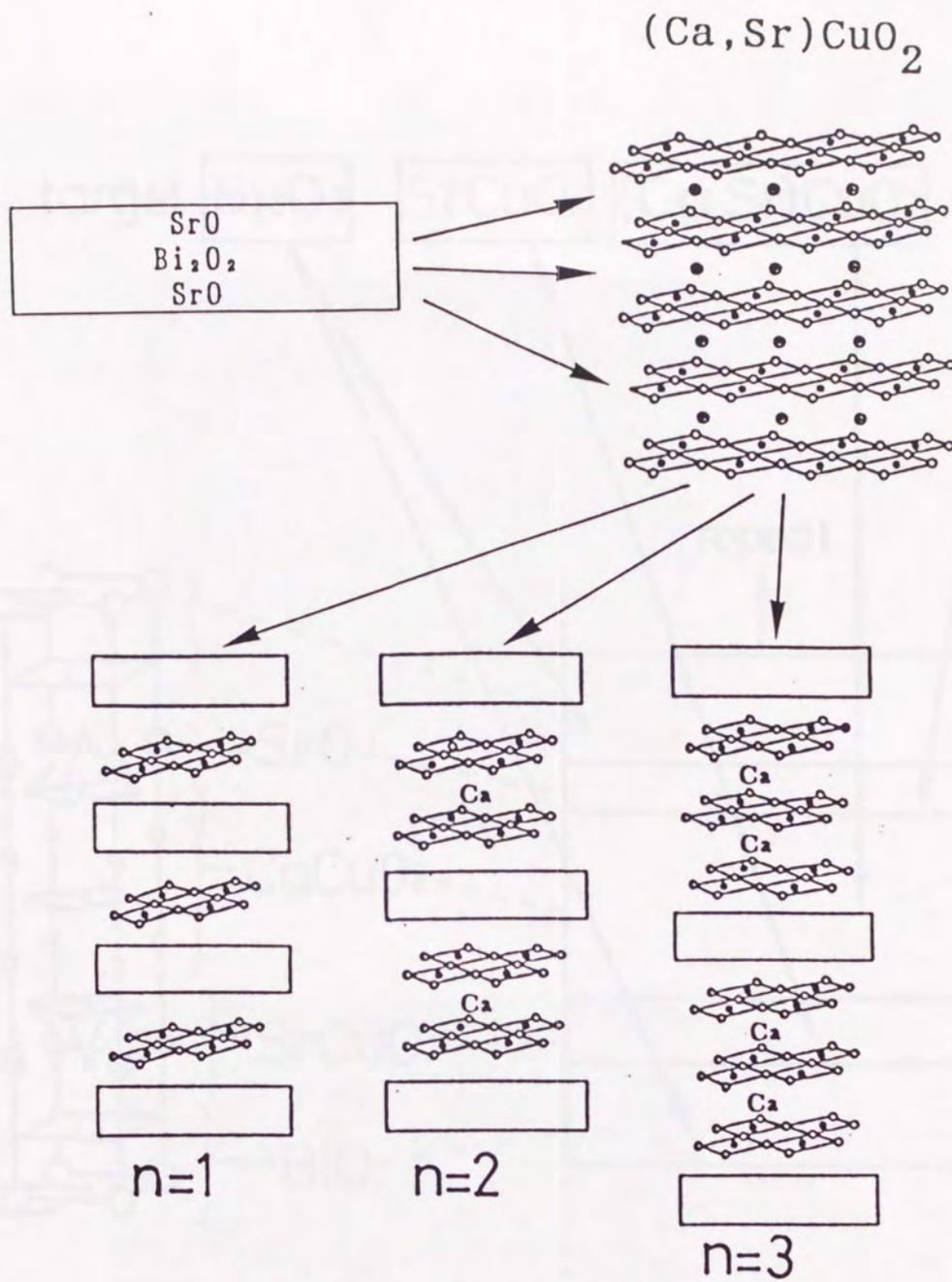
Fig.3 Basic concept of the layer-by-layer construction of $Bi_2Sr_2Ca_{n-1}Cu_nO_{2n+4}$ structure.
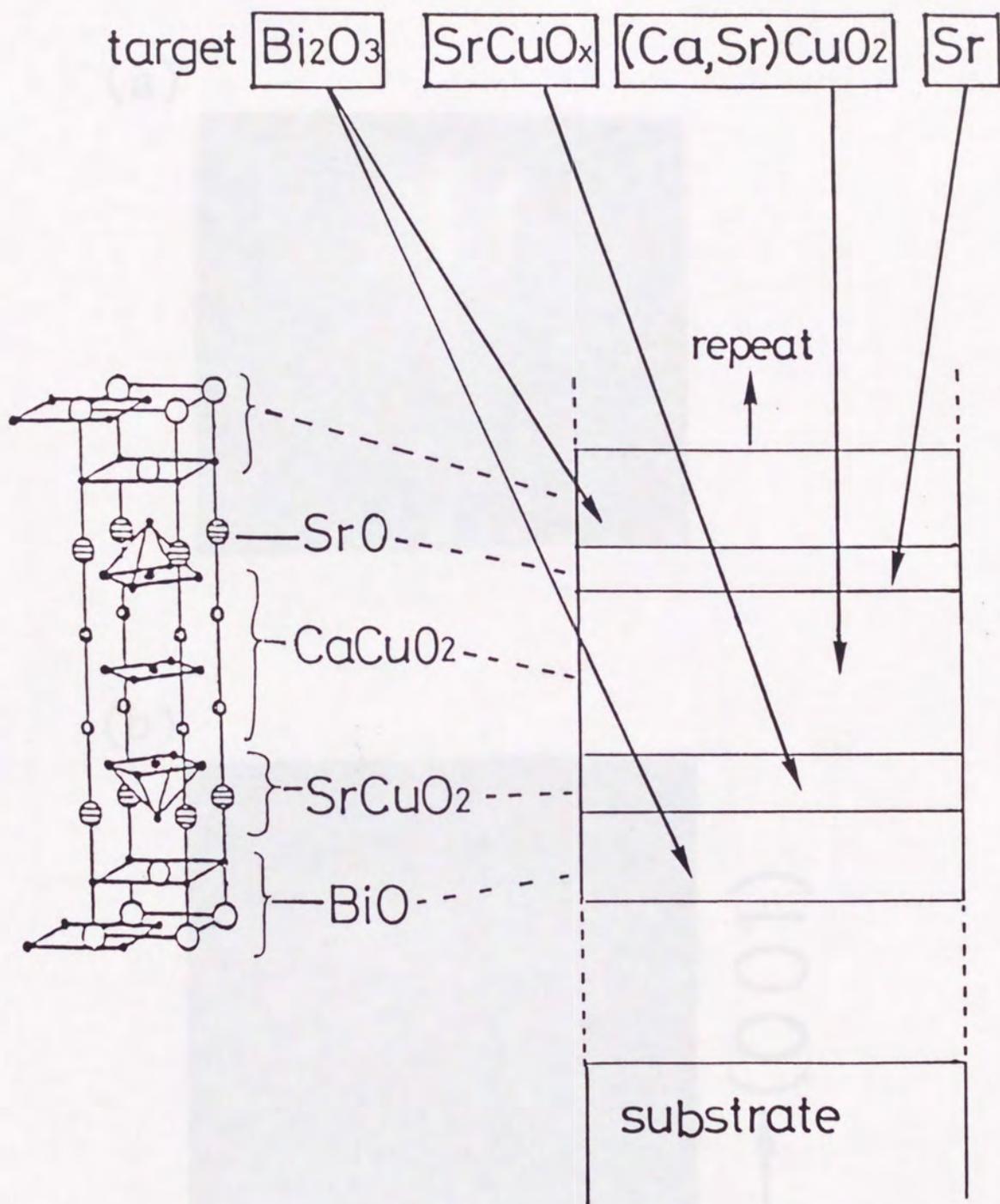
Fig.4   The profile of the layer-by-layer construction   of
$Bi_2Sr_2Ca_{n-1}Cu_nO_{2n+4}$ structure.

(a)

(b)
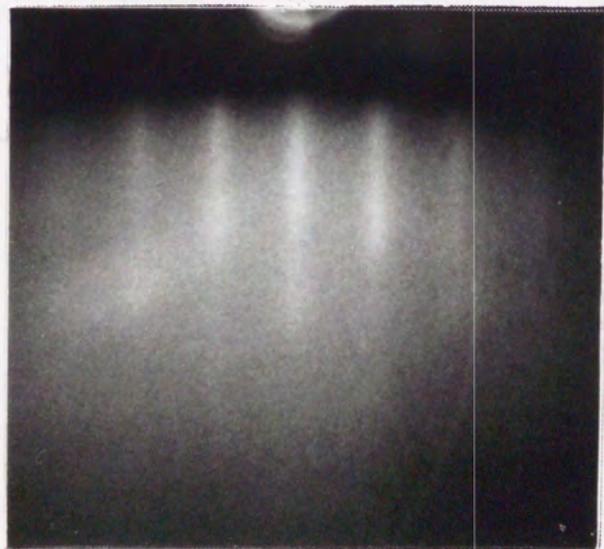
(001)

(100)

Fig.5 RHEED patterns for (a) $SrTiO_3$ (100) substrate and (b) as-grown $Ca_{0.86}Sr_{0.14}CuO_2$ films.

Fig.6   X-ray   diffraction pattern of   as-grown $Ca_{0.86}Sr_{0.14}CuO_2$
film.
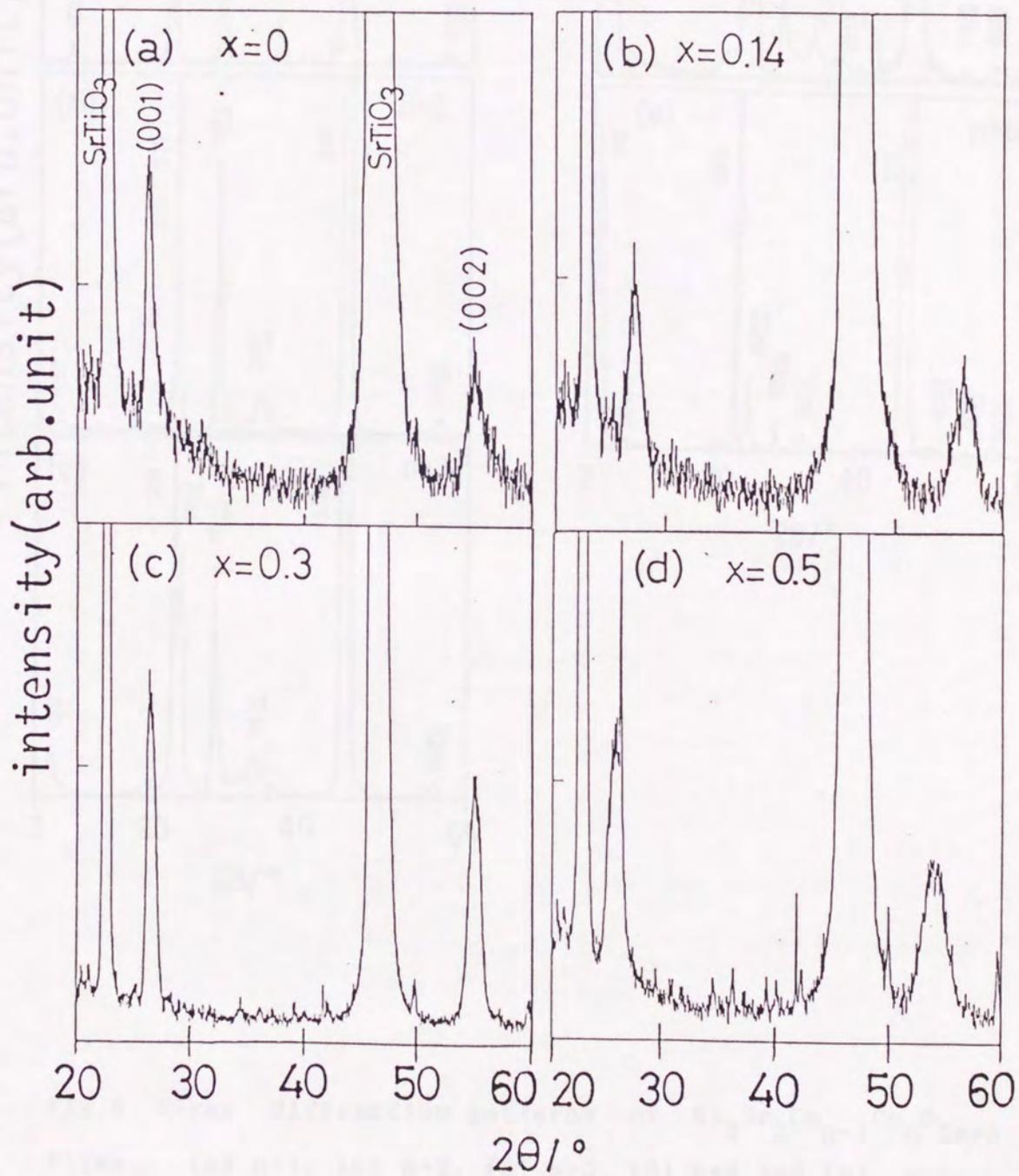
Fig.7 X-ray diffraction patterns of $Ca_{1-x}Sr_xCuO_2$ thin films with
(a) x=0, (b) x=0.14, (c) x=0.3 and (d) x=0.5.
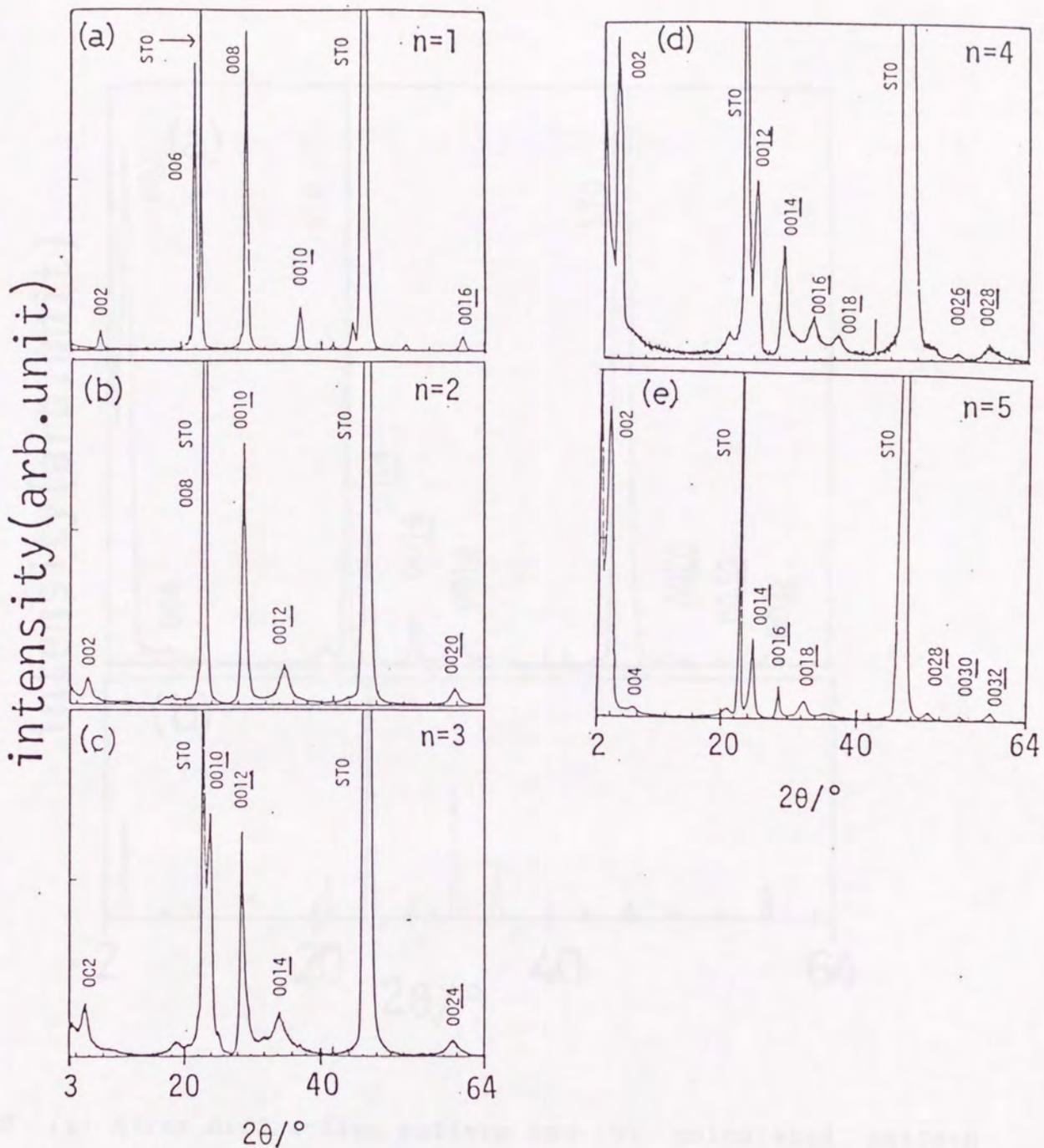
Fig.8 X-ray diffraction patterns of $Bi_2Sr_2Ca_{n-1}Cu_nO_{2n+4}$ thin
films.   (a) n=1, (b) n=2, (c) n=3, (d) n=4 and (e) n=5.   "STO"
shows the diffraction peaks of $SrTiO_3$ substrate.
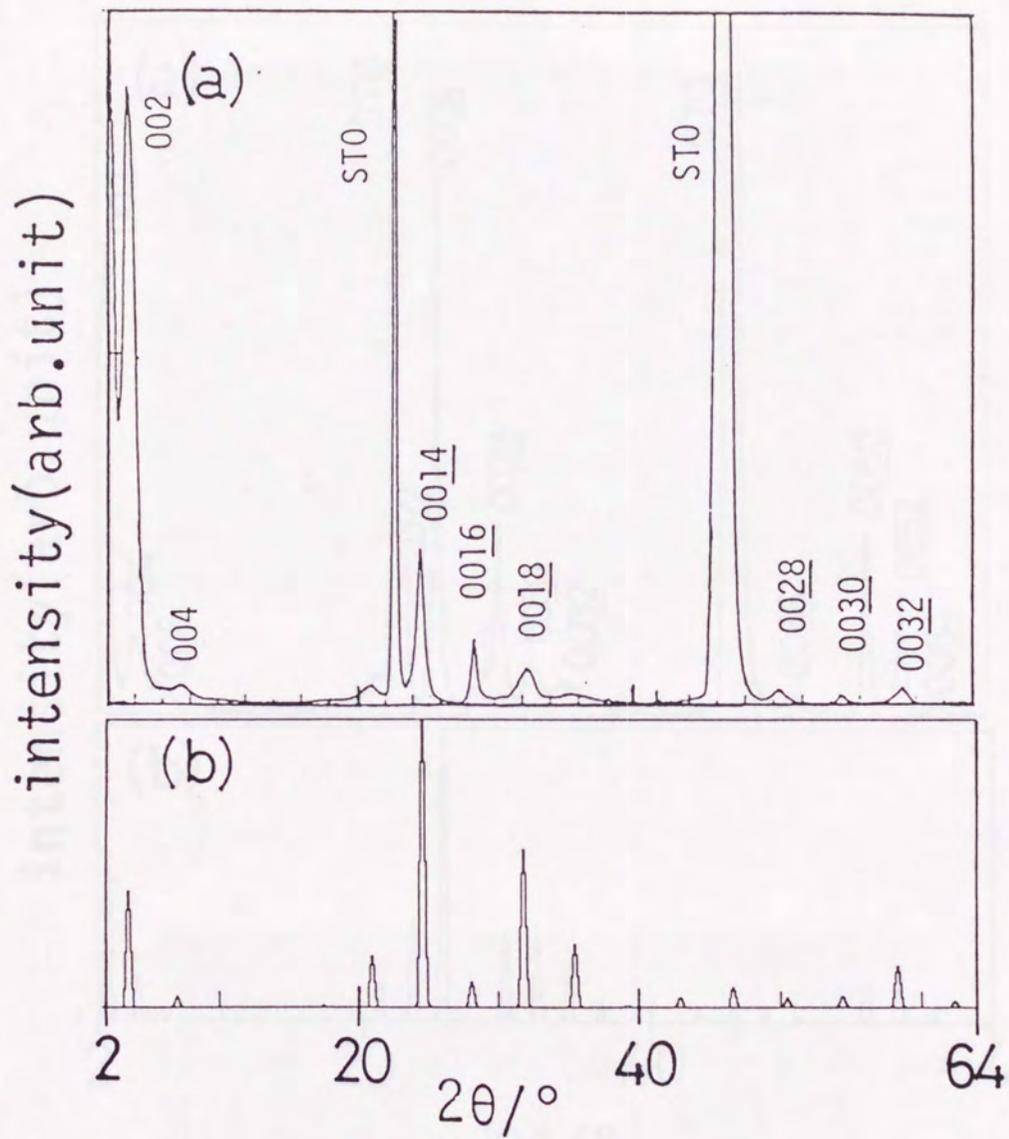
Fig.9 (a) X-ray diffraction pattern and (b) calculated pattern for $Bi_2Sr_2Ca_4Cu_5O_{14}$ with n=5. "STO" shows the diffraction peaks of $SrTiO_3$ substrate.
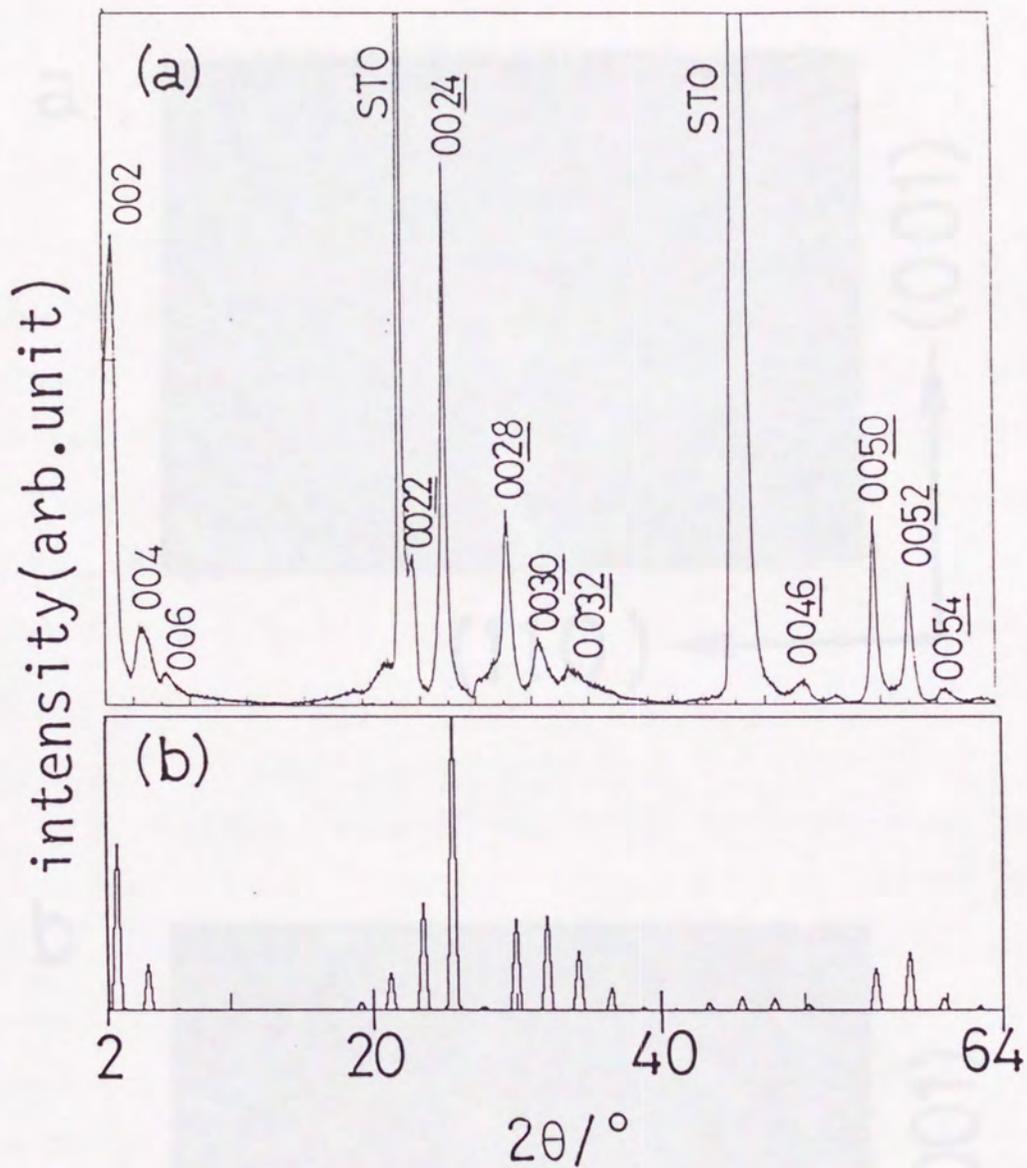
Fig.10 (a) X-ray diffraction pattern and (b) calculated pattern for $Bi_2Sr_2Ca_9Cu_{10}O_{24}$ with n=10. "STO" shows the diffraction peaks of $SrTiO_3$ substrate.

a

(001)

(110)

b

(001)

(010)
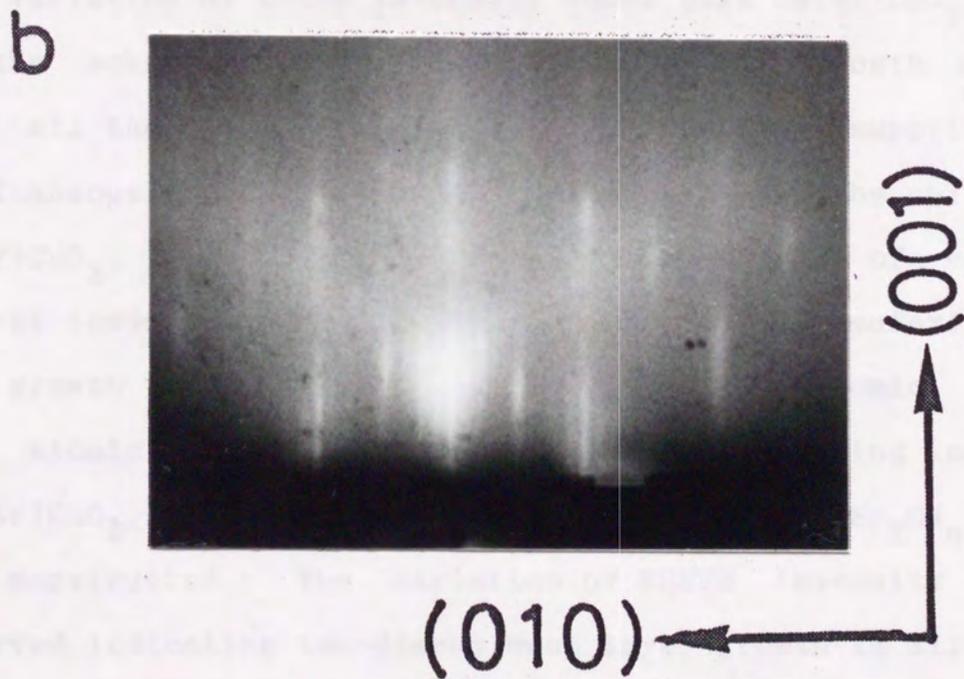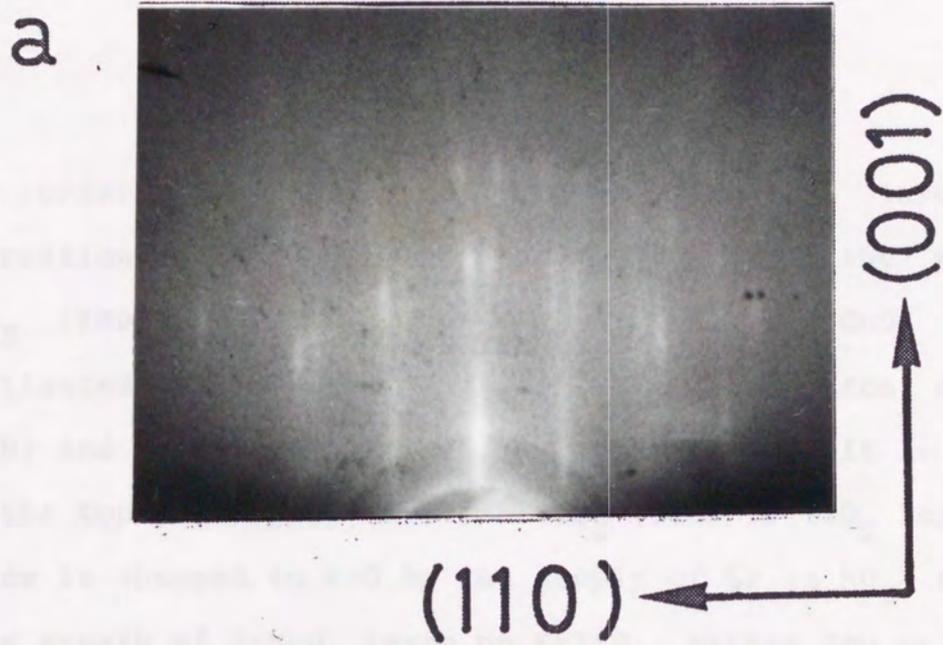
Fig.11   RHEED patterns after Bi_2O_2 deposition in layer-by-layer formation of $Bi_2Sr_2CaCu_2O_8$.

Chapter 4-2:

Layer-by-Layer Growth Mechanism of $Bi_2Sr_2Ca_{n-1}Cu_nO_{2n+4}$ and the Related Materials

Abstract

In order to study the growth mechanism in layer-by-layer construction of $Bi_2Sr_2Ca_{n-1}Cu_nO_{2n+4}$ thin films, the surface of $SrTiO_3$ (100) substrate and the growth of $Ca(Sr)CuO_2$ have been investigated using reflection high energy electron diffraction (RHEED) and Auger electron spectroscopy (AES). It is confirmed that the topmost of the native $SrTiO_3$ (100) is TiO_2 layer and the surface is changed to SrO by the supply of Sr in NO_2 atmosphere. In the growth of $SrCuO_x$ layer on $SrTiO_3$, either SrO or CuO_2 layer becomes surface layer depending upon the composition of the substrate surface, when Sr and Cu are supplied simultaneously. The variation of RHEED intensity shows that $Ca(Sr)CuO_2$ is grown on the substrate with two dimensional layer growth mechanism. When all the metal elements, Ca(Sr) and Cu, are supplied in NO_2 simultaneously, the unit of the layer growth is the unit-cell of $Ca(Sr)CuO_2$. Furthermore, the successive supply of each metal element leads to one atomic-layer growth of this material, namely the growth unit can be separated into Ca(Sr) atomic layer and CuO_2 atomic layer. By the layer-by-layer stacking of $SrCuO_x$, $(Ca,Sr)CuO_2$, SrO and Bi_2O_2, the structures of $Bi_2Sr_2Ca_{n-1}Cu_nO_{2n+4}$ are constructed. The variation of RHEED intensity is also observed indicating two-dimensional layer growth in all the steps of layer-by-layer stacking. Using the intensity variation, the

thickness of each layer is controlled within the monolayer accuracy.

Introduction

The structures of $Bi_2Sr_2Ca_{n-1}Cu_nO_{2n+4}$ with desired n value have been constructed by the insertion of Bi_2O_2/Sr_2O_2 layer into the parent structure of $(Ca,Sr)CuO_2$ using the layer-by-layer deposition technique. However, the problem remains whether the structure is really constructed with layer-by-layer growth mechanism, even if the final product is $Bi_2Sr_2Ca_{n-1}Cu_nO_{2n+4}$. For the real layer-by-layer construction of desired structures, the control of the surface atomic layer during the layer-by-layer growth must be essential. In order to achieve the atomic layer control, the initial stage of the growth, such as the substrate surface and the first deposited layer just on the substrate, are definitely important.

In this section, the growth mechanisms of $(Ca,Sr)CuO_2$ and $Bi_2Sr_2Ca_{n-1}Cu_nO_{2n+4}$ formed by layer-by-layer stacking were studied. Furthermore, the initial stage of the growth, which is the surface of $SrTiO_3$ (100) substrate or the growth of $SrCuO_x$ layer just on the substrate, has been investigated, and the control of the surface layer in $SrCuO_x$ has been tried. Here, the growth mechanism of the film has been investigated using reflection high energy electron diffraction (RHEED) and Auger electron spectroscopy (AES). In addition, the control of the layer-by-layer deposition process using RHEED intensity is described. This technique makes it possible to control the thickness of each layer in atomic layer scale.

Experimental

Details of the film formation have been described in Chapter 4-1. The targets of $Ca_{0.86}Sr_{0.14}CuO_2$, $Sr_{0.9}CuO_x$, Sr metal, Bi_2O_3, Cu metal and TiO_2 (Katayama, 99.9%) were used, and the substrates were $SrTiO_3$ (100). The surface of the film was investigated using in-situ RHEED observation (Physitec, RHG-1000) and Auger electron spectroscopy (ULVAC ULA-1000 controller, and ULVAC-PHI Model 10-120 LEED-Auger unit). The experimental apparatus has been shown in Chapter 1.

The RHEED pattern was observed with acceleration voltage of 15kV. During the film growth, the RHEED pattern was taken by a CCD camera (Hamamatsu C3077) and recorded by a VTR (Sony EDV-6000). The RHEED image was digitized and analyzed by a microcomputer (NEC PC-9801ES).

The AES unit was attached to the same vacuum chamber, so I could obtain the Auger spectra without the exposure of the films to air. The energy of incident electron for AES measurement was 2kV, and the spectra were obtained using lock-in amplifier (NF Electronic, 5600A).

The substrate surfaces were cleaned by heating them in 5×10^{-4} Pa of NO_2 at 923K. After the annealing, the Auger signal of carbon (271eV) was not detected on the surface, and the signals of Ti, Sr and O were observed. At first, the films of the parent material were prepared by the ablation of $Ca_{0.86}Sr_{0.14}CuO_2$ target or the successive ablation of Ca(Sr) and Cu, and the growths were studied. By the application of the observed growth process in the formation of $(Ca,Sr)CuO_2$, some surfaces were

79

formed on the substrate by the ablation of Sr and TiO_2 targets. The prepared surfaces were compared in order to investigate the substrate surface. Furthermore, $SrCuO_x$ layer and $Bi_2Sr_2Ca_{n-1}Cu_nO_{2n+4}$ film were formed, and the growth was investigated.

The films were prepared in 1×10^{-3} Pa of NO_2. The substrate temperature was between 873K and 923K. X-ray diffraction (XRD) patterns were obtained using CuK_α with $\theta - 2\theta$ scanning.

Result and Discussion

At first, the parent material was prepared by the ablation of $Ca_{0.86}Sr_{0.14}CuO_2$ target, and the growth mechanism with simultaneous supply of all elements was studied. Fig.1 (a) shows the variation of RHEED intensity in specular reflection area during the film growth. The oscillation of RHEED intensity can be observed during the preparation of $(Ca,Sr)CuO_2$.

The oscillation of RHEED intensity has been observed in the growth of semiconductors, such as GaAs[1,2], and it is well known that the oscillation is the intrinsic phenomenon accompanied by two-dimensional layer growth mechanism[3,4] (refer Appendix A). The clear oscillation in Fig.1(a) indicates that the parent material of $(Ca,Sr)CuO_2$ can be grown with two-dimensional layer growth mechanism similarly to the semiconductors. Fig.1 (b) shows the x-ray diffraction pattern of the as-grown film prepared with 20 cycles of the RHEED oscillation. The film thickness was estimated from the width of (001) diffraction peak using following equation, which is called "Scherrer's equation".[5]

$$t=0.9L/B\cos\theta_B \qquad (1)$$

Here, "t" is the film thickness/nm, the wavelength of x-ray is $L=0.154nm$ (CuK_α), the width of half maximum of the peak is $B=0.021rad$ and the position of (001) diffraction peak is $\theta_B=13.9°$. The calculated thickness was 6.7nm, from which the thickness of the layer with one oscillation of RHEED intensity was deduced to be 0.34nm. This value corresponds to the lattice constant c of the parent material of $(Ca,Sr)CuO_2$ $(c=0.320nm)$.[6] This result indicates that the unit of the layer growth is the

unit cell of $(Ca,Sr)CuO_2$, when all elements are supplied simultaneously. This growth mechanism is similar to that reported for $YBa_2Cu_3O_7$[7]

Second, the possibility of atomic-layer growth of the $(Ca,Sr)CuO_2$ has been examined. This material has a crystal structure, where Ca(Sr) layer and CuO_2 layer are stacked alternatively along the c-axis [see Chapter 4-1, Fig.2], so the parent material may be formed by the successive ablation of Ca(Sr) and Cu. The first step of the film formation affects the growth mechanism strongly, so SrO_x, CaO_x or CuO_x thin layer was prepared on the $SrTiO_3$ substrate separately, and the growth was studied at first. The layer was prepared on $SrTiO_3$ (100) substrates with the ablation of Sr, Ca or Cu target in 1×10^{-3} Pa of NO_2. Figs.2(a) and 2(b) show the RHEED patterns and the intensity variations during the formation of SrO_x and CuO_x thin films, respectively. At the beginning of the SrO_x deposition, clear RHEED oscillation could be observed, and the streak pattern was maintained during the early stage. When only CaO_x was deposited on $SrTiO_3$, a similar behavior was observed, although the disappearance of the intensity oscillation was slightly rapid compared with Sr. These behaviors suggest that the atomic-layer growths of SrO and CaO are possible in the first step of the growth, that is, in a few atomic layer just on the $SrTiO_3$. On the other hand, CuO_x on $SrTiO_3$ did not show an oscillation of RHEED intensity and the spotty RHEED pattern appeared immediately after the Cu deposition [see Fig.2 (b)]. Even if strontium (calcium) oxide was deposited after the CuO_x deposition, the

82

spotty pattern did not disappear, so the early stage of the film formation was significantly important. These results can be explained as follows. Since the charges of SrO and CaO layers are neutral, stacking of these layers is possible from the charge neutrality requirement. From the viewpoint of lattice matching, $SrTiO_3$ has a cubic perovskite structure, and bulk SrO and CaO have a cubic rock-salt type crystal structure. The (100) plane of $SrTiO_3$ consists of SrO layer and/or TiO_2 layer [see Fig.3]. The SrO layer in $SrTiO_3$ (100) and (100) plane of bulk SrO (or CaO) have same structure. In $SrTiO_3$, the bond length of Sr-O in SrO layer is 0.276nm. The length in bulk SrO is 0.258nm, and Ca-O in CaO is 0.240nm. SrO and CaO layers have neutral charge, and the structures are similar to that of the substrate, therefore these layers can be grown with two-dimensional layer growth at the earliest stage. The matches of lattice constants between the SrO (CaO) and $SrTiO_3$, however, are not so good, so the layer-growth mode fails after the deposition of a few layer. SrO layer has a better lattice matching with the substrate than CaO, thus the oscillation of RHEED intensity in CaO growth disappears rapidly compared with SrO growth. On the other hand, CuO_2^{2-} layer, which I want to form, has minus charge, so the stacking of this layer is impossible, and neutral CuO or Cu_2O may be formed immediately. The lattice matching between these oxides and $SrTiO_3$ (100) substrate is not so good. CuO has a monoclinic structure with a=0.468nm, b=0.343nm, c=0.513nm and $\beta = 99° 28'$. This structure does not fit $SrTiO_3$ (100). Cu_2O has a cubic cuprous-oxide structure with a=0.427nm, but this structure does not include a plane fitting the $SrTiO_3$ (100).[8] Thus, the

83

interface   energy between these oxides and the substrate must   be large and the three dimensional growth occurs easily.

Judging from these results,   SrO and CaO should be   deposited on   the   substrate at first for the $(Ca,Sr)CuO_2$ formation.   The target   must be replaced by the Cu target at the peak top of   the oscillation of the RHEED intensity to form CuO_2 atomic layer, and it must be replaced by Ca and Sr again at the next peak top.   The film   of $(Ca,Sr)CuO_2$ may be grown   by the   repetition   of   this process with atomic-layer growth.   Fig.4(a) shows the variation of   RHEED   intensity versus time during the film growth   by   this method.   The $Ca(Sr)O_x$ layer was formed by rapid exchange   of   Ca target   and   Sr target, and the ratio of Ca:Sr was about   8:2   in this experiment.   Oscillation of the intensity could be   observed and the streak pattern was maintained without the appearance of a spotty pattern.   Fig.4(b) shows the x-ray diffraction pattern   of the   film   formed   by this method with   30   cycles   of   alternate deposition   of   Ca(Sr) and Cu, where 1 cycle   of   the   deposition includes   two cycles of the oscillation of RHEED intensity.   The diffraction pattern indicates that $(Ca,Sr)CuO_2$ film can be   grown by   this   method. The film thickness   calculated   by   Scherrer's equation   (eq.1)   was 9.2nm,   and the   thickness   with   one-cycle deposition, which includes the deposition   of one $Ca(Sr)O_x$ layer and   that   of one CuO_x layer, was deduced to be   0.31nm.   This value   corresponds   to   the lattice constant   c   of $(Ca,Sr)CuO_2$. Namely,   two   cycles of the oscillation of RHEED   intensity   are observed   during   the growth of one unit cell of $(Ca,Sr)CuO_2$ in this process, while there is one oscillation in the   simultaneous

deposition process. These results indicate that atomic-layer growth of this material has become possible by a combination of the successive supply of each metal element and the growth control using the oscillation of RHEED intensity. In this growth process, strict control of the chemical composition is necessary. Otherwise, excess copper-deposition over one atomic-layer immediately leads to three-dimensional growth with a rough surface. The application of the oscillation of RHEED intensity permits a growth control within atomic-layer order, and makes it possible to control the chemical composition of the film strictly.

If the monolayer of Ca(Sr)O was deposited on the substrate, the two-dimensional CuO_2 layer could be grown within monolayer thickness. On the other hand, three-dimensional islands of CuO_x were formed immediately on the bare $SrTiO_3$ substrate. The reason of this behavior is that the deposition of CuO_2 monolayer on $Ca(Sr)O_x$ layer makes the stable substance of $(Ca,Sr)CuO_2$. However, even if the Ca(Sr)O is deposited on the substrate, supply of copper over one monolayer thickness immediately leads to the island growth because of the charge neutrality and the lattice matching of CuO_x.

The results shown above indicate that the relation between the substrate surface and the first layer just on the substrate governs the growth mechanism of the film. Therefore, I studied the substrate surface and the film growth at the initial stage carefully. The surface of the bare $SrTiO_3$ (100) was examined through the method described below. The monolayers of strontium

85

oxide and titanium oxide were deposited from Sr and TiO_2 targets with different sequences on the substrates, and the RHEED patterns were compared. The deposition of monolayer of SrO_x on $SrTiO_3$ (Sr/STO) led to the clear oscillation of RHEED intensity and streak RHEED pattern was maintained through the deposition. Figs.5(a) and 5(b) show the RHEED patterns of the substrate and Sr/STO, and Fig.5 (d) the intensity variation. The deposition of TiO_x monolayer on the SrO_x deposited substrate (Ti/Sr/STO) also showed the clear oscillation and the streak RHEED pattern [see Figs.5(c) and 5(d)]. This behavior shows that the SrO_x and TiO_x can be formed with two dimensional atomic layer growth. The thicknesses of the one atomic layers could be strictly controlled using the oscillation of RHEED intensity. On the other hand, direct deposition of TiO_x layer on the substrate (Ti/STO) did not indicate a clear intensity oscillation, and the RHEED pattern became blurred as shown in Fig.6. (Thus, in the preparation of Ti/STO and Sr/Ti/STO samples, the thicknesses of SrO_x and TiO_x layers were monitored by calibrated thickness monitor with quartz-crystal oscillator.) These behaviors suggest that the TiO_2 layer is the topmost layer of the bare $SrTiO_3$. In order to confirm this estimation, I have measured the Auger spectrum of each surface and compared the ratios of Auger intensities of Sr(110eV, MNN line) and Ti (387eV, LMM line). Since, the MNN Auger electron of Sr has very short escape depth, which corresponds to the thickness of about two atomic layers[9], the Auger intensity for Sr is so sensitive to the surface layer. Figs.7(a) and 7(b) show the Auger spectrum for the $SrTiO_3$

substrate and the relative intensity of Sr/Ti, respectively. The Sr/Ti intensity ratio on bare substrate surface has good agreement with that of Ti/Sr/STO surface, while the surfaces of other samples have different values. This result strongly supports that the topmost layer of the substrate is TiO_2 layer. This is consistent with the reported result of x-ray photoemission spectroscopy.[10] Thus, I conclude that the topmost of $SrTiO_3$ (100) is TiO_2 layer and the SrO layer is most suitable as the first layer just on the $SrTiO_3$ (100) substrate.

The RHEED data indicate that TiO_2 layer can be formed with layer-growth mode on SrO top-layer and not on TiO_2 top-layer. From the viewpoint of the charge neutrality, TiO_2 layer is neutral itself, so the stacking of TiO_2 layers will be possible. This result suggests the lattice matching affects the growth mode strongly compared with the charge neutrality. Bulk TiO_2 has three phases, which are anatase, blookite and rutile.[8] In these structures, titanium is coordinated by 6 oxygen to form a octahedron, and the octahedrons are connected with the edge sharing. Thus, the structure of TiO_x networks in bulk TiO_2 is different from that in $SrTiO_3$, and the growth of two-dimensional TiO_2 layer should be disturbed. From the viewpoint of the structure, TiO with rock-salt structure fits the $SrTiO_3$ (100) rather than TiO_2, but the production of divalent Ti^{2+} ion will be impossible under the oxidation condition of high substrate-temperature and NO_2 atmosphere.

The difference in relative Auger intensities for Sr/Ti/STO and Ti/Sr/STO, which is shown in Fig.7(b), shows that the structures of the films were constructed according to the sequence of the

87

deposition of the atomic layers, and the rearrangement of the atomic layers into a stable structure did not occur under the experimental condition. This behavior indicates that the structure control with one atomic-layer scale is possible in this method.

In next step, $SrCuO_2$ layer (called "SCO"), which is one of the components of layer-by-layer stacking of $Bi_2Sr_2Ca_{n-1}Cu_nO_{2n+4}$, was formed by simultaneous deposition of Sr and Cu from $SrCuO_x$ target. This layer was formed on the bare $SrTiO_3$ (100) (STO) or on strontium deposited substrate (Sr/STO), and the growth in initial stage of the layer-by-layer stacking was studied using AES. On both substrates, the deposition of one SCO layer led to a streak RHEED pattern and clear oscillation of RHEED intensity. Thus, the thickness of one unit layer was easily confirmed using the oscillation. This behavior is very similar to the growth of $(Ca,Sr)CuO_2$ [see Fig.1], and suggests the SCO layer has the same structure of the parent material, and the layer is grown with two-dimensional unit-cell layer growth. Interestingly, the Auger spectra had different intensity ratios of strontium / copper (840eV LMM line) for these two samples as shown in Fig.7 (c). The SCO layer on Sr/STO had much larger Sr/Cu value than that on bare $SrTiO_3$. This result indicates that the arrangement of atomic layers in $SrCuO_x$ layer is dependent on the topmost layer of the substrate material. Namely, the top of the SCO layer is SrO_x on the Sr/STO, and CuO_x layer on the bare $SrTiO_3$. This behavior is explained by the self-arrangement of

88

the atomic layers to form a stable interface between the layer and the substrate. On the TiO_2 topmost-layer of the bare $SrTiO_3$, SrO will be more stable than CuO_2 from the viewpoint of the perovskite crystal structure, resulting in the CuO_2 topmost in $SrCuO_2$. On the Sr/STO surface, the arrangement of the layers should be reversed [see Fig.8]. This result indicates that the topmost layer of the substrate is the determining factor for the construction of the film structure when the elements are supplied simultaneously. This behavior is different from that observed in the layer-by-layer stacking of atomic layers, in which the structure is constructed according to the sequence of supply of atoms.

The variation of RHEED pattern and intensity during the formation of SCO/Sr/STO are shown in Figs.9(a), 9(b), 9(c) and 9(e). The RHEED pattern of the SCO/Sr/STO showed that the surface has 2x2 superstructure above 773K. The same superstructure is observed on the surface of Sr/SCO/STO. I consider that the superstructure is due to the ordered oxygen deficiency in the SrO top layer. Since CuO_2^{2-} layer has minus charge, oxygen deficiency in SrO layer, which makes Sr^{2+}, will be necessary to satisfy the charge neutrality.

The deposition of bismuth oxide on the SCO/Sr/STO leads to the formation of $Bi_2Sr_2CuO_6$ structure with n=1. The 2x2 superstructure disappeared by the Bi deposition as shown in Fig.9(d). By the repetition of this deposition cycle, the thin film of $Bi_2Sr_2CuO_6$ was formed. The x-ray diffraction pattern showed that the structure of $Bi_2Sr_2CuO_6$ was actually formed through this process.

By similar way, the films of $Bi_2Sr_2Ca_{n-1}Cu_nO_{2n+4}$ were formed. The number of CuO_2 layer was controlled by the insertion of $(Ca,Sr)CuO_2$ between the SCO layer and SrO layer depositions. Fig.10 shows the variation of RHEED pattern during the layer-by-layer formation of $Bi_2Sr_2CaCu_2O_8$ with n=2. In this case, $SrCuO_x$, $(Ca,Sr)CuO_2$, Sr and Bi_2O_3 were successively ablated in NO_2 atmosphere. In all the steps of the layer-by-layer stacking, the oscillation of RHEED intensity was observed, and the streak pattern was maintained. This behavior is remarkably different from the previous report of the process through the three-dimensional growth[11], or the growth through random-oriented structure.[12] Under my experimental condition, two-dimensional layer growth was possible in all the steps of layer-by-layer stacking of $Bi_2Sr_2Ca_{n-1}Cu_nO_{2n+4}$. The oscillation of the RHEED intensity makes it possible to control the deposition thickness of each layer strictly. The x-ray diffraction patterns indicated that the structures of $Bi_2Sr_2Ca_{n-1}Cu_nO_{2n+4}$ with n=1 to 10 could be constructed by this method.

Conclusion

The growth mechanism in the formation of $(Ca,Sr)CuO_2$ and that in the layer-by-layer construction of $Bi_2Sr_2Ca_{n-1}Cu_nO_{2n+4}$ were investigated. The present results show the topmost layer of $SrTiO_3$ (100) substrate is TiO_2, and the SrO layer is suitable as the first layer of the film formation on this substrate. In the formation of $(Ca,Sr)CuO_2$, the film is formed with the unit-cell layer growth by the simultaneous supply of all the elements. Furthermore, the unit of layer growth can be separated into atomic layers of $Ca(Sr)O$ and CuO_2 when the elements are supplied separately. In this case, the structure is constructed according to the sequence of the deposition, and the rearrangement of the atomic layers does not occur. On the other hand, when the elements are supplied simultaneously, the atomic layers in the unit-cell layer are arranged to make more stable interface, so the arrangement is determined by the topmost layer of the substrate. The result also shows that the $Bi_2Sr_2Ca_{n-1}Cu_nO_{2n+4}$ structures can be grown with two-dimensional layer growth in all the steps of the layer-by-layer construction. The most important factor to determine the growth mode is the lattice matching between the film and the substrate, and better matching leads to a two-dimensional layer growth. In this growth mode, the variation of RHEED intensity enabled us to control the process of monolayer deposition strictly not only for parent material of $(Ca,Sr)CuO_2$ but also for $Bi_2Sr_2Ca_{n-1}-Cu_nO_{2n+4}$. This is a key technique to achieve the layer-by-layer construction of these materials.

References

(1) J.J.Harris and B.A.Joyce, Surf.Sci.Lett., 108, L90 (1981).

(2) T.Sakamoto, H.Funabashi, K.Ohta, T.Nakagawa, N.J.Kawai and T.Kojima, Jpn.J.Appl.Phys., 23, L657 (1984).

(3) J.H.Neave, B.A.Joyce, P.J.Dobson and N.Norton, Appl.Phys.A, 31, 1 (1983).

(4) J.M.van Hove, C.S.Lent, P.R.Pukite and P.I.Cohen, J.Vac.Sci.& Technol.B, 1, 741 (1983).

(5) B.D.Cullity, Elements of X-ray Diffraction 2nd Edition, (Addisson-Wesley, Massachusetts, 1977).

(6) T.Siegrist, S.M.Zahurak, D.W.Murphy and R.S.Roth, Nature, 334, 231 (1988).

(7) T.Terashima, K.Shimura, Y.Bando, Y.Matsuda, A.Fujiyama and S.Komiyama, Phys.Rev.Lett., 67, 1362 (1991).

(8) R.Kiriyama and H.Kiriyama, Structural Inorganic Chemistry I, (Kyoritsu Press, Tokyo, 1979).

(9) M.P.Seah and W.A.Dench, Surf.Interf.Anal., 1, 2 (1979).

(10) M.Kawai, S.Watanabe and T.Hanada, J.Cryst.Growth, 112, 745 (1991).

(11) D.G.Schlom, A.M.Marshall, J.T.Sizemore, Z.J.Chen, J.N.Eckstein, I.Bozovic, K.E.von Dessonneck, J.S.Harris Jr. and J.C.Bravman, J.Cryst.Growth, 102, 361 (1990).

(12) S.Yokoyama, T.Ishibashi, M.Yamagami and M.Kawabe, Jpn.J.Appl.Phys., 30, L106 (1991).

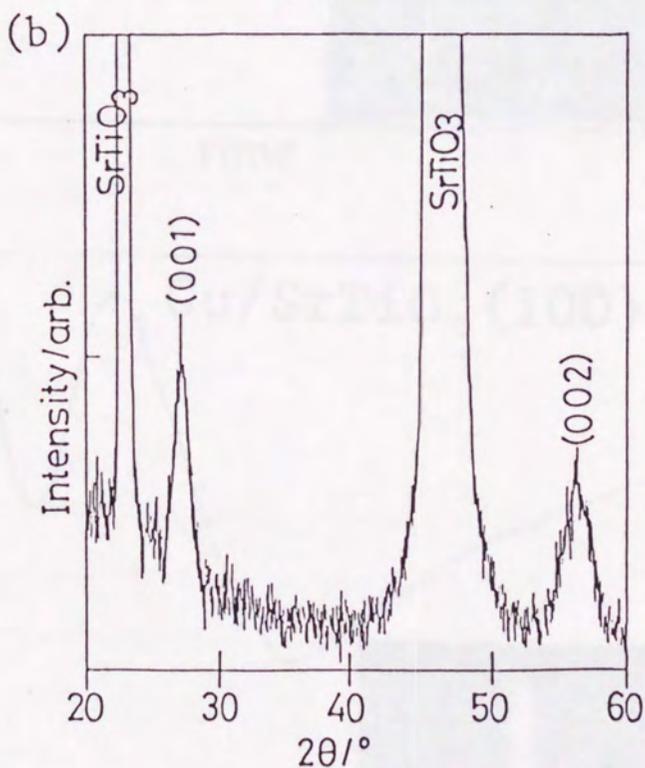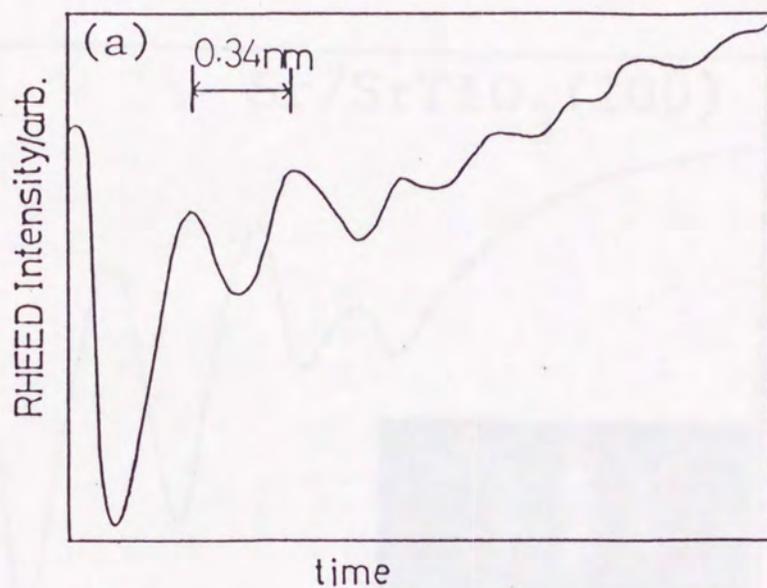Fig.1 (a) Variation of RHEED intensity with time during the film formation by the ablation of $Ca_{0.86}Sr_{0.14}CuO_2$. (b) XRD pattern of the as-grown film formed by deposition with 20-cycle oscillation of the RHEED intensity.
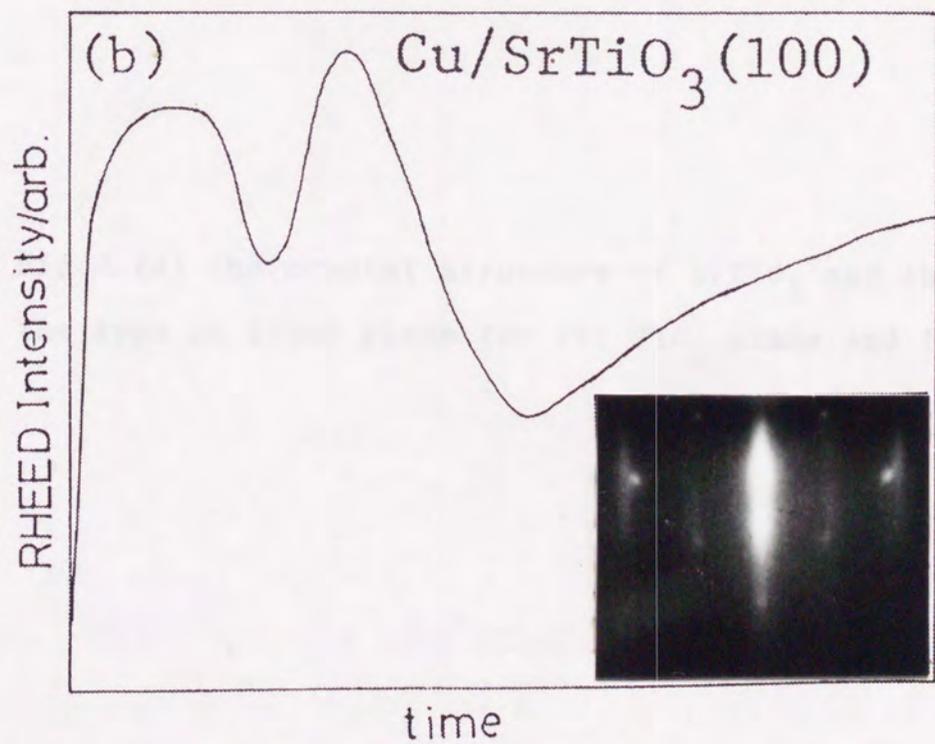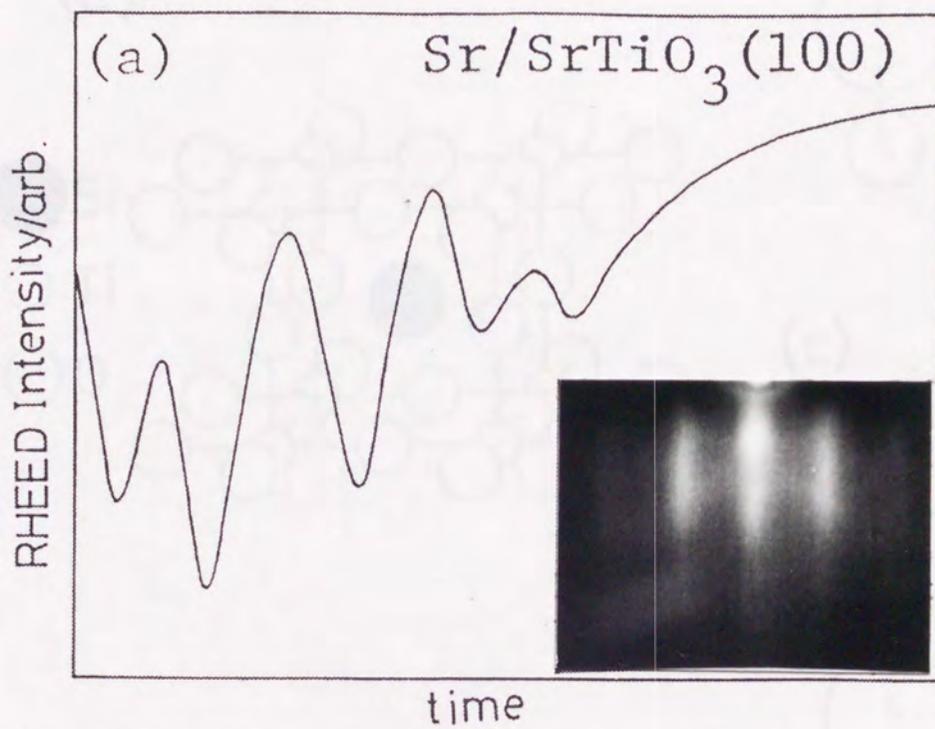
Fig.2 RHEED pattern and intensity variation of (a) Sr deposition
and (b) Cu deposition on SrTiO₃ substrates.
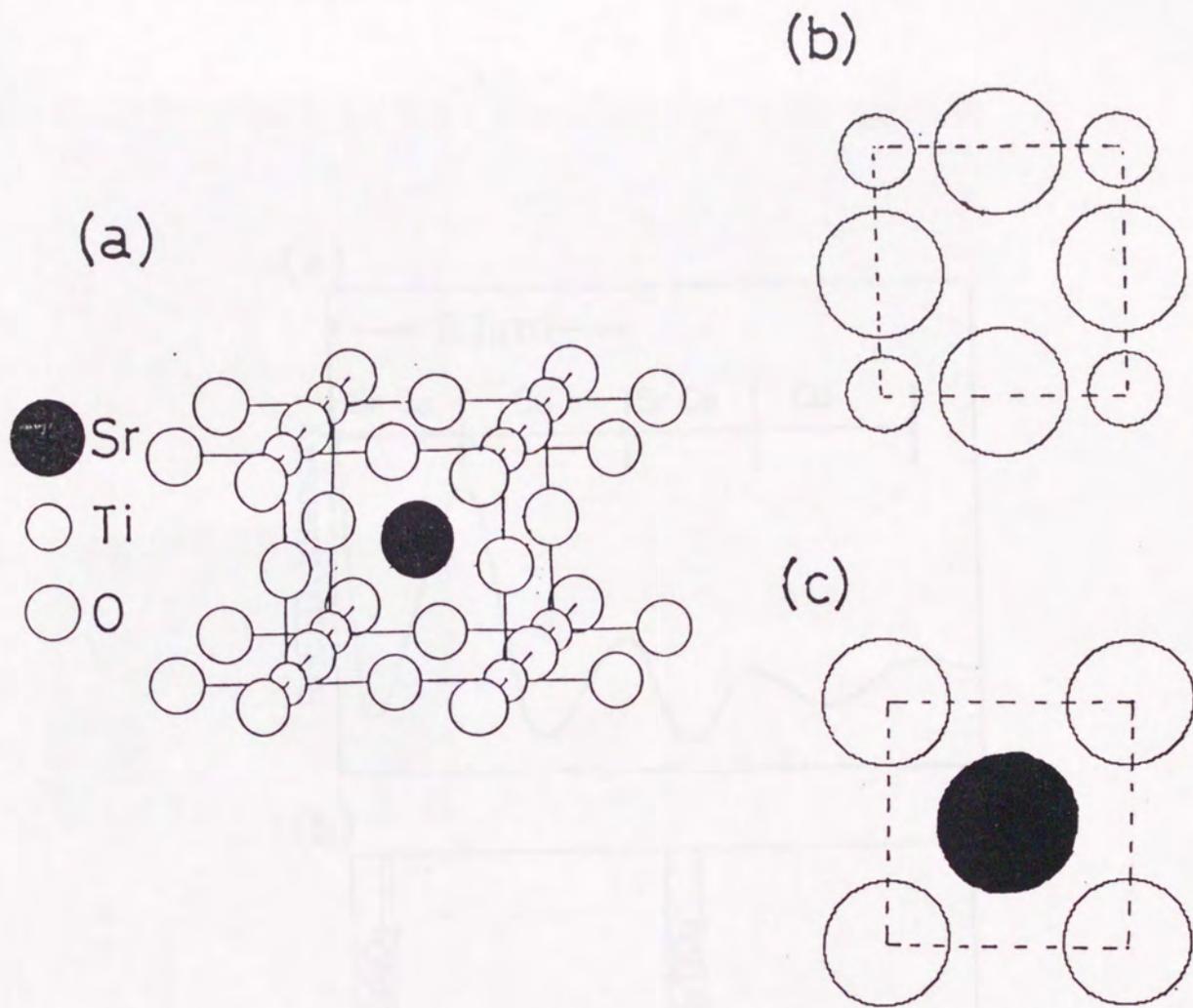
Fig.3 (a) The crystal structure of $SrTiO_3$ and the areangement of the ions in (100) plane for (b) TiO_2 plane and (c) SrO plane.
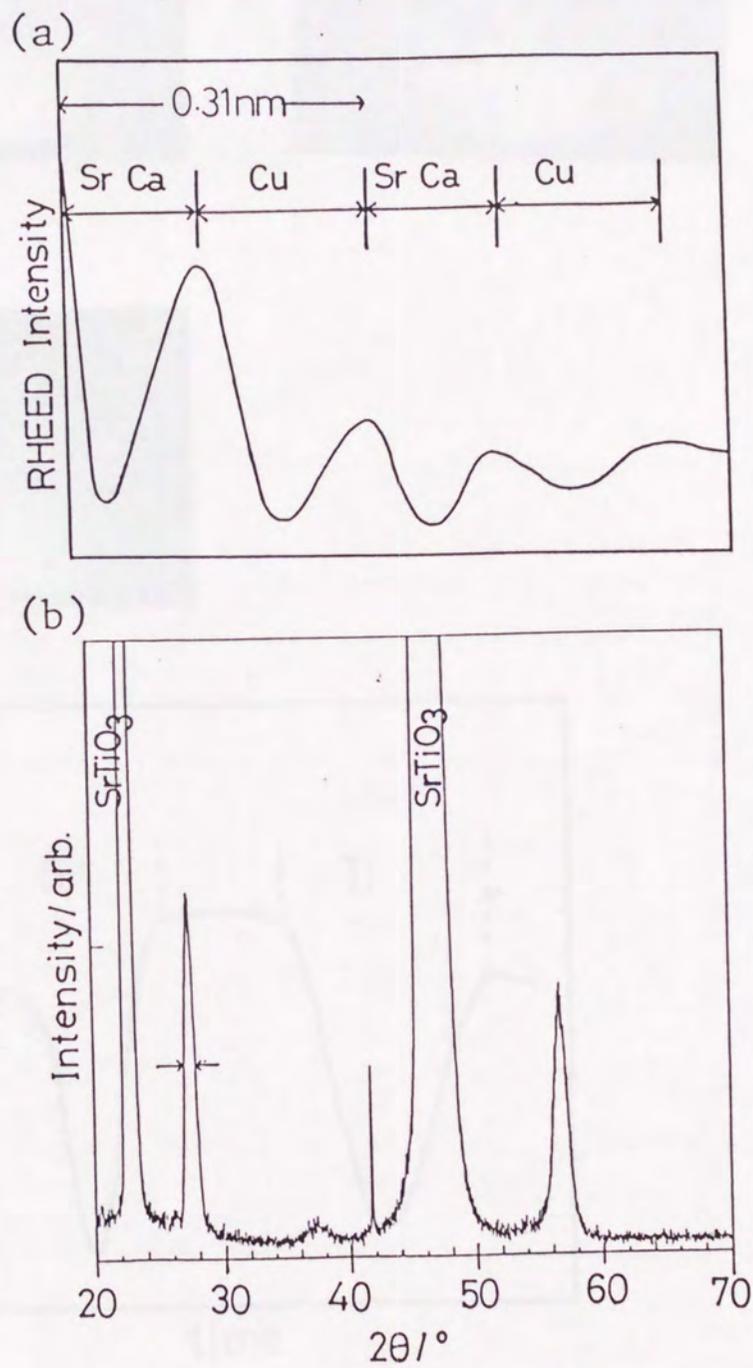
Fig.4 (a) Variation of RHEED intensity with time during the formation of $(Ca,Sr)CuO_2$ film by the successive ablation of Ca(Sr) and Cu. (b) XRD pattern of the as-grown film formed by 30-cycle deposition of Ca(Sr) and Cu. 1-cycle deposition includes two cycle oscillations of the RHEED intensity.
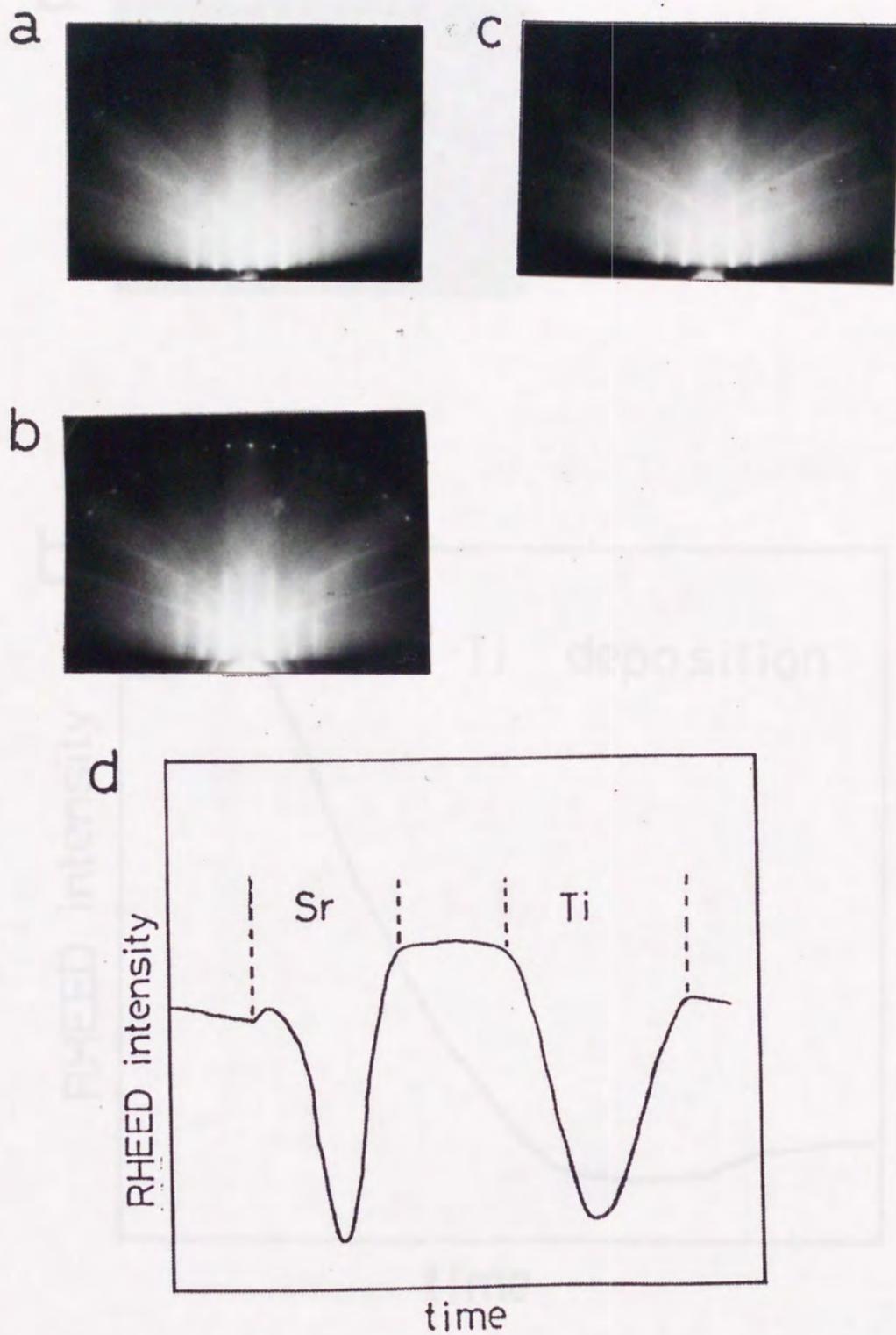
Fig.5 RHEED pattern for (a) SrTiO$_3$ (100) substrate, (b) SrO deposited substrate (Sr/STO) and (c) TiO$_2$ deposited Sr/STO (Ti/Sr/STO). (d) The variation of RHEED intensity during the formation.

a

b

RHEED intensity

Ti deposition

time
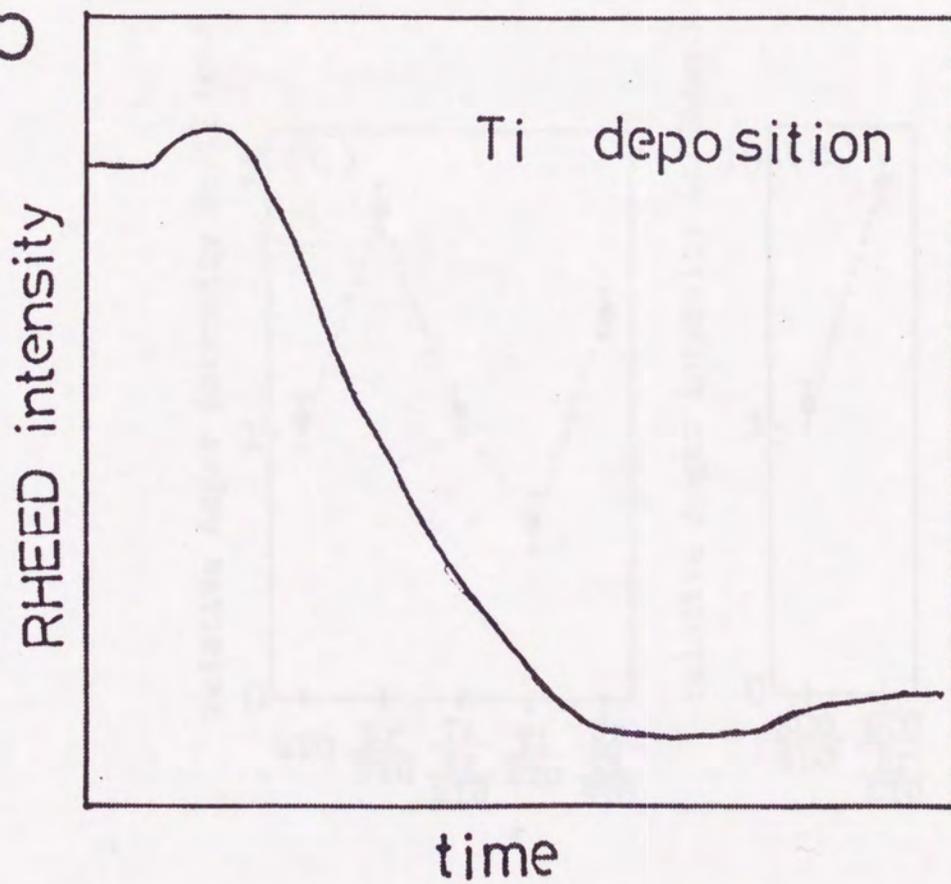
Fig.6 (a) RHEED pattern for TiO_x deposited $SrTiO_3$ (100) substrate. (Ti/STO). (b) The variation of RHEED intensity during the formation.
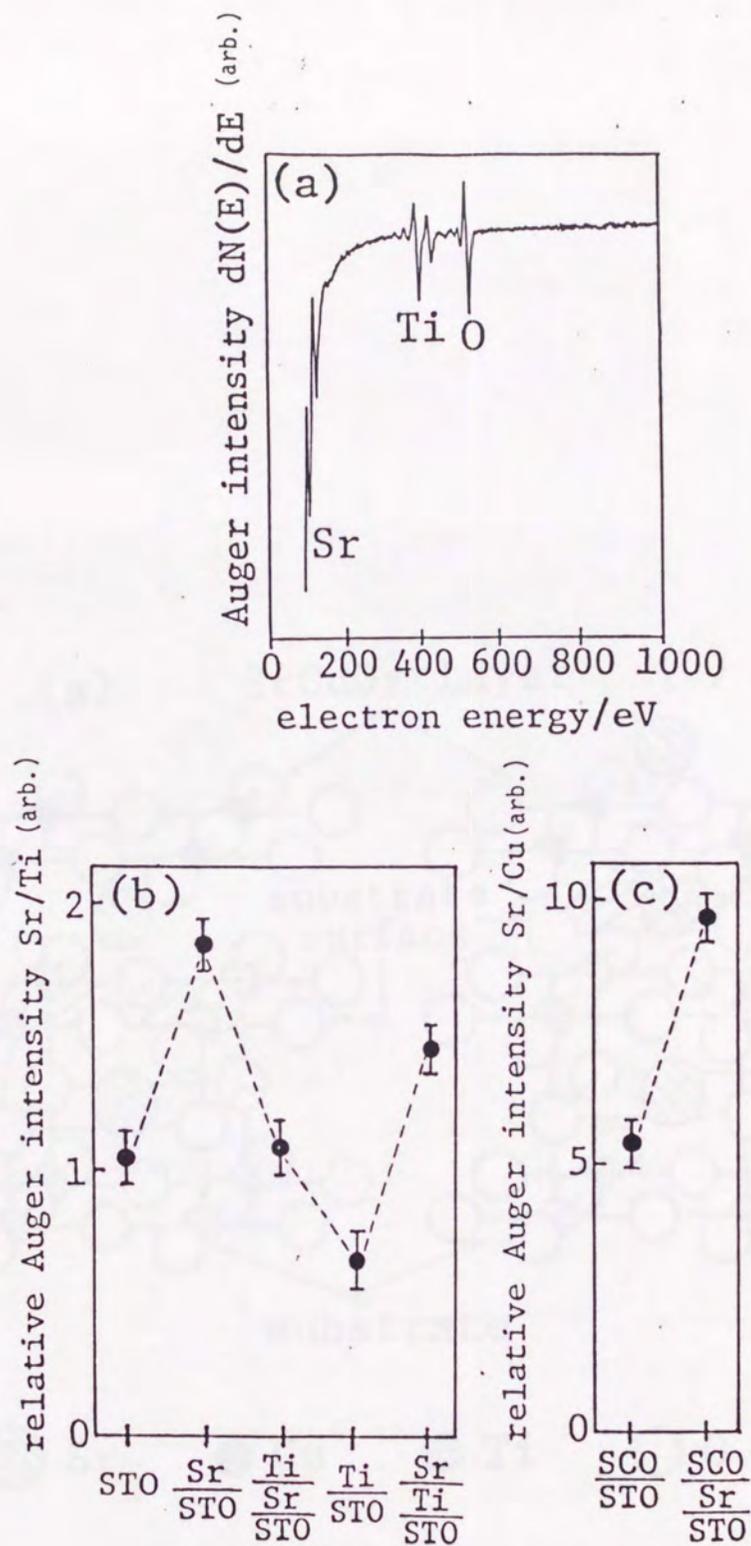
Fig.7 (a) The Auger spectrum of $SrTiO_3$ substrate, (b) the relative Auger intensities of Sr/Ti of STO:$SrTiO_3$, Sr/STO:SrO_x on STO, Ti/Sr/STO:TiO_x on Sr/STO, Ti/STO:TiO_x on STO, Sr/Ti/STO:SrO_x on Ti/STO, and (c) relative Auger intensities of Sr/Cu for SCO/STO:$SrCuO_x$ layer on STO, SCO/Sr/STO:SrO_x layer on Sr/STO
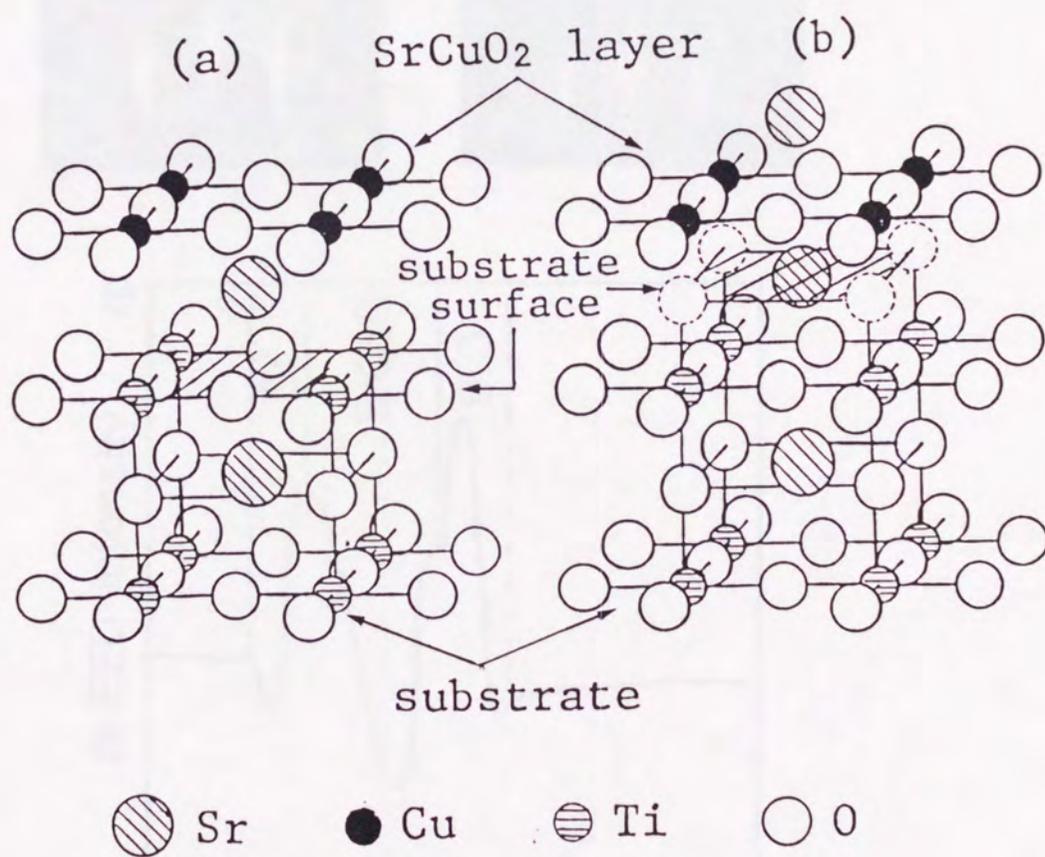
Fig.8 The profiles of the structure of $SrCuO_2$ thin layer (a) on $SrTiO_3$ (100) substrate and (b) on Sr deposited $SrTiO_3$ substrate. The arrangement of SrO layer and CuO_2 layer is changed dependent on the surface layer of the substrate.
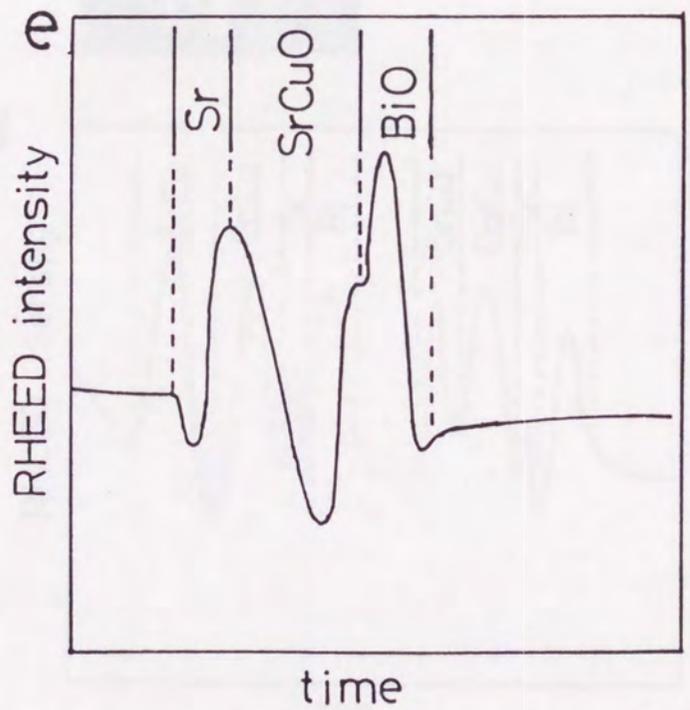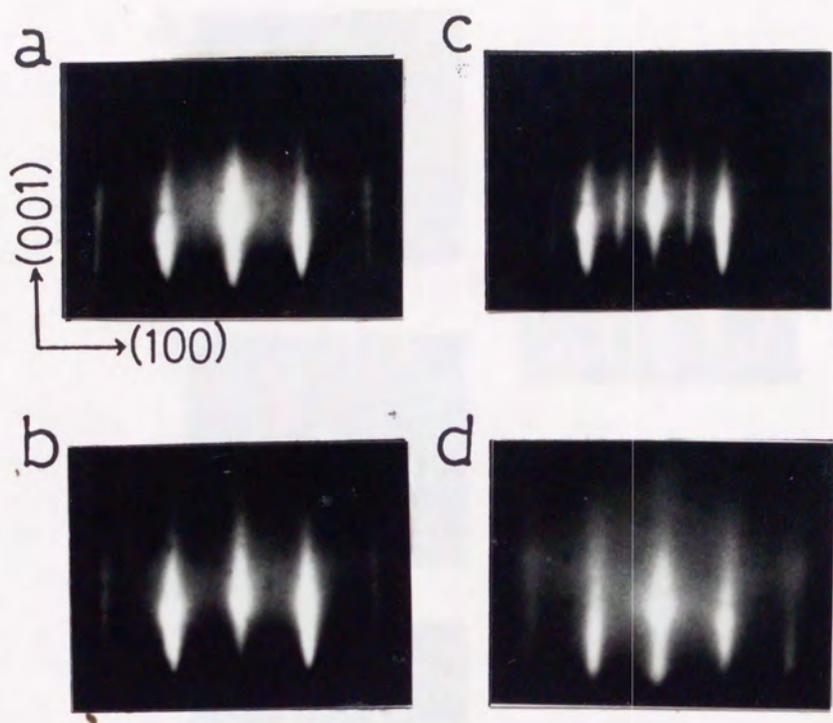
Fig.9 The changes of RHEED pattern and intensity for the deposition of Sr/SrCu/Bi for $Bi_2Sr_2CuO_6$ formation. (a) RHEED pattern of bare $SrTiO_3$ substrate, after SrO_x deposition, (c) after $SrCuO_x$ deposition, (d) after Bi_2O_x deposition and (e) the variation of RHEED intensity.
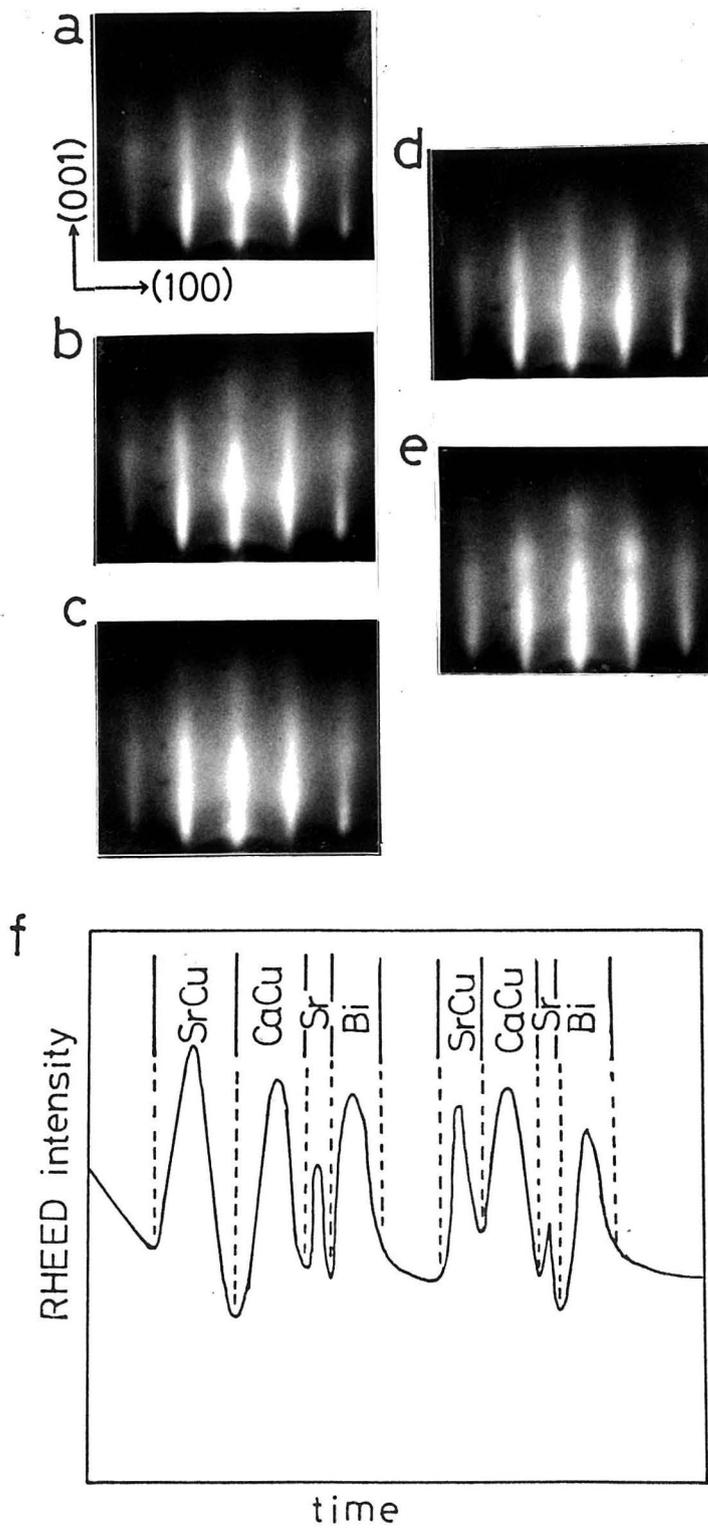
Fig.10 The changes of RHEED pattern and intensity through the formation of $Bi_2Sr_2CaCu_2O_8$ structure. (a) RHEED pattern after Bi_2O_x deposition, (b) after $SrCuO_x$ deposition, (c) after $(Ca,Sr)CuO_x$ deposition, (d) after SrO_x deposition, (e) after Bi_2O_x deposition, and (f) the variation of RHEED intensity.

Chapter 4-3:

Site-Selective Substitution in $(Bi,Pb)_2Sr_2CaCu_2O_8$ Thin Film by Layer-by-Layer Growth Process

Abstract

By the application of layer-by-layer deposition technique, "Tailored superconducting films" are fabricated. In this section, Bi ions in $Bi_2Sr_2CaCu_2O_8$ have been site-selectively substituted by Pb in order to control the superconductivity. Composition and structure analyses have revealed that Pb is actually substituted for Bi with the amount as I introduced. The superconducting zero-resistance temperature can be risen with the increase of Pb up to 30% of the Bi amount.

93

Introduction

The superconducting property of cuprate superconductor is strongly dependent on the carrier concentration, which can be controlled either by substitution of metal ions or variation of oxygen content.[1-3] The property also varies against the change of the number of CuO_2 planes (n) in $Bi_2Sr_2Ca_{n-1}Cu_nO_{2n+4}$, so both the crystal structure and the carrier concentration must be controlled in order to study the determining factor of the transition temperature (T_c) in this system.

The structure control by layer-by-layer stacking has been performed as shown in Chapter 4-1. For the control of the carrier concentration, the substitution of metal ion is effective. For example, it has been reported that yttrium substitution for Ca site in $Bi_2Sr_2CaCu_2O_8$ decreases the hole concentration and T_c.[4] On the other hand, possible way to increase the hole concentration is a substitution of Pb^{2+} for Bi^{3+} together with the control of oxygen amount. In the sample prepared solid state reaction, however, it is not clear whether the Pb ion really substitutes the Bi site or not, because the metal ions in this system may easily migrate into the other ion site during the reaction at high temperature as shown in Chapter 3-2. Therefore, the site-selective substitution of Pb for Bi is necessary to elucidate the correlation in a well-defined system. In this section, a site-selective substitution of Pb^{2+} for Bi^{3+} is carried out by the application of layer-by-layer construction, and the effect of the substitution on the superconducting properties is studied in $(Bi,Pb)_2Sr_2CaCu_2O_8$.

94

Experimental

Six kinds of $(Bi,Pb)_2Sr_2CaCu_2O_8$ thin films with different Pb contents were prepared by layer-by-layer growth process. The films were prepared by successive ablation of $Bi_{1-x}Pb_xO_y$, $SrCuO_x$, $CaCuO_x$, Sr [see Chapter 4-1]. The nominal composition of $Bi_{1-x}Pb_xO_y$ was varied with x=0, 0.1, 0.2, 0.3, 0.4 and 0.5. The experimental setup has been shown in Chapter 2. The films were prepared on MgO (100) substrate under N_2O gas flow. Substrate temperature was varied from 773K to 873K, and the pressure of N_2O was 1 to 10 Pa. In this method, the Pb ion is forced to enter the Bi site.

Resistivity-temperature curves (R-T curves) were measured by standard four-probe method in He refrigerator from 10K to 300K. The constant current source (Keithley, 224) and voltmeter (Keithley 181) were used in the measurement. Typical current in the measurement was $1A/cm^2$. and the lowest resistivity I could be measured was 1×10^{-6} ohm·cm. The temperature was measured by a semiconductor sensor. X-ray diffraction patterns were obtained using CuK_α with $\theta-2\theta$ scanning. The chemical composition of the film was determined by electron probe micro analysis (EPMA) with wavelength-dispersion measurement by Shimazu EMX-2A.

95

Results and Discussion

Fig.1 shows the relation between Pb concentrations in the films, which was determined by EPMA, and nominal concentrations in the targets. Here Pb concentration (x) in is expressed by Pb/(Bi+Pb) in molar ratio. The Pb concentration in the film was nearly proportional to that in the target within the range from x=0 to 0.5. Compositions except Bi and Pb in these films were nearly equal to $Sr_2Ca_1Cu_2O_y$. Thus, the $(Bi_{1-x}Pb_x)_2Sr_2CaCu_2O_y$ films with systematically altered Pb content have been prepared by this method.

The x-ray diffraction patterns of these films are shown in Fig.2, in which nominal target compositions are x=0, 0.2, 0.3 and 0.5. The patterns indicate that all the films have almost single-phase of $(Bi,Pb)_2Sr_2CaCu_2O_8$ structure. Large peaks of other phases are not observed. Thus, together with the x-ray diffraction and EPMA, it was concluded that the $(Bi_{1-x}Pb_x)_2$-$Sr_2CaCu_2O_8$ films with the same structure including different Pb concentrations up to x=0.5 were prepared.

The R-T curves of these films are shown in Fig.3. All films exhibited the decrease of the resistivity due to the superconducting transition around 80K. It is clear that zero-resistance temperature (T_c^{zero}) increases, as I expected, against the increase of Pb substitution from x=0 to 0.3. The films with larger Pb content than x=0.3, such as x=0.5, showed two steps in the decrease of the resistivity leading to lower T_c^{zero}. For the samples with Pb concentration within x=0 to 0.3, impurity phases were not observed, and the change of the T_c^{zero} was

96

systematically.   In the $La_{2-x}Sr_xCuO_4$ superconductor, it has been revealed that T_c increases with the increase of Sr in the small x region, and T_c decreases with large Sr concentration.[1]   In the $(Bi_{1-x}Pb_x)_2Sr_2CaCu_2O_8$ case, the similar behavior have been observed, thus I considered that the control of the superconductivity could be successfully carried out by the change of hole concentration accompanied by the Pb substitution.

On the other hand, T_c^{onset} are same for the films with different Pb concentrations. T_c^{onset} is the highest temperature where the superconductivity can be observed. The reason is considered as follows. T_c^{onset} emerges even when a little amount of superconducting component exists, that is, even the existence of a filamental current path shows a drop in resistivity. I consider that excess oxygen in the system may create a small amount of holes in the Pb-nondoped crystal to show just an onset of the resistivity drop but not zero resistance.

Conclusion

Site-selective substitution of Pb^{2+} for Bi^{3+} in Bi_2O_2 layer has been performed to control the superconductivity of $(Bi,Pb)_2Sr_2CaCu_2O_8$ superconductor by layer-by-layer deposition method. The T_c^{zero} of this system increased with the increase of the Pb amount in the range of $x=0$ to 0.3, which indicate that the superconductivity is controlled by the site-selective Pb substitution at the Bi_2O_2 layer, which leads to the increase of hole concentration in this system.

References

(1) Y.Tokura, J.B.Torrance, T.C.Huang and A.I.Nazzal, Phys.Rev.B, 38, 7156 (1988)

(2) J.B.Torrance, Y.Tokura, A.I.Nazzal, A.Bezinge, T.C.Huang and S.S.Parkin, Phys.Rev.Lett., 61, 1127 (1988).

(3) E.Sonder, B.C.Chakoumakos and B.C.Sales, Phys.Rev., 40, 6872 (1989).

(4) T.Tamegai, K.Koga, K.Suzuki, M.Ichihara, F.Sakai and Y.Iye, Jpn.J.Appl.Phys., 28, L112, (1989).

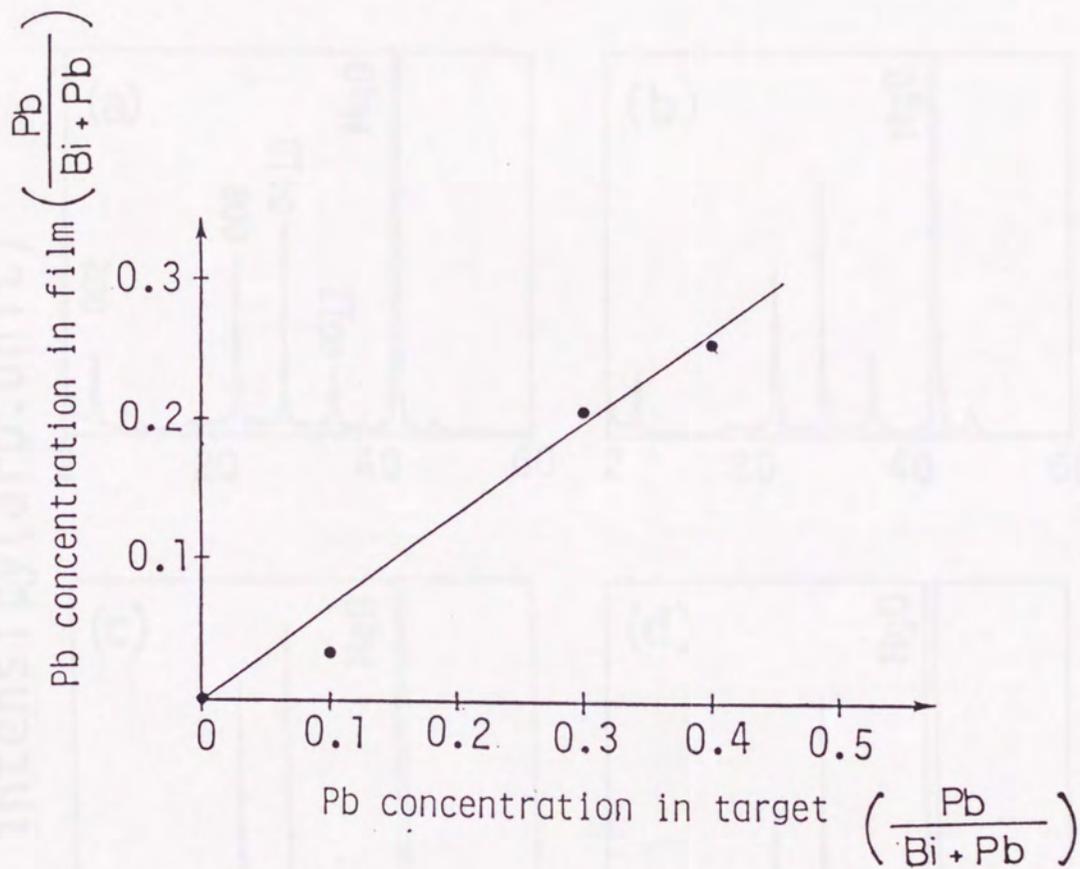Fig.1 The relation between Pb concentration in the films and the nominal compositions in the targets.
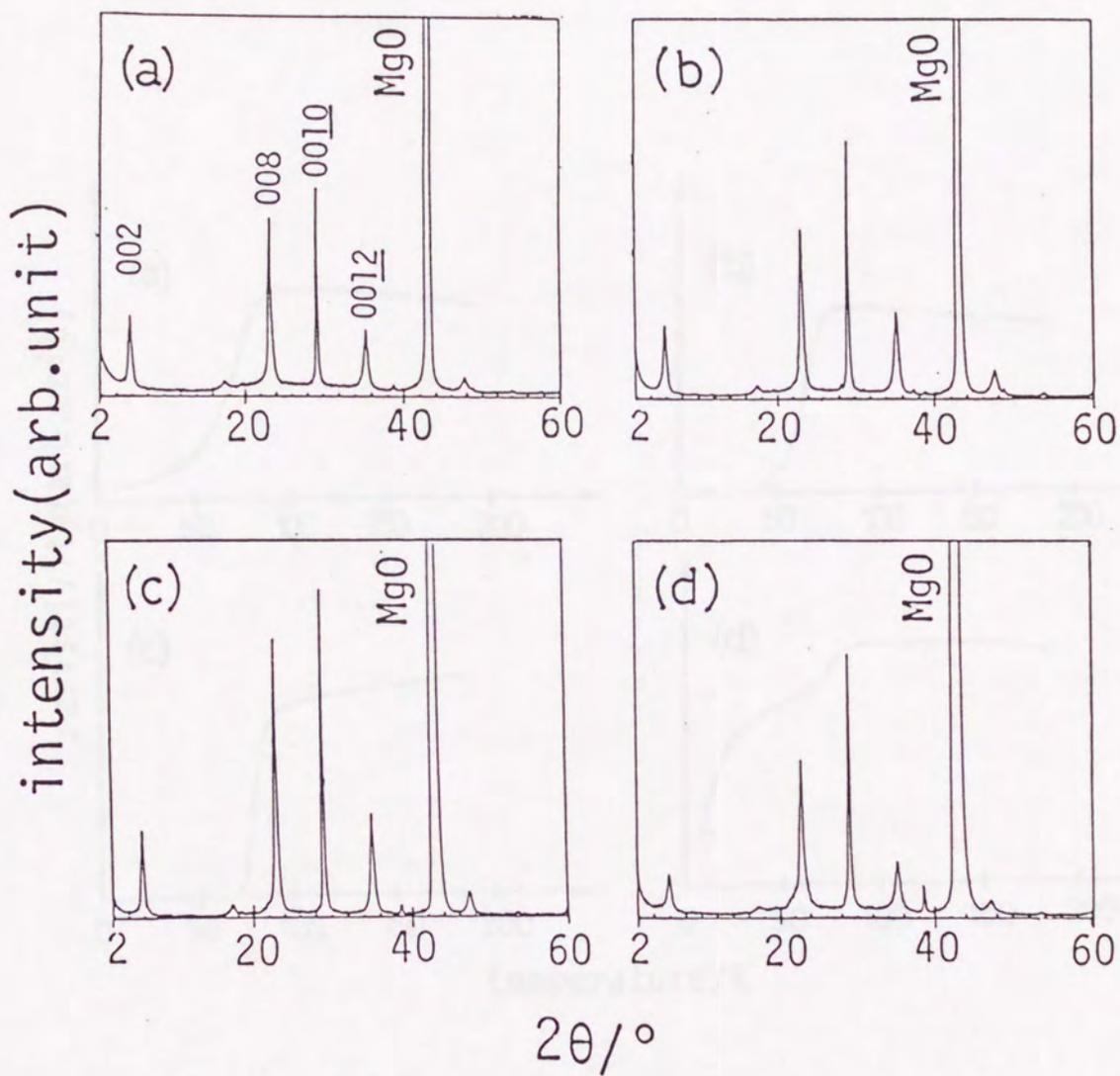
Fig.2 X-ray diffraction patterns of $(Bi_{1-x}Pb_x)_2Sr_2CaCu_2O_8$ thin films for (a) x=0, (b) x=0.2, (c) x=0.3 and (d) x=0.5.
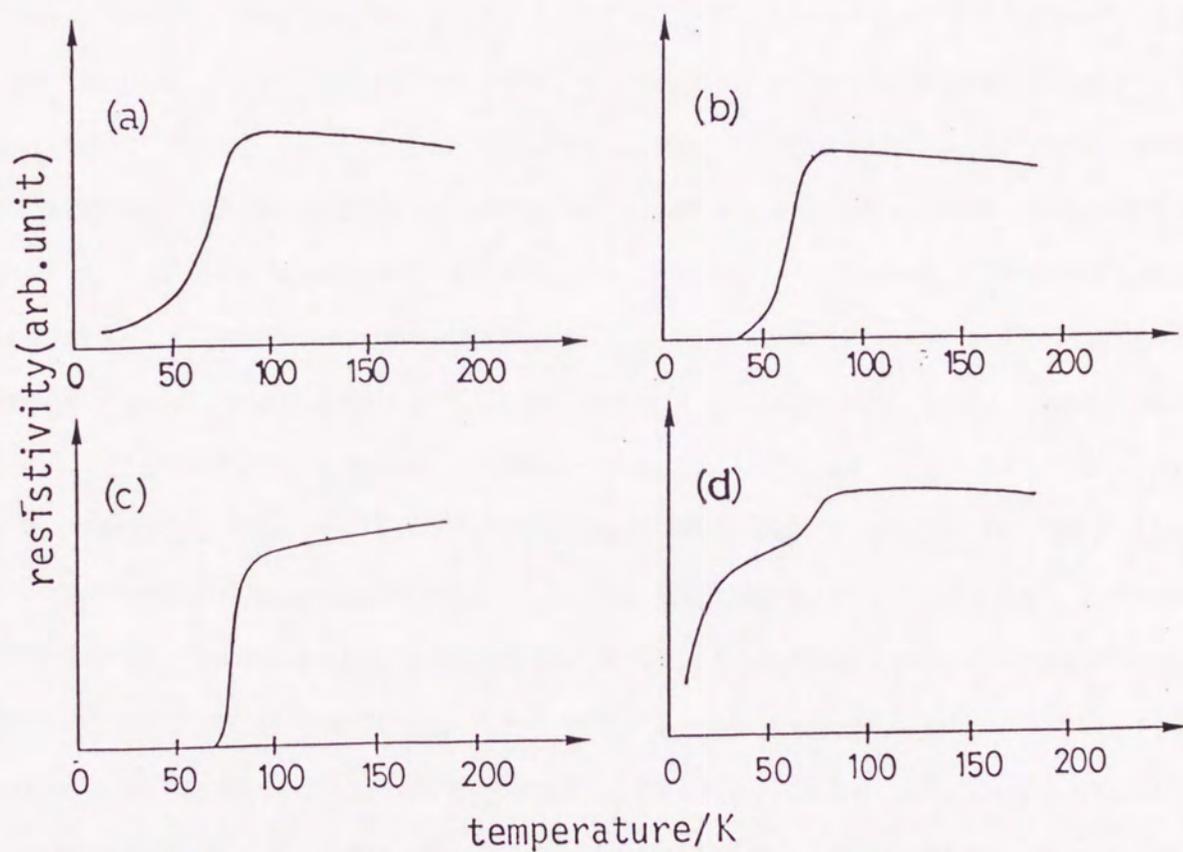
Fig.3   R-T curves of $(Bi_{1-x}Pb_x)_2Sr_2CaCu_2O_8$ thin films   for   (a) x=0, (b) x=0.2, (c) x=0.3 and (d) x=0.5.

Chapter 5
Superconducting Properties of $Bi_2Sr_2Ca_{n-1}Cu_nO_{2n+4}$

Chapter 5-1:

Two-Dimensional Superconductivity in Artificial Superlattice Based on $Bi_2Sr_2(Ca_{1-x}Y_x)Cu_2O_8$

Abstract

Two-dimensional nature in the high T_c superconductor of $Bi_2Sr_2CaCu_2O_8$ is examined on a superconducting superlattice prepared by the stacking of superconducting and nonsuperconducting layers. The superlattices have been formed by stacking of two kinds of $Bi_2Sr_2(Ca_{1-x}Y_x)Cu_2O_8$ layers containing different yttrium concentrations. One layer contains lower yttrium concentration (x=0.15) to be a superconductor, and the other contains higher concentration (x=0.5) to be a semiconductor. These layers are periodically stacked to form the superconducting superlattice. These superlattices exhibit same resistivity-temperature curves with the original superconducting film with x=0.15, and the properties are independent of the stacking periodicity in the superlattices. This behavior can be explained by the strong two-dimensional character in the $Bi_2Sr_2(Ca_{1-x}Y_x)Cu_2O_8$ system.

101

Introduction

The $Bi_2Sr_2Ca_{n-1}Cu_nO_{2n+4}$ structures have been controlled using the layer-by-layer growth method. By the application of this technique, the structure which can not be obtained in bulk samples can be prepared. The properties of the artificially constructed superconductor give us a new information about the intrinsic character of this material. In this section, an artificial construction of superconducting superlattice structure is attempted, and the properties are investigated.

The key component of cuprate superconductors is two-dimensional CuO_2 plane. Consequently, the crystal structures[1,2], band structures[3] and the electric conductivities[4-6] of these materials show a strong two-dimensional nature. In order to study the two-dimensional nature in superconductivity, ultrathin films with several nanometer thickness have been used, and worse superconductivity in thinner film has been reported.[7] In such films, however, the effect of the substrate such as lattice mismatch, which deteriorates the superconductivity in the thin layer near the substrate, cannot be neglected. Accordingly, it is indefinite that the observed properties really reflect the intrinsic nature. To avoid this problem, I have examined the superconducting superlattice. The superlattice with periodical stacking of ultrathin layers of superconductor and nonsuperconductor may give us one possible diagnostic to estimate the two dimensional nature of superconductivity without the substrate effect.

In order to evaluate the intrinsic nature of thin

superconducting layer in the superlattice, the lattice matching between superconductor and nonsuperconductor must be good. If not so, the construction of superlattice becomes difficult, and the mismatch deteriorates the superconductivity. I have examined the superlattice based on $Bi_2Sr_2CaCu_2O_8$ with double CuO_2 planes (n=2) structure. This superconductor has hole carriers.[8] Thus, the substitution of trivalent ion such as Y^{3+} for divalent Ca^{2+} decreases the carrier concentration of this system, and high Y concentration changes the superconductor into a semiconductor.[9] So the superlattice can be prepared by the combination of $Bi_2Sr_2(Ca_{1-x}Y_x)Cu_2O_8$ superconducting layer with low Y concentration and semiconducting layer with high Y concentration. Since these two layers have almost same crystal structures and good lattice matching, this combination is suitable for the synthesis of superlattice. This superlattice has a modulation of Y concentration, that is, a modulation of carrier concentration along the c-axis direction. The two-dimensional nature of the superconductivity in $Bi_2Sr_2(Ca_{1-x}Y_x)Cu_2O_8$ is evaluated by the variation of superconducting property against the periodicity of the modulation in the superlattices.

103

Experimental

The superlattices were formed by the applications of layer-by-layer growth and site-selective substitution. $Bi_2Sr_2(Ca_{1-x}Y_x)$-Cu_2O_8 is a stable phase, so this structure can be formed relative easily. Thus, there is no need to separate the structure into four components like the way in Chapter 4. In this experiment, the $Bi_2Sr_2(Ca_{1-x}Y_x)Cu_2O_8$ was constructed by the stacking of two components of Bi-O and Sr-(Ca,Y)-Cu-O. The sintered discs of $Bi_{0.7}Pb_{0.3}O_y$ and $Sr_2Ca_{1-x}Y_xCu_{2.2}O_y$ with x=0.05, 0.15, 0.25 and 0.5 were used to form each layer in $Bi_2Sr_2(Ca_{1-x}Y_x)Cu_2O_8$. A normal film was prepared by stacking of the layers of Bi(Pb)-O and Sr-(Ca,Y)-Cu-O. The cycle of the deposition was repeated in 40 times to form a film. The superlattices were constructed by periodic deposition of $Sr_2(Ca_{1-x}Y_x)Cu_{2.2}O_y$ layer with different yttrium concentrations of x=0.15 and x=0.5 between adjacent Bi(Pb)-O layers. The profile of the formation is shown in Fig.1. The experimental setup has been shown in Chapter 2.

The samples were deposited on MgO (100) substrates under the mixed atmosphere of O_2 (1.5Pa) and N_2O (3.5Pa) with substrate irradiation of ArF laser. Typical thickness of the sample was 60nm. The properties of cuprate superconductors are very sensitive to the carrier concentration[9,10] and the concentration changes with a small variation of oxygen content.[11] Therefore, all the films were annealed at 1113K for 1 hour in O_2 atmosphere after the deposition in a furnace to introduce enough amount of oxygen into the crystal structure.

Resistivity-temperature curves (R-T curves) were measured by

104

standard four-probe method. X-ray diffraction patterns were obtained using CuK_α with $\theta-2\theta$ scanning.

Here, transition midpoint (T_c^{mid}) was used as critical temperature. T_c^{mid} was determined as follows. The R-T curve above T_c was approximated as straight line and extrapolated below T_c. Intersecting point between a half height of the approximated line and R-T curve was defined as T_c^{mid}. This is a normal way of definition of T_c^{mid}.

Result and Discussion

Fig.2 shows the variation of resistivity-temperature curves of normal $Bi_2Sr_2(Ca_{1-x}Y_x)Cu_2O_8$ films versus the change of Y concentration. The concentrations of yttrium at Ca site were 5%, 15% and 25%. These are called Y(5%), Y(15%) and Y(25%), respectively. The x-ray diffraction patterns indicated that all the films consisted of single-phase of $Bi_2Sr_2(Ca_{1-x}Y_x)Cu_2O_8$ with double CuO_2 planes (n=2) in as-grown states. The films were oriented with their c-axes perpendicular to the substrate surfaces. The Y(5%) and the Y(15%) films indicated superconducting transition midpoints of 85K and 65K, and the Y(25%) showed a semiconducting behavior, respectively [see Figs.2(a), 2(b) and 2(c)]. The variation is due to the decrease of carrier concentration with the increase of trivalent Y^{3+} ion at the divalent Ca^{2+} site.[9]

The combination of two kinds of layers of Y(15%) for superconductor and Y(50%) for semiconductor has been selected to fabricate a superlattice with a modulation of carrier concentration. The reason for the selection of Y(15%) as the superconducting layer is that the superconductivity of the Y(15%) layer is very sensitive to the changes of the Y concentration, and yttrium inflow from Y(50%) layer to Y(15%) layer during the sample preparation can be detected by the deterioration of the superconductivity. In the construction of the superlattice, the ratio of the Y(15%) and the Y(50%) layers is fixed at 2:1, and only the periodicity of the stacking has been changed. The superlattices were formed by the repetition of stacking of eight

layers of Y(15%) and four layers of Y(50%), four layers of Y(15%) and two layers of Y(50%), or two layers of Y(15%) and one layer of Y(50%), in which the one layer indicates the layer with 1.5nm thickness corresponding to half of the lattice constant c (3.0nm) of $Bi_2Sr_2(Ca_{1-x}Y_x)Cu_2O_8$ [see Fig.1].

The x-ray diffraction pattern and the calculated intensity for the superlattice with four layers of Y(15%) and two layers of Y(50%) are shown in Fig.3. The calculation was performed on the large unit cell with c-axis of 9.0nm. The equation of the x-ray diffraction intensity has been described in Chapter 3-1.[12,13] The calculated result shows that any satellite peak due to the superstructure should not appears, if the superlattice is really formed. In this superlattice, the satellite peaks are made by only the modulation of Y (and Ca) concentration, but the difference of the scattering factor between Ca^{2+} and Y^{3+} is screened off by the much larger scattering by heavy Bi^{3+}, and satellite peaks do not appear.

The R-T curve for the superlattice of two Y(15%) layers and one Y(50%) layer is shown in Fig.2(d), and the superconducting transition temperatures of the superlattices are summarized in Fig.4 showing transition midpoints (T_c^{mid}) as representatives. The superlattices, even with the periodic stacking of two Y(15%) layers and one Y(50%) layer, exhibit the same resistivity-temperature behavior with the original superconducting film made of only Y(15%) [Figs.2 (b) and (d)]. This result indicates the following two facts. One is that the inter-diffusion of yttrium, which is randomize the effective carrier concentration, did not

107

occur between Y(15%) layers and Y(50%) layers during the sample preparation. If the mixing of yttrium concentration occurs, the average Y concentration is about 27% leading to a semiconducting behavior [Fig.2 (c)]. This is so different from the property of the superlattice [Fig.2 (d)]. The other fact is strong two dimensional nature of the $Bi_2Sr_2(Ca_{1-x}Y_x)Cu_2O_8$ superconductor. The same behavior in the R-T curves of the superlattice and the original Y(15%) superconducting film indicates that the carriers in this system distribute two-dimensionally in each layer. Namely, averaging the carrier concentration across the Bi_2O_2/Sr_2O_2 layer hardly occurs and each layer maintains its own property. Furthermore, no deterioration of superconducting property even in the superlattice with Y(15%):Y(50%)= 2 layers: 1 layer suggests that the ultrathin $Bi_2Sr_2(Ca,Y)Cu_2O_8$ layer with only 3.0nm thickness is sufficient to emerge the superconductivity similar to that of the thick superconducting film. These results show the strong two dimensional nature of superconductivity in Bi-Sr-Ca-Cu-O superconductor.

A model of interactions in $Bi_2Sr_2(Ca,Y)Cu_2O_y$ is shown in Fig.5. The results suggest that the substitution of Y for Ca affects only the nearest CuO_2 planes beside the Ca site. The interaction is strongly blocked by the thick Bi_2O_2/Sr_2O_2 layer and does not reach the next unit-cell. Thus, I call the Bi_2O_2/Sr_2O_2 layer "blocking layer". In the area sandwiched by adjacent blocking layers, the interaction is strong, and that across blocking layer is very weak. This explains the strong two-dimensional nature in $Bi_2Sr_2(Ca,Y)Cu_2O_y$.

Recently, it has been reported in $YBa_2Cu_3O_7/PrBa_2Cu_3O_7$

108

superlattice that the superconductivity of $YBa_2Cu_3O_7$ layer becomes worse when the thickness becomes thinner than 3.6nm. This deterioration will be due to a weak three-dimensional nature in Y-Ba-Cu-O system.[14,15] Blocking layer in Y-Ba-Cu-O system is BaO/CuO(chain)/BaO (refer Chapter 3-1 about the structure of Y-Ba-Cu-O). This blocking layer is thinner than Bi_2O_2/Sr_2O_2 in Bi-Sr-Ca-Cu-O, and includes a CuO chain unit, which has a property similar to the CuO_2 planes. Therefore, the interaction is not blocked effectively by the BaO/CuO/BaO layer, and the two-dimensional CuO_2 planes are softly connected in Y-Ba-Cu-O system, namely weak three-dimensional nature appears. The two or three-dimensional nature of a cuprate superconductor is strongly dependent on the type of blocking layers. The strong two-dimensional nature is a characteristic feature of $Bi_2Sr_2Ca_{n-1}Cu_nO_{2n+4}$ system including Bi_2O_2/Sr_2O_2 blocking layer, I consider.

Conclusion

I have fabricated
$[Bi_2Sr_2(Ca_{0.85}Y_{0.15})Cu_2O_8]_n/[Bi_2Sr_2(Ca_{0.5}Y_{0.5})Cu_2O_8]_m$
superconductor/semiconductor superlattices with n:m = 2:1 in
order to evaluate the two dimensional nature in the high T_c Bi-
Sr-Ca-Cu-O superconductor. The result shows that carriers in
this system have two-dimensional distribution, and an interaction
across the Bi_2O_2/Sr_2O_2 blocking layer is so weak. The
superconducting layer even with 3.0nm thickness has a
superconducting property similar to that of the thick
superconducting film. This behavior seems to be attributed to
the strong two-dimensional nature of the Bi-Sr-Ca-Cu-O system
originated from the two-dimensional crystal structure.

References

(1) F.Izumi, H.Asano, T.Ishigaki, E.Takayama-Muromachi, Y.Uchida, N.Watanabe and T.Nishikawa, Jpn.J.Appl.Phys., 26, L649 (1987).

(2) J.M.Tarascon, Y.Le Page, P.Barboux, B.G.Bagley, L.H.Greene1, W.R.McKinnon, G.W.Hull, M.Giroud and D.M.Hwang, Phys.Rev.B, 37, 9382 (1988).

(3) H.Krakauer and W.E.Pickett, Phys.Rev.Lett., 60, 1665 (1988).

(4) S.J.Hagen, T.M.Jing, Z.Z.Wang, J.Horath and N.P.Ong, Phys.Rev.B, 37, 7928 (1988).

(5) S.Martin, A.T.Fiory, R.M.Fleming, L.F.Schneemeyer and J.V.Waszczak, Phys.Rev.Lett., 60, 2194 (1988).

(6) M.Tachiki and T.Takahashi, Solid State Commun., 72, 1083 (1989).

(7) X.X.Xi, J.Geerk, G.Linker, Q.Li and O.Meyer, Appl.Phys.Lett 54, 2367 (1989).

(8) P.Mandel, A.Poddar, A.N.Das, B.Ghosh, P.Choudhury, Phys.Rev.B, 40, 730 (1989).

(9) T.Tamegai, K.Koga, K.Suzuki, M.Ichihara, F.Sakai and Y.Iye, Jpn.J.Appl.Phys., 28, L112 (1989).

(10) H.Takagi, T.Ido, S.Ishibashi, M.Uota, S.Uchida and Y.Tokura, Phy.Rev.B., 40, 2254 (1989).

(11) K.Takeuchi, M.Kawasaki, M.Yoshimoto, Y.Saito and H.Koinuma, Jpn.J.Appl.Phys., 29, L70 (1990).

(12) K.Imai, I.Nakai, T.Kawashima, S.Sueno and A.Ono, Jpn.J.Appl.Phys., 27, L1661 (1988).

(13) Y.Gao, P.Lee, P.Coppens, M.A.Subramanian and A.W.Sleight, Science, 241, 954 (1988).

(14) J.N.Triscone, O.Fisscher, O.Brunner, L.Antognazza, A.D.Kent

and M.G.Karkut, Phys.Rev.Lett., 64, 804 (1990).

(15) B.Oh, K.Char, A.D.Kent, M.Naito, M.R.Beaseley, T.H.Geballe,
R.H.Hammond, A.Kapitulnik and J.M.Graybeal, Phys.Rev.B, 37, 7861
(1988).

Fig.1   Schematic diagram for the successive depositions to form
Y(15%)/Y(50%) superlattices.
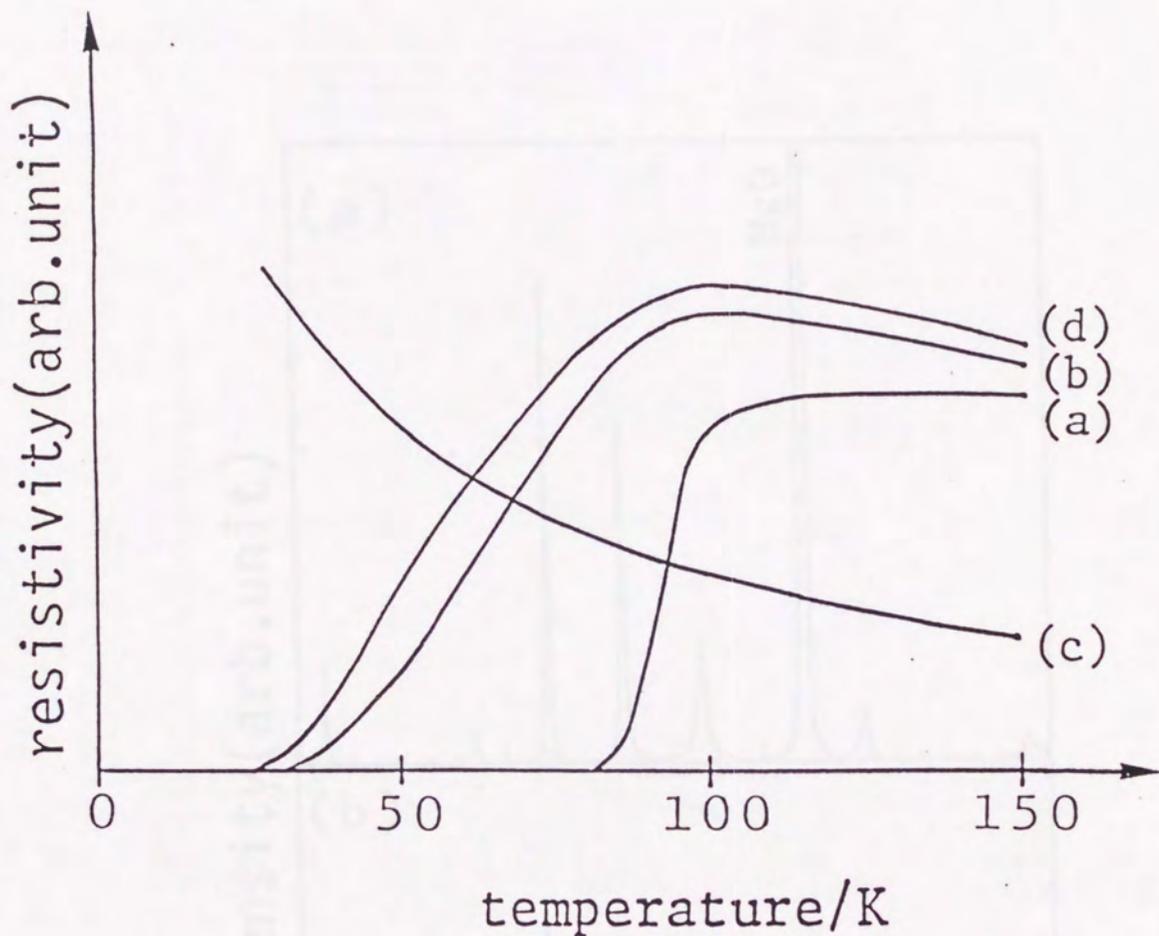
Fig.2 R-T curves of $Bi_2Sr_2(Ca_{1-x}Y_x)Cu_2O_8$ films with (a) x=0.05, (b) x=0.15, (c) x=0.25 and (d) superlattice consisting of the stacking of two layers of Y(15%) and one layer of Y(50%).
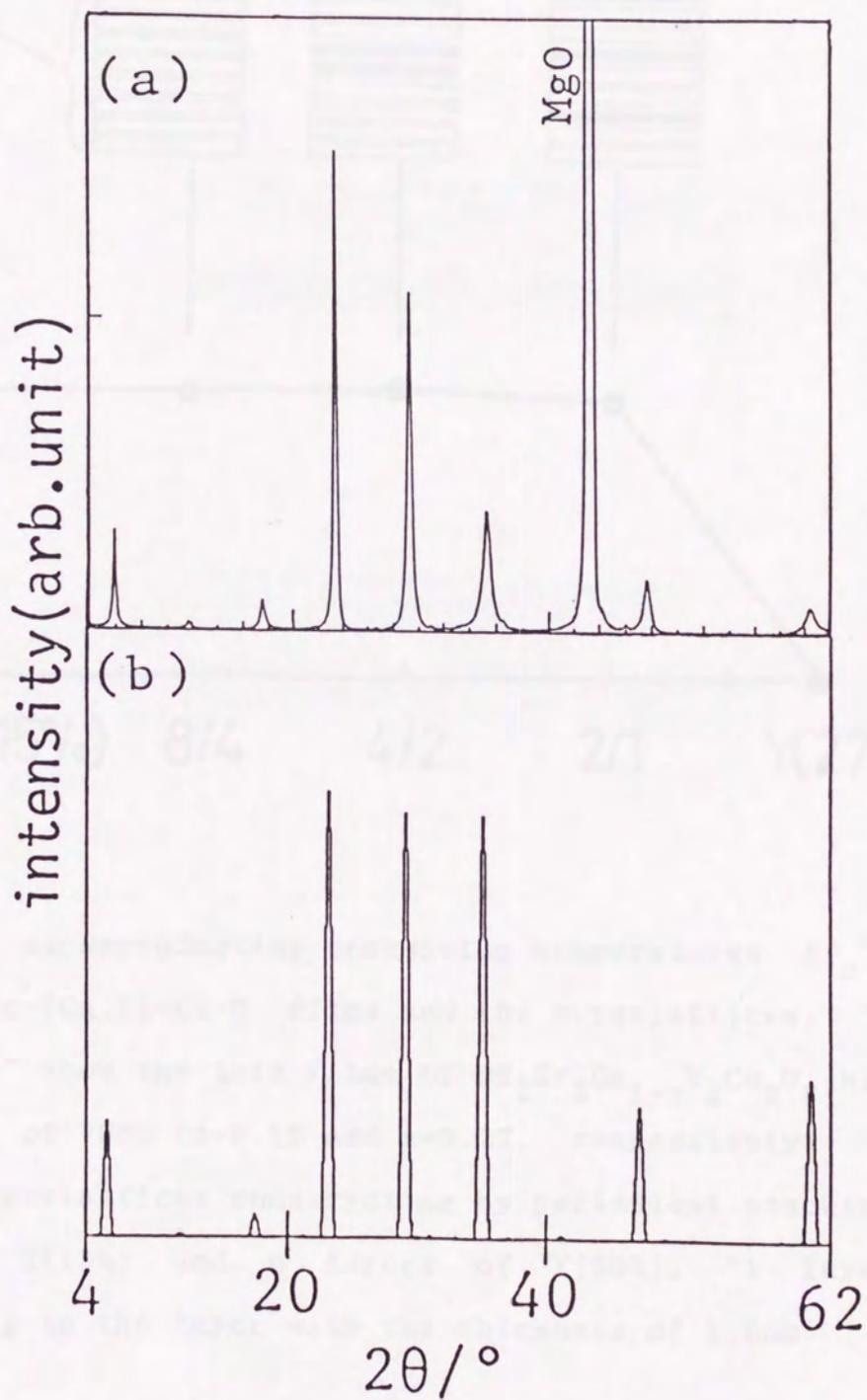
Fig.3 (a) X-ray diffraction patterns and (b) calaculated diffraction pattern for superlattice consisting of the stacking of four layers of Y(15%) and two layers of Y(50%).
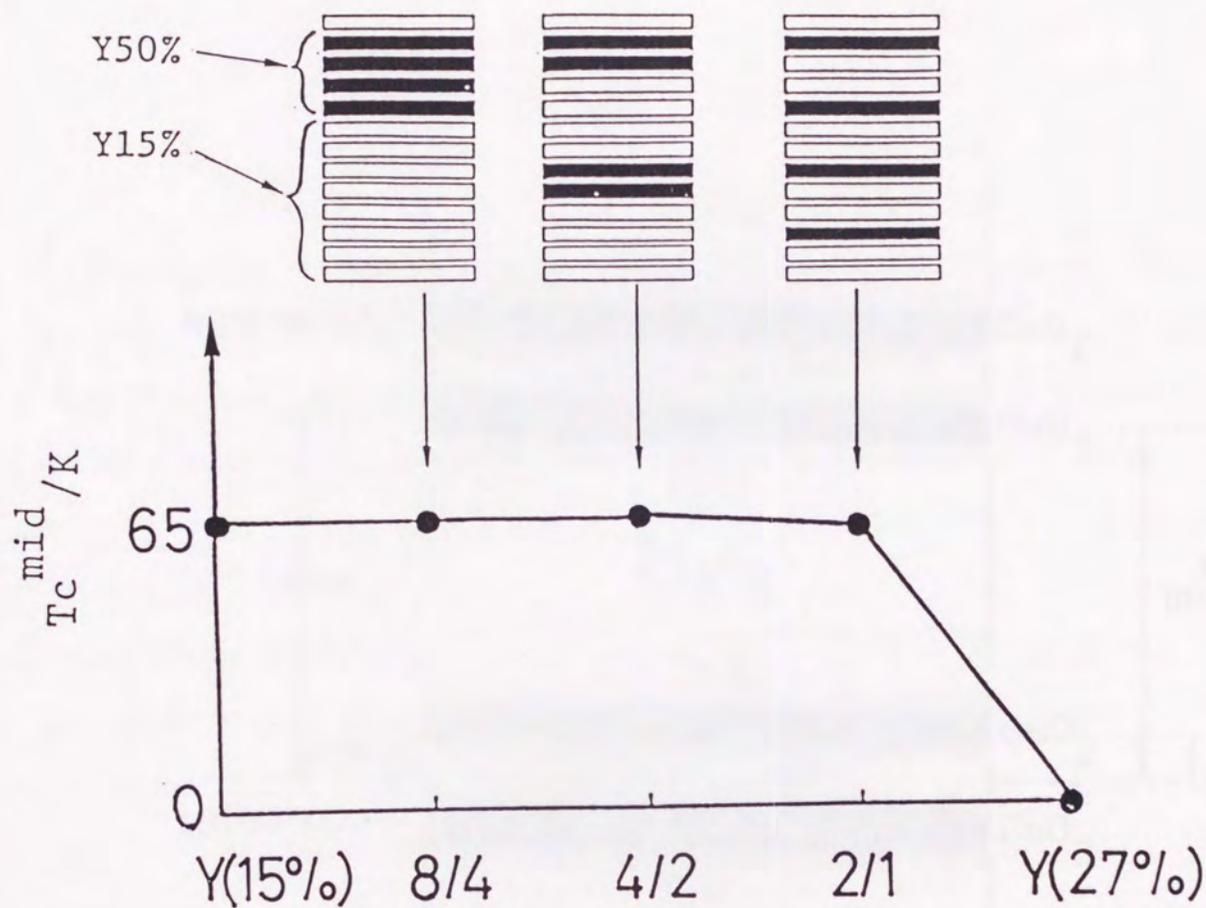
Fig.4   The superconducting transition temperatures (T_c^{mid}) of normal Bi-Sr-(Ca,Y)-Cu-O films and the superlattices. "Y(15%)" and "Y(27%)" show the thin films of $Bi_2Sr_2Ca_{1-x}Y_xCu_2O_8$ with the thicknesses of 75nm (x=0.15 and x=0.27, respectively).   "m/n" shows the superlattices constrycting by periodical stacking of m layers   of Y(15%) and n layers of Y(50%). "1 layer"   is corresponding to the layer with the thickness of 1.5nm.
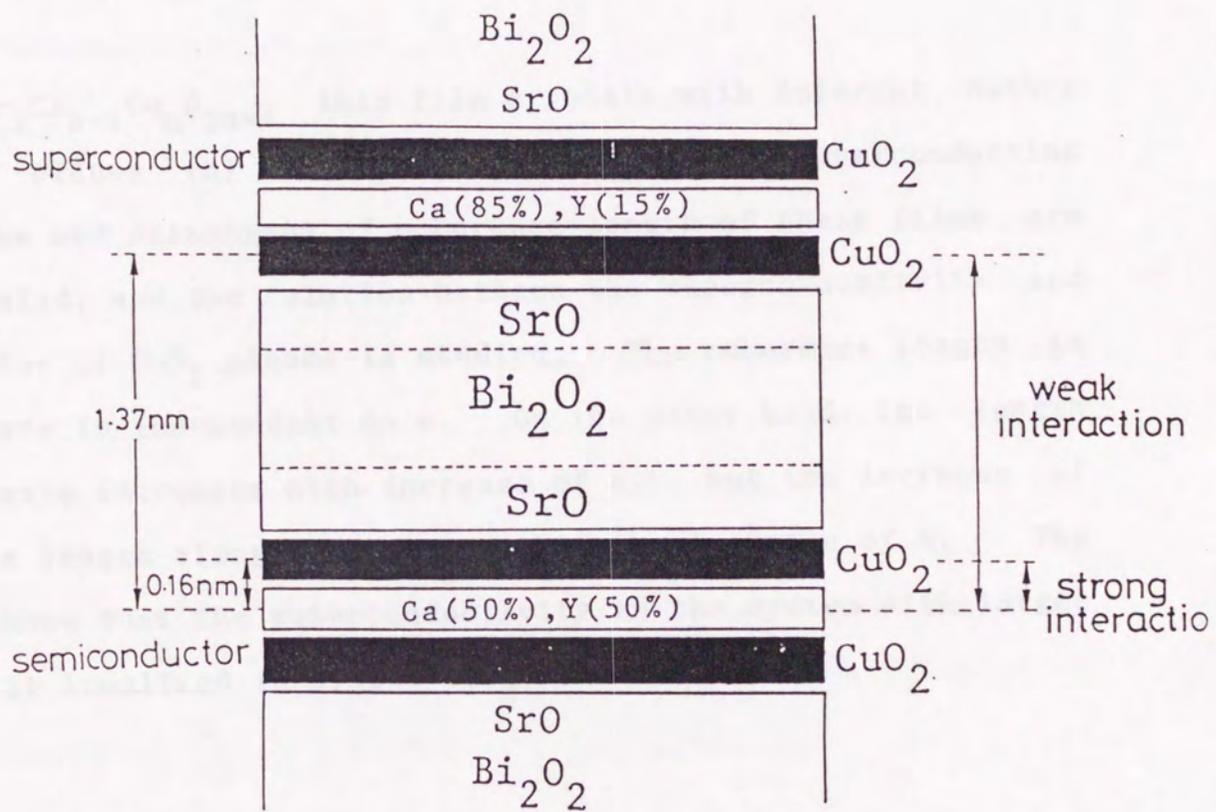
Fig.5 Profile of a model of interactions   in $Bi_2Sr_2(Ca,Y)Cu_2O_8$.

Chapter 5-2:

Superconducting Property and Anisotropy of Coherence Length in $Bi_2Sr_2Ca_{n-1}Cu_nO_{2n+4}$

Abstract

$Bi_2Sr_2Ca_{n-1}Cu_nO_{2n+4}$ thin film crystals with deferent number of CuO_2 planes (n) have been grown. The superconducting properties and anisotropy of coherence length of these films are investigated, and the relation between the superconductivity and the number of CuO_2 planes is studied. The coherence length in CuO_2 plane is independent on n. On the other hand, the length along c-axis increases with increase of n, but the increase of coherence length along c is slower than the increase of n. The result shows that the superconductivity in the system with larger n is still localized in single CuO_2 plane.

113

Introduction

The property of the superconducting superlattice shows a strong two-dimensional nature of $Bi_2Sr_2CaCu_2O_8$ as shown in Chapter 5-1. The two-dimensional nature will be attributed to the two-dimensional crystal structure, especially due to the Bi_2O_2/Sr_2O_2 blocking layer. In this section, the superconductivity in $Bi_2Sr_2Ca_{n-1}Cu_nO_{2n+4}$ with different n was studied. This system has the same blocking layer, so the change of the superconductivity with the variation of n can be observed. For the quantitative evaluation of two-dimensional nature, the coherence length is estimated from the transition broadening under magnetic field using anisotropic Ginzburg-Landau theory. Coherence length means the spatial expanse of Cooper pair in superconductors.[1-3] From the superconductivity and the anisotropy of coherence length, intrinsic characters of superconductivity in this system are discussed.

114

The growth of $Bi_2Sr_2Ca_{n-1}Cu_nO_{2n+4}$ thin film crystal has been described in Chapter 4. The coherence length (ξ) was obtained by following way. Resistivity-temperature curves were measured in magnetic field by standard four-probe technique, and the relation between the critical temperature (T_c) and the magnetic field was obtained. The magnetic field was generated by a superconducting magnet, and the maximum field was 7.5T. Critical field (H_{c2}) was defined by the applied magnetic field. The value of $-dH_{c2}/dT$ was obtained from the slope in T_c-H_{c2} curve. This value is dependent on the direction of the magnetic field, and two values were obtained. One is for the magnetic field parallel to the c-axis of the film, and the other for the field perpendicular to the c-axis. From the value of $-dH_{c2}/dT$, H_{c2} at 0K ($H_{c2}(0)$) was estimated by the extrapolation using Werthamer-Helfand-Hohenberg theory.[2] The relation is given by following equation.

$$H_{c2}(0)=0.69T_c(-dH_{c2}/dT)_{Tc} \qquad (1)$$

The relation between the coherence length (ξ) and H_{c2} is given by Ginzburg-Landau theory.[3] The equation (2) is obtained by the solving linearized Ginzburg-Landau equation under static and homogenous magnetic field.[5] The maximum magnetic field (H_{c2}) satisfying the Ginzburg-Landau equation is

$$H_{c2}(0)=\Phi_0/(2\pi\xi^2(0)) \qquad (2)$$

where Φ_0 is flux quantum. By the consideration of anisotropy ($\xi_a=\xi_b\neq\xi_c$), eq.(2) leads to

$$\xi_a^2(0)=\Phi_0/(2\pi H_{c2}(0)) \qquad (3)$$

$$\xi_c(0)=\Phi_0/(2\pi H_{c2}(0)\xi_a(0)) \qquad (4)$$

From eqs.(1), (3) and (4), the coherence length in ab plane (ξ_a)
and that along c-axis (ξ_c) were estimated.

Results and Discussion

The resistance-temperature curves under magnetic field of $Bi_2Sr_2Ca_2Cu_3O_{10}$ thin film are shown in Fig.1. The magnetic field was varied between 0T and 7.5T, and the direction of the field is parallel to the c-axis [Fig.1(a)] or perpendicular to the c-axis [Figs.1(b)]. Here, the transition midpoint (T_c^{mid}) was used as transition temperature, because T_c^{mid} corresponds to the transition temperature defined by mean-field theory.[6] The variation of T_c^{mid} versus magnetic field is shown in Fig.2. The obtained data can be approximated by a linear line. Thus, the critical magnetic field at 0K ($H_{c2}(0)$) can be estimated using equation (1), and coherence length can be calculated by anisotropic Ginzburg-Landau theory [eqs.(3) and (4)]. The calculated coherence lengths in $Bi_2Sr_2Ca_{n-1}Cu_nO_{2n+4}$ with n=2 to 4 are shown in Fig.3. The coherence length in ab plane is almost independent of the number of CuO_2 plane (n). On the other hand, that along the c-axis has a tendency to be lengthened with increase of n. This behavior can be understood qualitatively from the viewpoint of the crystal structures in this system. The fundamental component of high T_c superconductivity is two-dimensional CuO_2 plane, thus the coherence length in ab plane shows that in the CuO_2 plane. The crystal structures of this system have same CuO_2 networks in ab plane, even if the number of CuO_2 is different. Therefore, the same coherence lengths in ab planes are very reasonable. Along the c-axis, however, the interaction is blocked by the Bi_2O_2/Sr_2O_2 blocking layer as shown in Chapter 5-1. The distance between the adjacent blocking

117

layers becomes larger with the increase of n, so the coherence length along the c-axis will be elongated. The coherence length in ab plane obtained here was about 3.5nm, and that along c ranged 0.13nm for n=2 and 0.18nm for n=4. The values show that the superconducting anisotropy is decreased with increase of n in this system, but the system with n=4 still has a strong two-dimensional character in the superconductivity

The result also shows that the coherence length along c is not proportional to the number of CuO_2 planes and saturates in the system with larger n. Quantitatively, the value along c-axis is so small. The distance between the nearest CuO_2 planes is about 0.32nm. The coherence length is smaller than that distance. This result shows that the superconductivity in this system occurs in each CuO_2 plane, separately [see Fig.4].

The transition temperature (T_c) of $Bi_2Sr_2Ca_{n-1}Cu_nO_{2n+4}$ has maximum value for n=3 and 4. For n=5, T_c decreases below 30K[7], and the superconductivity has not been observed for the system with n > 5. However, I observed the superconducting transition in $Bi_2Sr_2Ca_6Cu_7O_{18}$ (n=7) thin film crystal, recently. The x-ray diffraction pattern and R-T curve for n=7 are shown in Fig.5 and Fig.6, respectively, The variation of T_c with increase of n is shown in Fig.7 This result gives another evidence for the two-dimensional superconductivity of this system.

The decrease of T_c in the system with larger n has been usually explained as follows. The properties in cuprate superconductors have very strong correlation with carrier concentration.[8] The system is antiferromagnetic insulator in

118

the area with low carrier concentration. With increase of carrier, the system becomes superconductor, and superconducting transition temperature increases. At the proper carrier concentration, T_c has a maximum value and decreases above the concentration. At much higher concentration, the system becomes normal metal. In $Bi_2Sr_2Ca_{n-1}Cu_nO_{2n+4}$ system, the hole carrier is supplied by the excess oxygen in Bi_2O_2 layer, so the carrier concentration per unit cell must be constant independent of the number of CuO_2. For this reason, the carrier per CuO_2 plane decreases with increase of the number of CuO_2 planes. This is a usual explanation for the decrease of T_c. The superconductivity for n=7 in Fig.6, however, shows that this explanation is insufficient, because the carrier concentration per CuO_2 plane is very low for n=7 system leading to a semiconducting behavior in common sense. This result shows that the carrier distribution is inhomogeneous in the system with larger n, and the carrier concentration is different in each CuO_2 plane. Namely, the system with larger n has both superconducting CuO_2 layer and semiconducting CuO_2 layer in one unit cell. This speculation also explains the saturation of ξ_c with increase of n. In the system with large n, the superconductivity appears not in all CuO_2 planes but in a part of CuO_2, so the coherence length is not proportional to the number of CuO_2 planes. From these results, I consider that the cause of the strong two-dimensional nature in $Bi_2Sr_2Ca_{n-1}Cu_nO_{2n+4}$ system is not only the effect of Bi_2O_2/Sr_2O_2 blocking layer but also the effect of inhomogeneous carrier distribution. The calculation based on Madelung potential shows the carriers exist only in the CuO_2 planes nearest to the Bi_2O_2

119

plane [see Chapter 5-3]. This calculation supports the speculation that the carriers non-uniformly distribute in this system, and the superconductivity occurs in each CuO_2 plane separately.

In the area with n=1 to 3, the T_c of this system increase with increase of n, but the reason is not clear in this step. I consider that the interaction between adjacent CuO_2 layers is determining factor in this area. Actually, some workers suggest the explanation based on such interaction.[9] In general, the interaction between CuO_2 planes is weak[10]. Thus it works only between the nearest CuO_2 planes, and does not reach the next unit cell beyond the blocking layer. Therefore, such interaction is almost same in the system with n>3, and in this area, the carrier concentration will be the determining factor of T_c.

120

Conclusion

The superconducting properties of $Bi_2Sr_2Ca_{n-1}Cu_nO_{2n+4}$ with different n were studied. The anisotropy of coherence length shows very strong two-dimensional nature and suggests that the superconductivity appears in each CuO_2 plane separately. The coherence length in ab plane is about 3.5nm, and that along c-axis is 0.13nm for n=2 and 0.18nm for n=4. Qualitatively, the variation of coherence length along c is explained by the variation of the distance between blocking layers, but for the quantitative explanation, it is necessary to take into account the inhomogeneous carrier-distribution. The observed super-conductivity for n=7 system is also explained by the same consideration. The strong two-dimensional nature in this system is attributed to the effect of the Bi_2O_2/Sr_2O_2 blocking layer and non-uniform distribution of the carriers.

References

(1) L.N.Cooper, Phys.Rev., 104, 1189 (1956).

(2) J.Bardeen, L.N.Cooper and J.R.Schrieffer, Phys.Rev., 108, 1175 (1957).

(3) V.L.Ginzburg and L.D.Landau, Zh.Eksperim.i Teo.Fiz., 20, 1064 (1950).

(4) N.R.Werthamer, E.Helfand and P.C.Hohenberg, Phys.Rev, 147, 295 (1966).

(5) M.Tinkham, Introduction to Superconductivity, (McGraw-Hill, New York, 1975).

(6) M.A.Paalanen and A.F.Fiory, Appl.Phys.Lett., 45, 794 (1984).

(7) I.Tsukada and K.Uchinokura, Jpn.J.Appl.Phys, 30, L1114 (1991).

(8) J.B.Torrance, Y.Tokura, A.I.Nazzal, A.Bezinge, T.C.Huang and S.S.P.Parkin, Phys.Rev.Lett., 61, 1127 (1988).

(9) J.M.Wheatley, T.C.Hsu and P.W.Anderson, Nature, 333, 121 (1988).

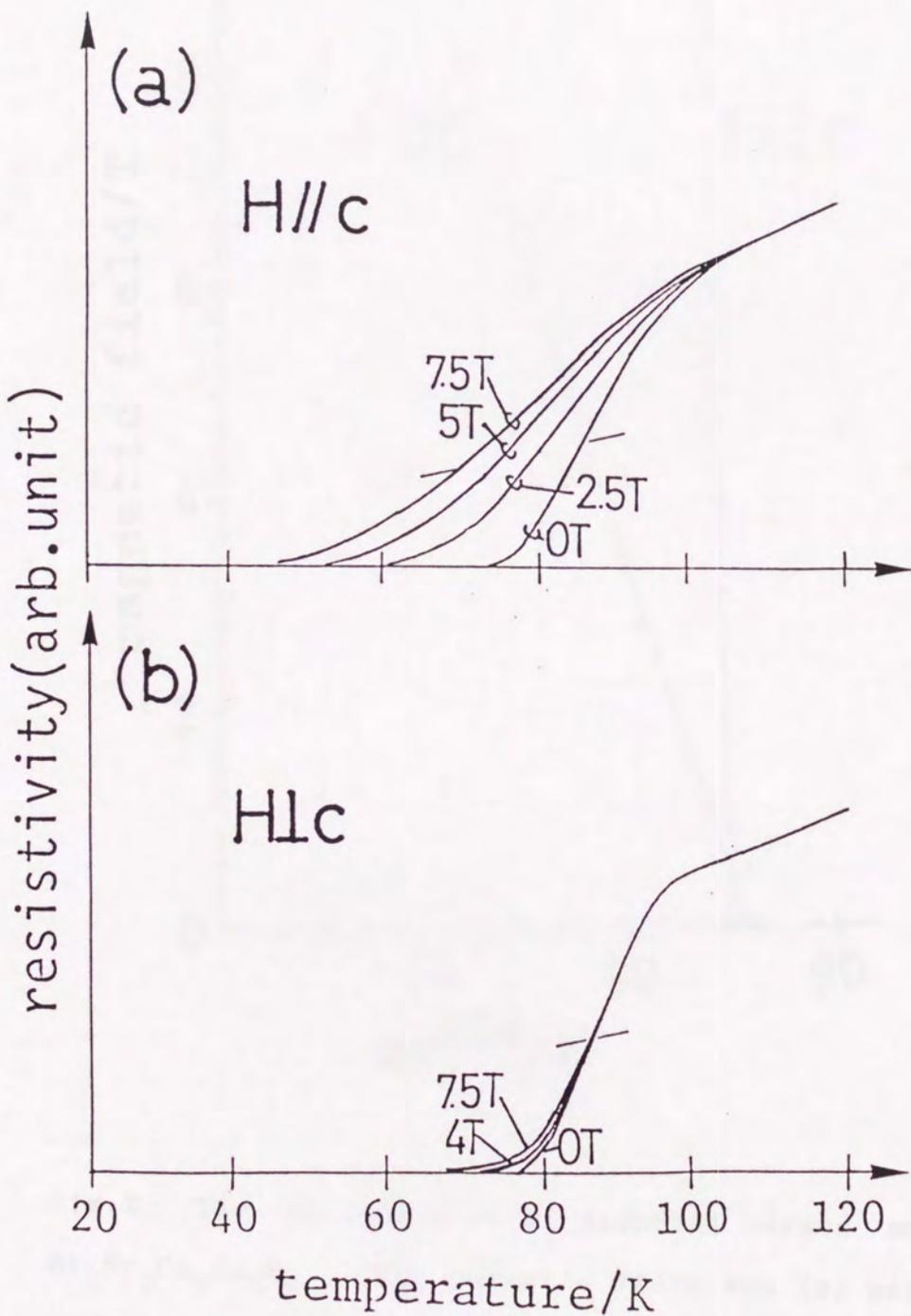(10) H.Kadowaki, M.Nishi, Y.Yamada, H.Takeya, H.Takei, S.M.Shapiro and G.Shirane, Phys.Rev.B, 37, 7932 (1988).

Fig.1   R-T curves of $Bi_2Sr_2Ca_2Cu_3O_{10}$ thin films   under   magnetic field (a) parallel to c-axis (b) perpendicular to c-axis.

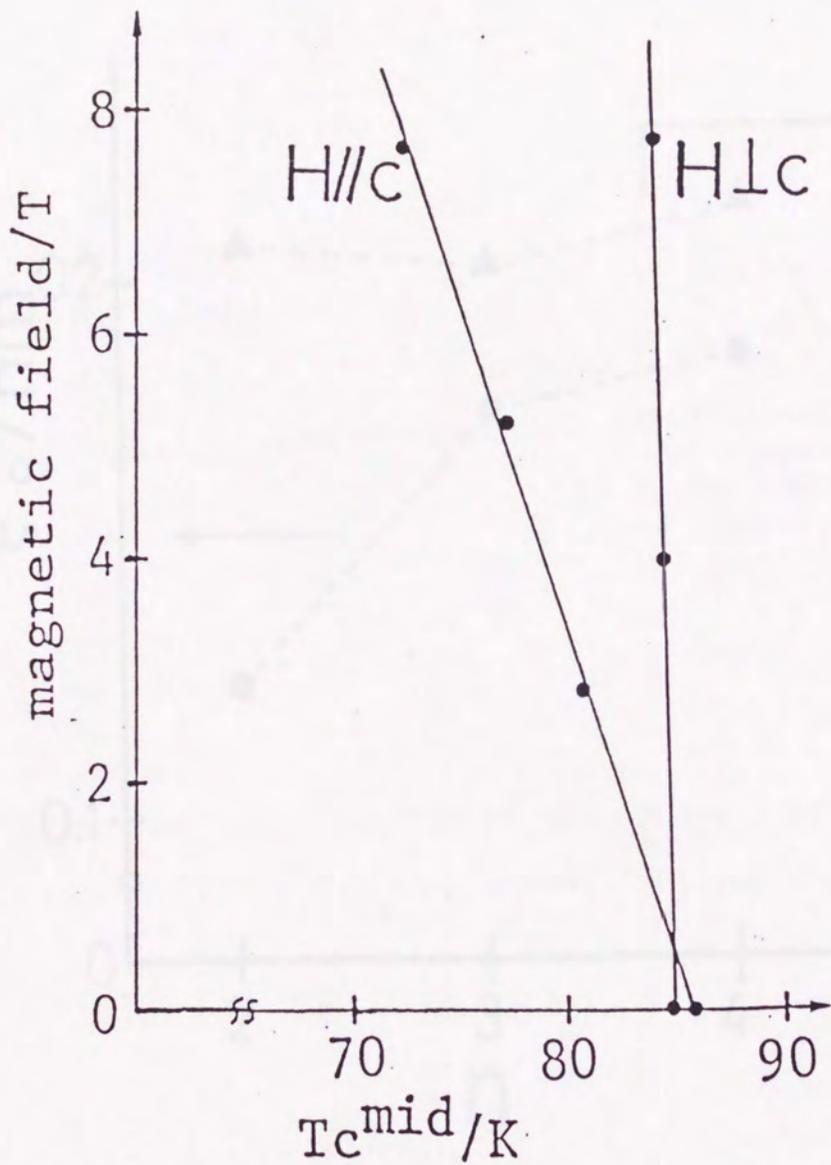Fig.2 The variation of T_c midpoint versus magnetic field in $Bi_2Sr_2Ca_2Cu_3O_8$. The magnetic field was (a) parallel to c-axis, and (b) perpendicular to c-axis.
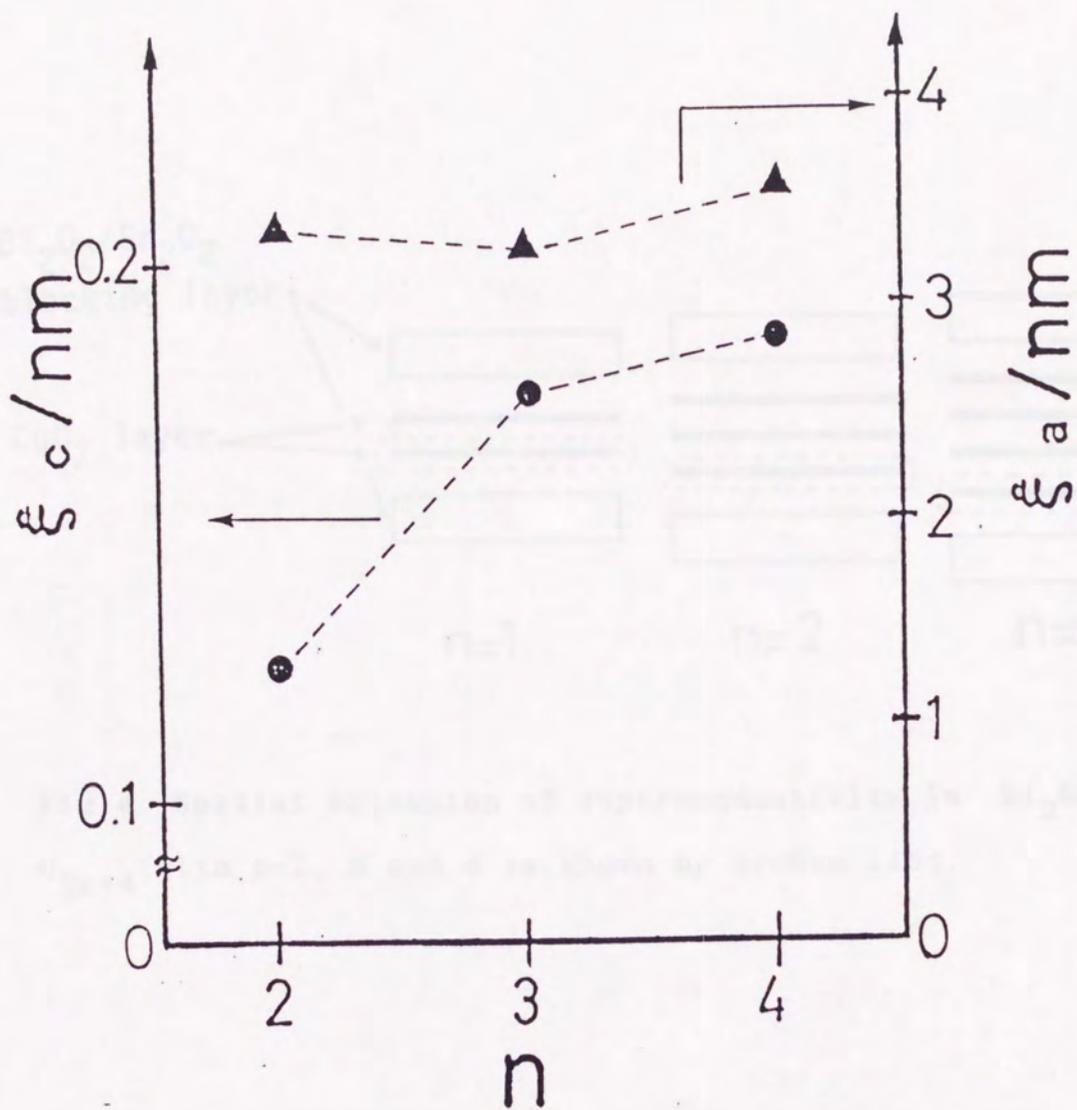
Fig.3 The coherence length in ab plane (ξ_a) and along c-axis (ξ_c) of $Bi_2Sr_2Ca_{n-1}Cu_nO_{2n+4}$ with n=2,3 and 4.

Bi$_2$O$_2$/Sr$_2$O$_2$
blocking layer

CuO$_2$ layer

n=1   n=2   n=3
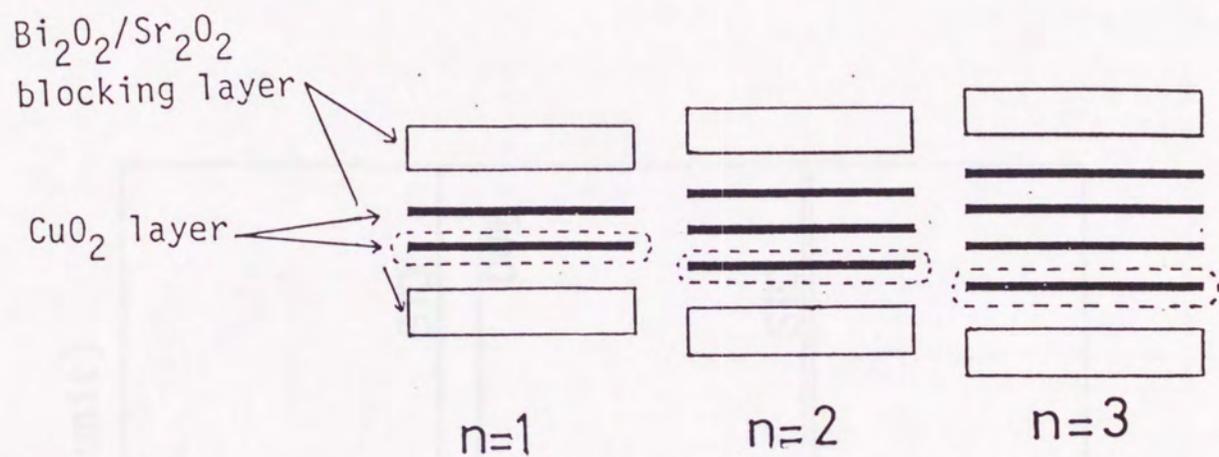
Fig.4   Spatial extension of superconductivity in   Bi$_2$Sr$_2$Ca$_{n-1}$Cu$_n$O$_{2n+4}$ with n=2, 3 and 4 is shown by broken line.
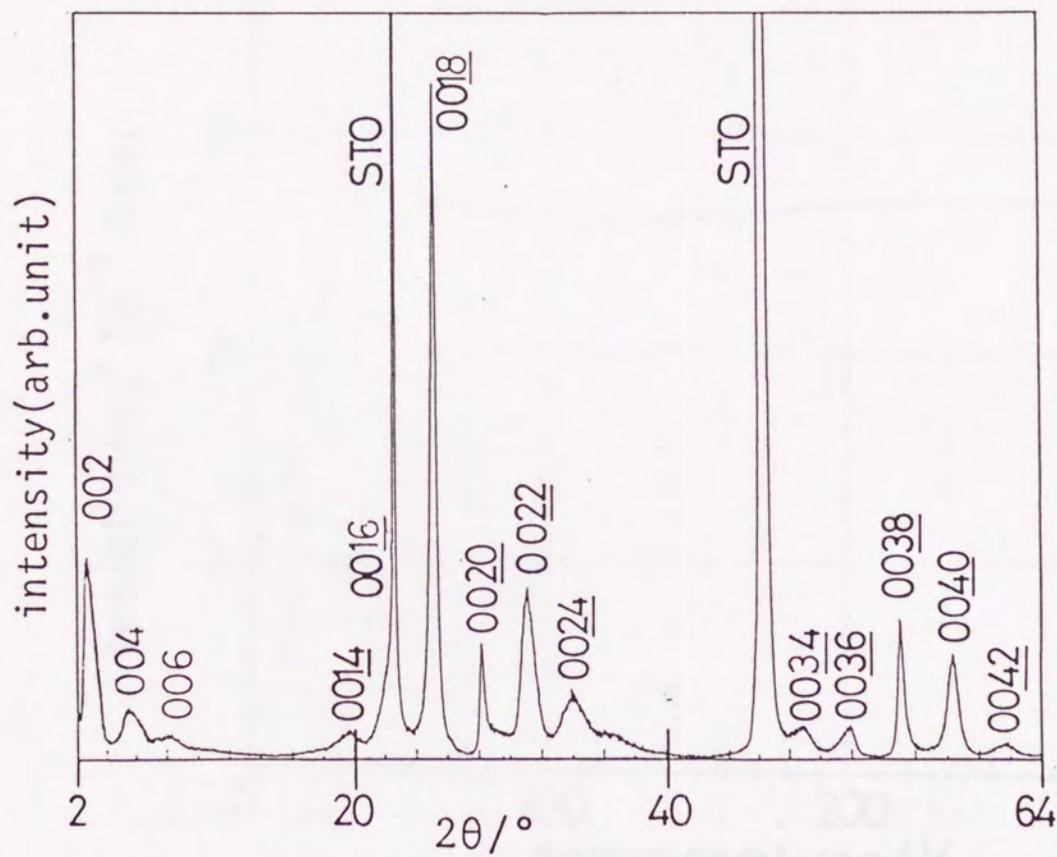
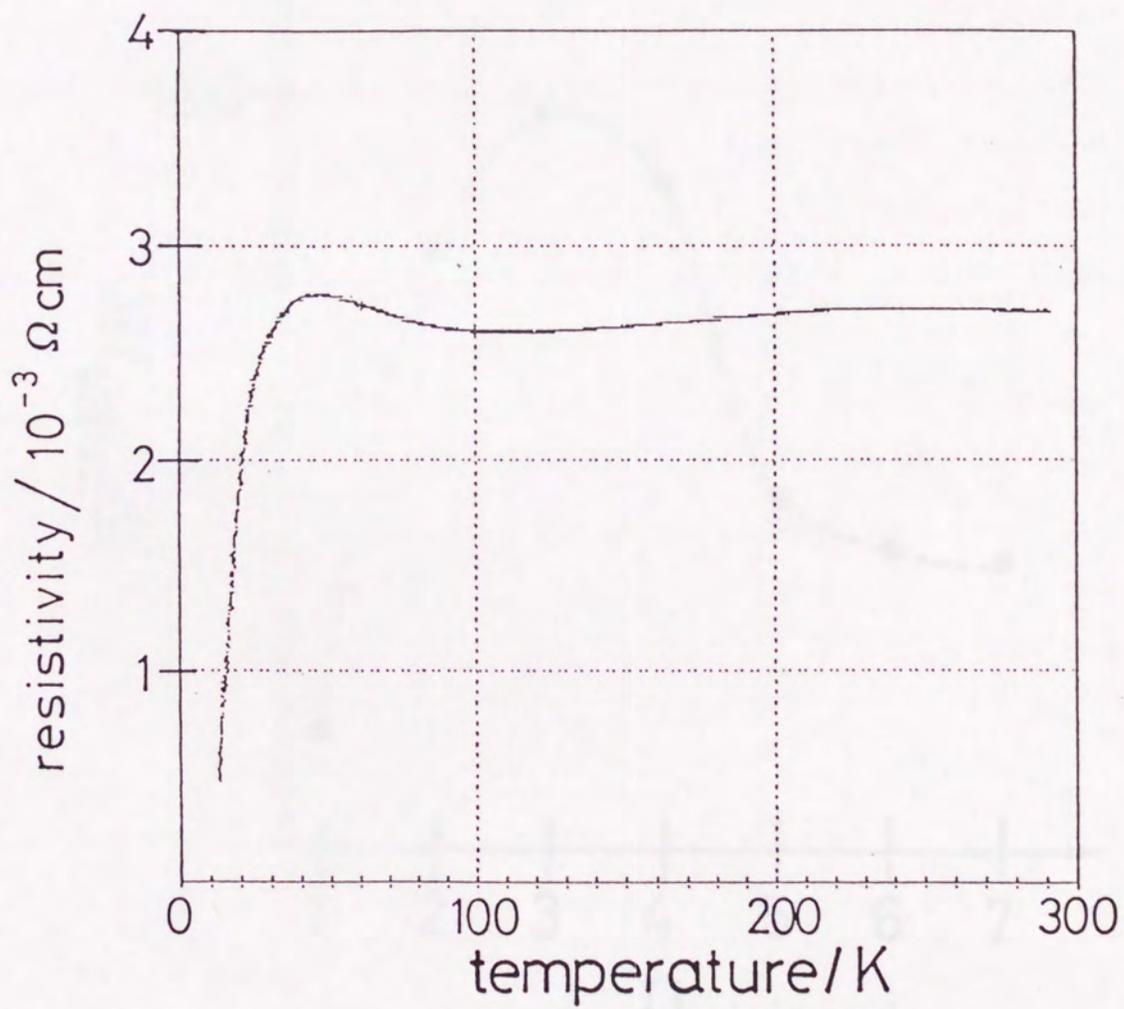Fig.5 X-ray diffraction pattern of $Bi_2Sr_2Ca_6Cu_7O_{18}$ thin film with n=7.
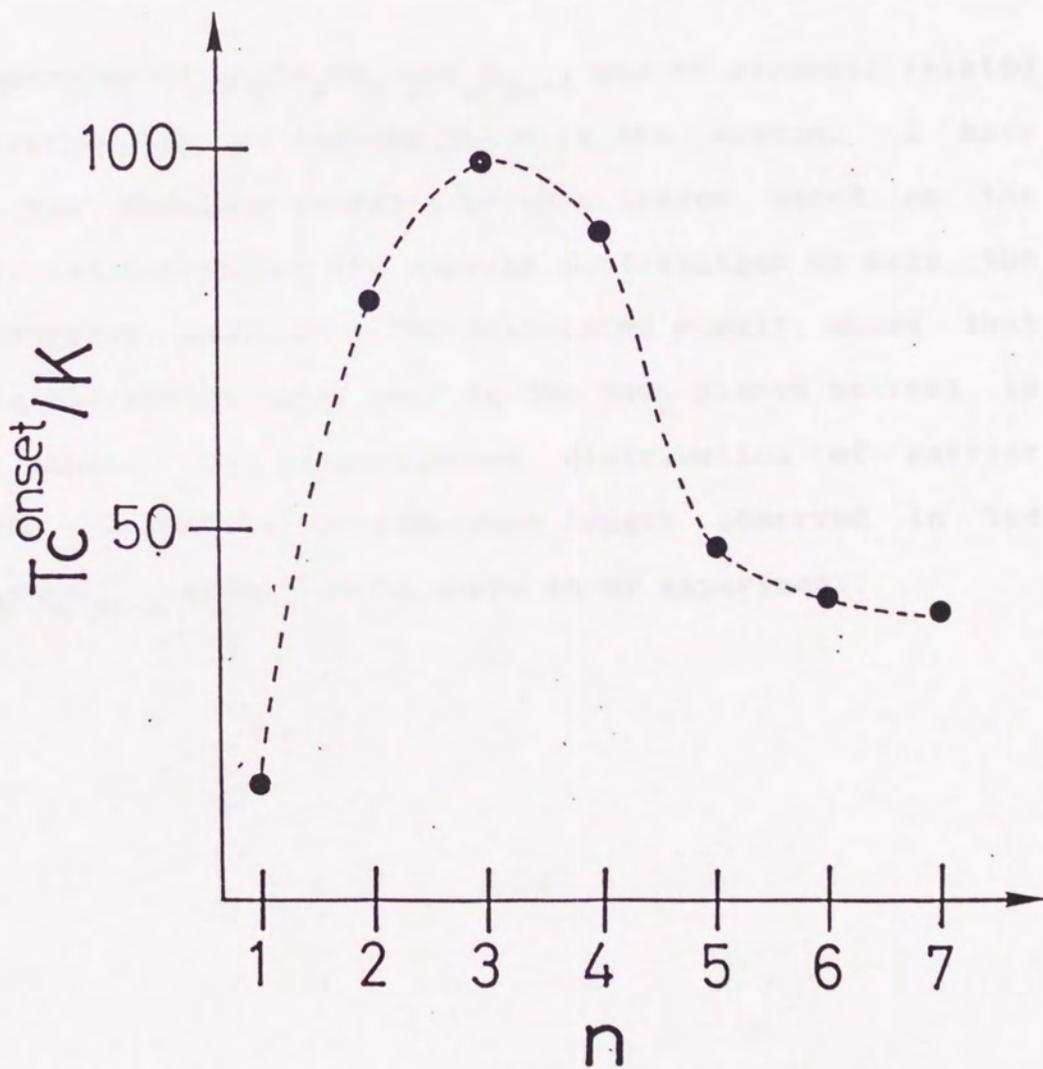
Fig.6 R-T curve of $Bi_2Sr_2Ca_6Cu_7O_{18}$ thin film with n=7.

Fig.7 Variation of superconducting transition temperature (T_c) in $Bi_2Sr_2Ca_{n-1}Cu_nO_{2n+4}$ with change of n.

Chapter 5-3:

Charge Distribution Based on the Calculation of Madelung Energy
and the Superconductivity in $Bi_2Sr_2Ca_{n-1}Cu_nO_{2n+4}$

Abstract

The properties of $Bi_2Sr_2Ca_{n-1}Cu_nO_{2n+4}$ may be strongly related
to the distribution of carrier holes in the system. I have
calculated the Madelung energies of this system based on the
ionic model, and determined the carrier distribution to make the
Madelung energies smallest. The calculated result shows that
carriers in the system exist only in the CuO_2 planes nearest to
the Bi_2O_2 layer. The inhomogeneous distribution of carrier
agrees with the behavior of coherence length observed in the
$Bi_2Sr_2Ca_{n-1}Cu_nO_{2n+4}$ thin-film crystals in my experiment.

Introduction

The observed superconducting behavior in $Bi_2Sr_2Ca_{n-1}Cu_nO_{2n+4}$ thin film crystals showed the strong two-dimensional nature of this system, and I concluded that the two-dimensional nature should be attributed to the inhomogeneous carrier distribution. In order to support this consideration, charge distribution has been calculated for $Bi_2Sr_2Ca_{n-1}Cu_nO_{2n+4}$ with different n. From the standpoint that these oxides are essentially ionic crystals, I considered that the determining factor of charge distribution in this system was Madelung energy. The distribution was determined to make the energy minimum has good agreement with my speculation.

Calculation

The basic concept of the calculation is shown below. In $Bi_2Sr_2Ca_{n-1}Cu_nO_{2n+4}$ system, excess oxygen in Bi_2O_2 layer supplied the hole carriers.[1,2] I assumed that the amount of excess oxygen is independent of the number of CuO_2 planes (n), so the carrier concentration per unit-cell is constant independently of n. It has been confirmed that the holes in this system exist at oxygen sites by electron energy loss and x-ray absorption experiment.[3,4] Thus, a constant amount of hole is injected to oxygen sites, and the distribution of hole is determined to make the Madelung energies minimum.

The calculation of Madelung energies followed the way used by Kondo et al.[5] Let Q_i be the average charge on the i site, where i may be Bi, Sr, Ca, Cu, O(1) to O(n). Let α_i be the number of equivalent sites for i species in the unit-cell. From charge neutrality,

$$\Sigma \alpha_i Q_i = 0 \qquad (1)$$

Let U_i be the Madelung potential at i site, which is linear function of Q_i's under the restriction (1).

$$U_i = \Sigma c_{ij} \alpha_j Q_j) \qquad (2)$$

The Madelung energy per unit-cell is given by

$$E_M = (\Sigma c_{ij} \alpha_i \alpha_j Q_i Q_j)/2 \qquad (3)$$

It should be mentioned that c_{ij} is not the potential at the i site for the charge distribution such that $\alpha_i Q_i = 1$ and other Q's=0. Such a charge assignment violates eq.(1). Instead of that, I used $\alpha_i Q_i = 1$, $\alpha_j Q_j = -1$ and other Q's=0. Under this condition, eq.(2) gives

125

$$U_i = c_{ii} - c_{ij} = b_{ij} \qquad (4)$$

Only such a difference between c's is meaningful. Using b_{ij} defined by eq.(4), following equations are obtained

$$U_i = \Sigma b_{ij} \alpha_j Q_j \qquad (5)$$
$$E_M = (\Sigma b_{ij} \alpha_i \alpha_j Q_i Q_j)/2 \qquad (6)$$

under the restriction of eq.(1). So the calculation of b_{ij} is necessary to treat the Madelung energies.

In $Bi_2Sr_2Ca_{n-1}Cu_nO_{2n+4}$ system, excess oxygen is included in Bi_2O_2 layer and the oxygens supply the hole carrier into the system. The excess oxygen, however, forms a complicated modulated structure[1,6], so it makes the calculation very difficult. Thus, I assumed the simple tetragonal structure for the calculation [see Fig.1]. Instead of the incorporation of excess oxygen, Bi^{3+} or O^{2-} in Bi_2O_2 layers is replaced by $Bi^{3-\delta}$ or $O^{-2-\delta}$, and the hole carriers are supplied to compensate the δ. For both replacements, the almost same result was obtained. Thus, I considered that the effect of excess oxygen in Bi_2O_2 layer could be treated by these replacements.

In this calculation, the hole concentration per unit-cell was fixed at 1.2. In $Bi_2Sr_2CaCu_2O_8$, this value is corresponding to a formal charge of Cu of +2.3, which is consistent with the value obtained from the Hall coefficient of this material.[7] Under that condition, Q_1 at the oxygen site was varied with the restriction of eq.(1) and the charge distribution is determined to make the energies minimum.

Result and Discussion

Here, the calculated result for $Bi_2Sr_2Ca_2Cu_3O_{10}$ (n=3) crystal is shown. This phase has four inequivalent oxygen and two Cu sites in the structure [see Fig.1].

O(1): oxygen in inner CuO_2 plane, which is far from Bi_2O_2 layer

O(2): oxygen in outer CuO_2 plane, which is nearer to Bi_2O_2

O(3): oxygen in SrO layer, which is apex oxygen of Cu

O(4): oxygen in Bi_2O_2 layer

Cu(1): copper in inner CuO_2

Cu(2): copper in outer CuO_2

The coefficients of b_{ij} for this structure are calculated by eq.(4). The obtained result is listed in Table 1.

For the calculation of the Madelung potential of each site, the nominal charge of each ion is assumed as +3 for Bi, +2 for Sr, Ca and Cu, and -2 for oxygen. The potential obtained by eq.(5) is listed in Table 2. They are the potentials for an electron in units of eV. Table 2 indicates that the potential in CuO_2 plane (U_{Cu}, U_{O1}, U_{O2}) are much higher than those in BiO plane (U_{Bi}, U_{O4}) or SrO layer (U_{Sr}, U_{O3}). Therefore, the consideration that the hole carrier with positive charge is distributed at CuO_2 is natural. However, the potential at O(1) in inner CuO_2 is very close to that at O(2) in outer CuO_2, so the further calculation is necessary to determine the carrier distribution.

When the hole carriers are supplied to O(1) and O(2) sites, the charges at the oxygen sites are given by

$$Q_{O1} = -2 + n_1$$
$$Q_{O2} = -2 + n_2$$
(7)

where n_1 and n_2 are hole content of the oxygen site. The carrier concentration was assumed to be 1.2 per unit-cell, and one unit-cell includes four O(1) and eight O(2) ions. Therefore, the equation

$$4n_1 + 8n_2 = 1.2$$
(8)

must be satisfied. From the charge neutrality, the charge at Bi site should be +2.7. (Instead of that, the charge of -2.3 at O(4) site is also possible, but these give the almost same result.)

$$Q_{Bi} = 2.7$$
(9)

Under the condition with eqs.(7), (8) and (9), the n_1 and n_2 are determined to make the eq.(6) minimum. The calculation showed that the minimum energy was given when all the hole existed at the outer O(2) site. The similar result was obtained for the system with larger n value, and holes are supplied only to the most outer CuO_2 plane. This behavior was independent of the number of CuO_2 planes. The results for n=2 to 4 are shown in Fig.2.

The cause of this behavior is that the hole supplier of this system exists at Bi_2O_2 layer. From the viewpoint of Madelung energy, it is hopeful that the hole carriers are close to the hole supplier. The calculation of hole distribution based on the Madelung energies is too simple and has a tendency to localize the carrier at single site. It is difficult to believe that such non-uniform distribution of carrier exists in the real crystal, and the distribution of holes will spread over the next

128

CuO$_2$ planes.   The Coulomb interaction, however, is the most important factor to determine the charge distribution in ionic solids, so the tendency of inhomogeneous charge-distribution must remain in the real system. I consider that a large part of holes in this system exists at oxygen site in outer CuO$_2$ plane, and in Bi$_2$Sr$_2$Ca$_{n-1}$Cu$_n$O$_{2n+4}$ with larger n, both superconducting CuO$_2$ layer with rich carriers and semiconducting layer with poor carriers are generated inside one unit-cell.   This consideration is very consistent with the superconducting behavior observed in this system.   This calculation shows that the speculation shown in   Chapter 5-2, which is that the inhomogeneous charge distribution   causes   the   strong   two-dimensional   nature,   is appropriate.

Conclusion

The charge distribution in $Bi_2Sr_2Ca_{n-1}Cu_nO_{2n+4}$ was estimated from the Madelung potential. The simple calculation shows that the hole carrier of this system is injected to the CuO_2 plane and not to SrO or BiO plane. In the system with larger n, a large amount of the holes exists at the oxygen site in the most outer CuO_2 plane, which is the plane nearest to the Bi_2O_2 layer. The non-uniform distribution of the carrier is consistent with the two-dimensional superconductivity of this system.

References

(1) K.Takeuchi, M.Kawasaki, M.Yoshimoto, Y.Saito and H.Koinuma, Jpn.J.Appl.Phys, 29, L70 (1990).

(2) C.C.Torardi, J.B.Parise, M.A.Sablamanian, J.Gopalakrishnan and A.W.Sleight, Physica C, 157, 115 (1989).

(3) H.Matsuyama, T.Takahashi, H.Katayama-Yoshida, T.Kashiwakura, Y.Okabe, A.Yagishita, K.Tanaka, H.Fujimoto and H.Inokushi, Physica C, 160, 567 (1989).

(4) N.Nucker, J.Fink, J.C.Fuggle, P.J.Durham and W.M.Temmerman, Phys.Rev.B, 37, 5158 (1988).

(5) J.Kondo, Y.Asai and S.Nagai, J.Phys.Soc.Jpn., 57, 4334 (1988).

(6) T.Onozuka, T.Kajitani, M.Hirabayashi, H.Sato and T.E.Mitchell, Jpn.J.Appl.Phys., 28, L1775 (1989).

(7) Y.Lu, Y.F.Yan, H.M.Duan, L.Lu and L.Li, Phys.Rev.B, 39, 729 (1989).
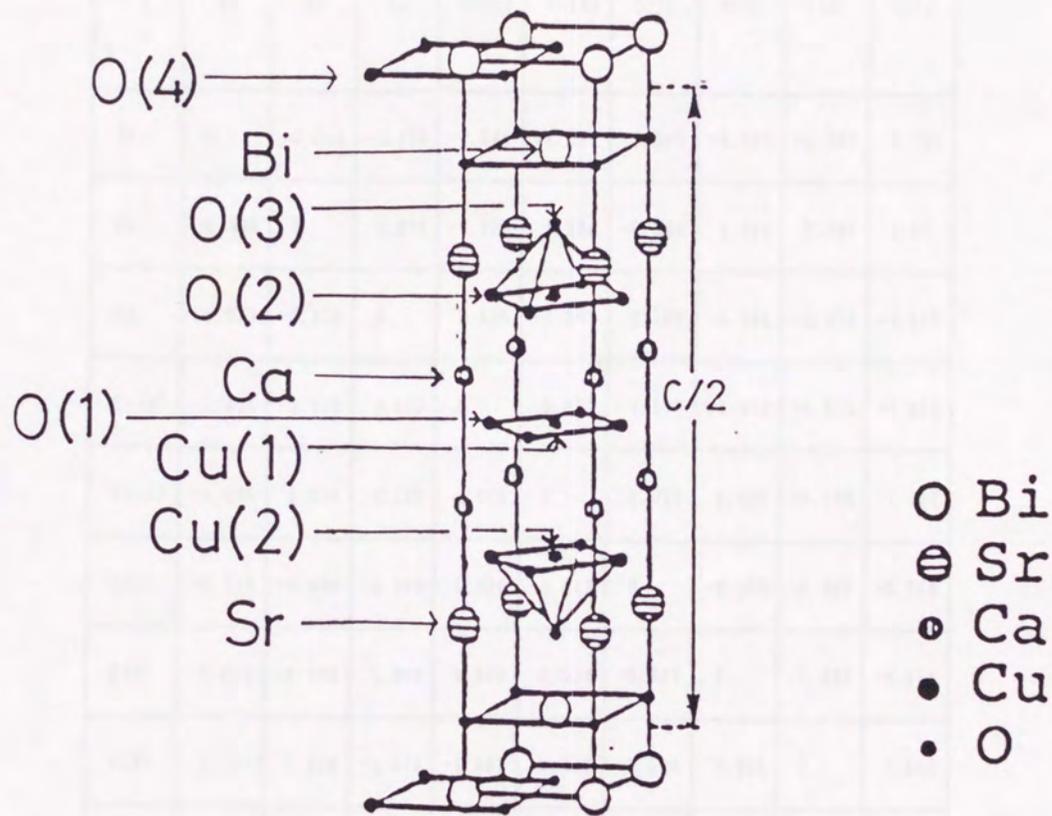
Fig.1 Crystal structure of $Bi_2Sr_2Ca_2Cu_3O_{10}$.

Table 1 Matrix of the calculated coefficient b_{ij} for $Bi_2Sr_2Ca_2Cu_3O_{10}$.

i\j	Bi	Sr	Ca	Cu(1)	Cu(2)	O(1)	O(2)	O(3)	O(4)
Bi	0	-2.010	-5.590	-6.041	-4.284	-6.041	-4.287	-4.937	2.190
Sr	0.926	0	0.074	-0.398	1.180	-0.395	1.315	2.037	1.01
Ca	-5.657	-2.929	0	2.820	-0.207	3.107	-0.054	-3.928	-5.657
Cu(1)	-6.613	-3.906	2.315	0	-0.917	5.197	-0.959	-4.878	-6.613
Cu(2)	-1.980	0.549	2.164	1.960	0	1.918	2.598	-0.169	-1.980
O(1)	-8.766	-6.056	0.449	3.045	-3.111	0	-3.105	-7.032	-8.766
O(2)	-3.059	-0.393	1.241	0.842	1.522	0.847	0	-1.333	-3.059
O(3)	2.121	1.716	-1.246	-1.691	0.142	-1.692	0.054	0	1.822
O(4)	2.190	-1.921	-5.590	-6.041	-4.289	-6.041	-4.287	-0.794	0

Table 2 Madelung potential (U) for each site of $Bi_2Sr_2Ca_2Cu_3O_{10}$
The potential is for a electron in units of eV.

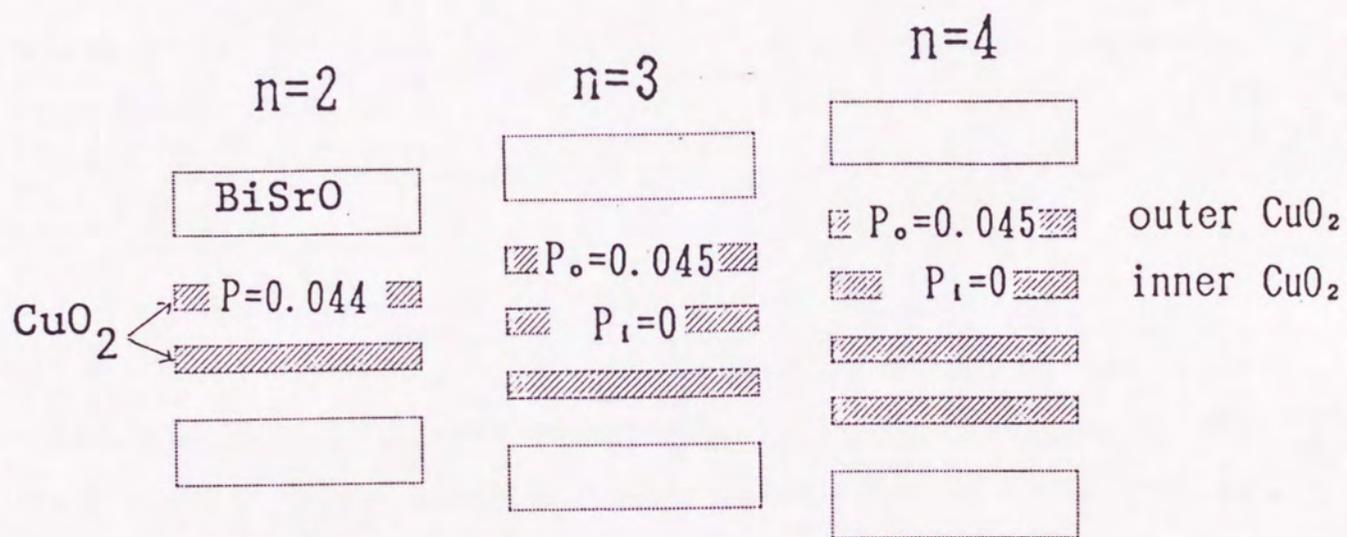|	Bi	Sr	Ca	Cu(1)	Cu(2)	O(1)	O(2)	O(3)	O(4)
U	15.89	22.73	29.01	33.72	33.90	-13.31	-13.98	-21.70	-30.97

Fig.2　　Profile　of　the　calculated　carrier　distribution　　in $Bi_2Sr_2Ca_{n-1}Cu_nO_{2n+4}$ for n=2 to 4.　　"p" shows hole　concentration per an oxygen ion.　　"p" shows hole concentration per oxygen ion.

Chapter 6

Summary and Future

132

Thin films of cuprate superconductors and the related materials have been grown using the ablation phenomenon induced by ArF laser irradiation. Furthermore, the crystal structure of the film has been artificially constructed by the layer-by-layer successive deposition. The growth mechanism of layer-by-layer formation and the properties of the films has been also investigated. The results and the considerations are summarized as follows.

In order to investigate the process of the film formation, the species generated from the oxide and metal targets by laser ablation were investigated by mass and emission spectroscopies. By the laser irradiation, the solid surface is decomposed into atoms and ions. Clusters or molecules are not produced. The species have high kinetic energy, and a part of them is in electronically excited state. The excess energy of the excited species may be effective for the improvement of crystallinity of the films. Compared with other methods, "laser ablation method" has an advantage which is that chemical composition of a film is almost same with that of a target, so this method is very suitable for the film formation including many elements.

In next step, the structure of $Bi_2Sr_2Ca_{n-1}Cu_nO_{2n+4}$ film was artificially constructed by layer-by-layer successive deposition method according to the guiding principle which is that the structure can be constructed by the insertion of blocking layers into the parent structure of $(Ca,Sr)CuO_2$. Thin film of this material is grown with two-dimensional layer-growth mechanism, and the structure is constructed according to the sequence of the

supply of the elements. For the layer growth, the substrate surface is a very important factor. By this method, the crystal structure can be controlled within an order of atomic layer, and metastable structures can be prepared.

By application of this method, superconductor/semiconductor superlattice structure and metastable $Bi_2Sr_2Ca_{n-1}Cu_nO_{2n+4}$ structure with large n were synthesized. This method makes it possible to prepare the structures, which cannot be obtained in bulk samples. The properties of these samples show the strong two-dimensional nature of $Bi_2Sr_2Ca_{n-1}Cu_nO_{2n+4}$ system. The two-dimensional nature is attributed to the thick blocking layer of $SrO/Bi_2O_2/SrO$ and non-uniform distribution of hole carriers in this system.

In my experiment, laser ablation method was established as one way of film formation, and the formation process in this method became clear. Furthermore, the structure control by successive stacking of atomic layers, which has been applied only to a part of semiconductors with very simple structure, was developed by my experiment, and it became clear that this structure-control could be applied to oxides, which included many elements and had complicated structures. By application of this technique, a new structure such as superlattice and metastable structure was synthesized. They were new substances, which could not be prepared by other methods. From the properties of these materials, a new information concerning the strong two-dimensional nature in $Bi_2Sr_2Ca_{n-1}Cu_nO_{2n+4}$ was found. This

134

information would not be obtained, if the structure could not be controlled in atomic-layer scale.

The layer-by-layer growth process used in my experiment can be the first step of "ultimate method of material synthesis", in which materials are constructed within atomic scale according to the designed structures. My experiment shows that the technique and the guiding principle, which has been used only in simple systems, can be adapted to the preparation and the structure-control of complicated oxide systems. I consider that this work is so meaningful, because it shows a possibility of the designing, synthesis and structure-control of various material using layer-by-layer deposition technique.

As a plan in future, I consider that structure-control in one-dimension should be attempted. The layer-by-layer formation is control in two-dimension, so the one-dimensional superconductor will be prepared by the processing of such two-dimensional superconducting sample. For this purpose, super-fine processing will be necessary. One possibility is a combination with scanning tunnel microscopy (STM), because the needle of STM can be used for such micro-processing. The cuprate superconductor has two-dimensional nature, so the thin layer of the superconductors showed superconductivity. If the superconductor has a one-dimensional line shape, what property the superconductor shows? It is very interesting problem. Of course, the STM observation of the growth process of the film is also interesting.

Furthermore, the study of the laser ablation process is

insufficient in this stage. The study of the earliest process in the ablation will be difficult, because the process is occur in very small area on the target surface and the time-scale is very short. However, the state of the ablated species should be studied more closely. In addition, the ablated particles include many types of species, which are atom, ion, excited species and so on. Thus I want to sort out the ablated species by a perturbation such as electric field or magnetic field. If it is possible, the effect of the each classified species on the film formation can be studied.

136

Acknowledgments

The author expresses his appreciation and gratitude to Professor S.Kawai of Osaka University for his encouragement during the course of this investigation. The author is greatly indebted to Assistant Professor T.Kawai of Osaka University for his helpful discussions , continuing guidance, and encouragement. The author would like to thank Assistant Professor T.Asai of Kansai University and Dr. K.Kitahama for his significant suggestions on the analysis of x-ray diffraction. The author would like to thank Assistant Professor C.Miyamoto of Osaka University and Dr. K.Tanihata for their considerable assistance on resistivity measurement at low temperature. The author expresses his special thanks to Mr.I.Matsubara in Industrial Research Institute of Osaka Prefecture for his considerable assistance for the resistivity measurement and helpful discussion concerning the superconductivity under magnetic field. The author expresses his thanks to Mr.T.Tanaka in Material Analysis Center of ISIR for his advice in XRD and EPMA measurements. The author also expresses his thanks to Mr.A.Koreeda and Mr.T.Ishibashi for observation and analysis of the electron diffraction. In final, the author appreciates the kind cooperation and encouragement of all members of his laboratory.

Appendix A: Growth Mechanism of Thin Films and Reflection High Energy Electron Diffraction (RHEED).

The schematic diagram of RHEED observation is shown in Fig.1. The RHEED method has a low incident angle of the electron beam in a few degree, so this way is very sensitive to the surface atoms. Generally speaking, there are two types in a growth mode of thin films. One is three-dimensional island growth [Fig.2 (a)], and the other is two-dimensional layer growth [Fig.2(b)]. The relation between the growth mode and RHEED pattern is shown in Fig.3. If the island is formed during the growth, the electron beam transmitting through the island particle makes the transmittance electron diffraction pattern, which is spotty pattern[1] [see Fig.3(a)]. In two-dimensional layer growth, on the other hand, the streak RHEED pattern is observed due to the flat surface[1] [see Fig.3(b)]. At the same time, the oscillation of RHEED intensity is often observed in the layer-growth mode.[2,3] Though, the mechanism of the intensity oscillation has not been established yet, the explanation by single-scattering[4,5] or multiple-scattering approximation[6,7] is suggested. The simple explanation of single-scattering approximation is shown here in Fig.4. In the two-dimensional growth mode, the deposition on the flat substrate surface makes the steps between the top surface and substrate surface. At this time, the diffraction intensity becomes weak by the interference between the beam scattered by the substrate surface and that scattered by the top surface [see Fig.4]. When

the top layer is completed by further deposition, the surface flatness is recovered, and the intensity becomes strong again. This process is repeated during the film growth, so the intensity oscillation can be observed in the layer-growth mode. However, the inversion of the intensity, where the weakest intensity is given by the completed flat surface, is often observed, in practice. This behavior cannot be explained by the single-scattering approximation. The calculation based on the multiple-scattering approximation was performed to explain this behavior, but the development is insufficient in this step. Here, I show only one example. Dobson et al reported that the dominant process of electron scattering is multiple scattering by the step edge on the surface. They suggested that the oscillation of RHEED intensity is responsible for the variation of the number of step edges. [6]

References

(1) S.Takeuchi, Diffraction Crystallography, (Maruzen, Tokyo, 1981).

(2) J.J.Harris and B.A.Joyce, Surf.Sci.Lett., 108, L90 (1981).

(3) J.H.Neave, B.A.Joyce, P.J.Dobson and N.Norton, Appl.Phys.A, 31, 1 (1983).

(4) C.S.Lent and P.I.Cohen, Surf.Sci., 139, 121 (1984).

(5) S.V.Ghaisas and A.Madhukar, J.Vacuum Sci.& Technol.B, 3, 540 (1985).

(6) P.J.Dobson, B.A.Joyce and J.H.Neave, J.Cryst.Growth, 81, 1, (1987).
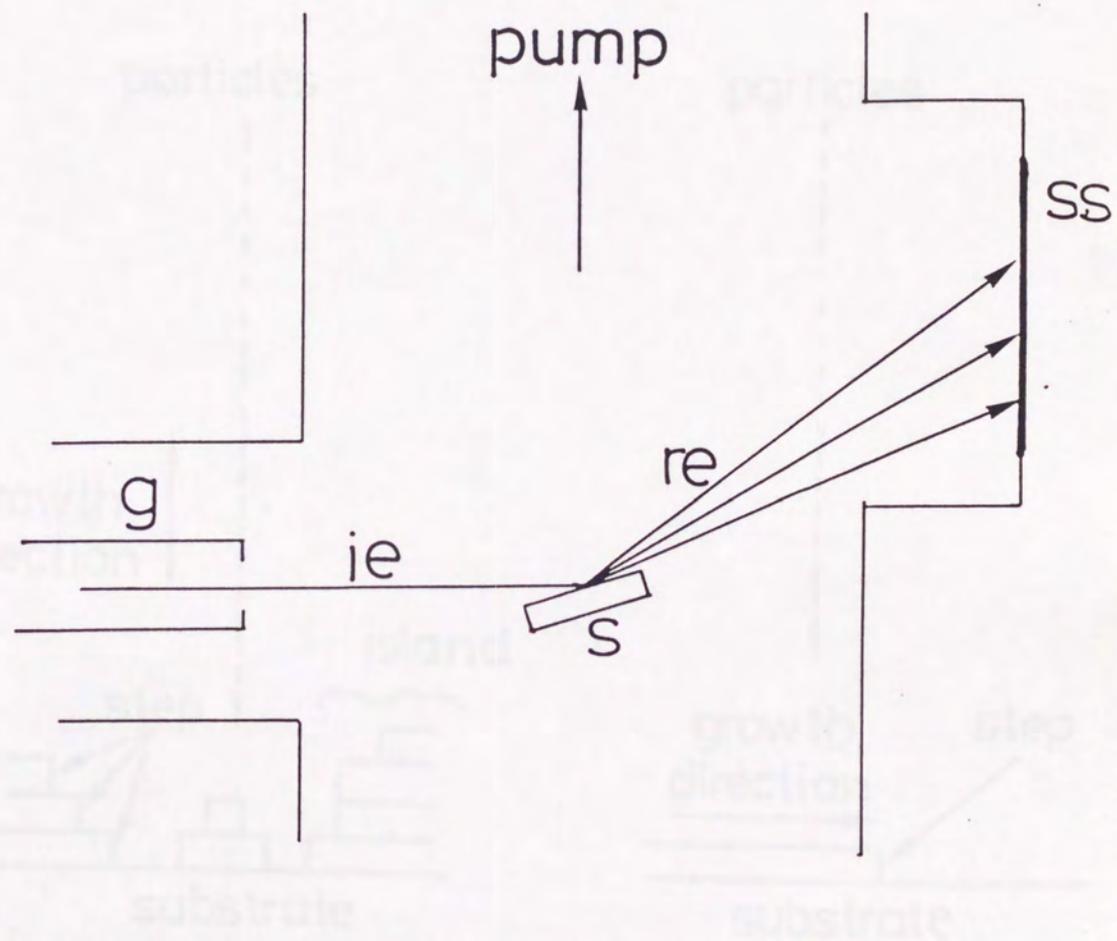
(7) T.Kawamura and P.A.Maksym, Surf.SCi., 161, 12 (1985).

Fig.1   The schematic diagram of RHEED observation, where g:electron gun, s:sample, ie:incident electron beam, re:reflected electron beam and ss:fluorescent screen.
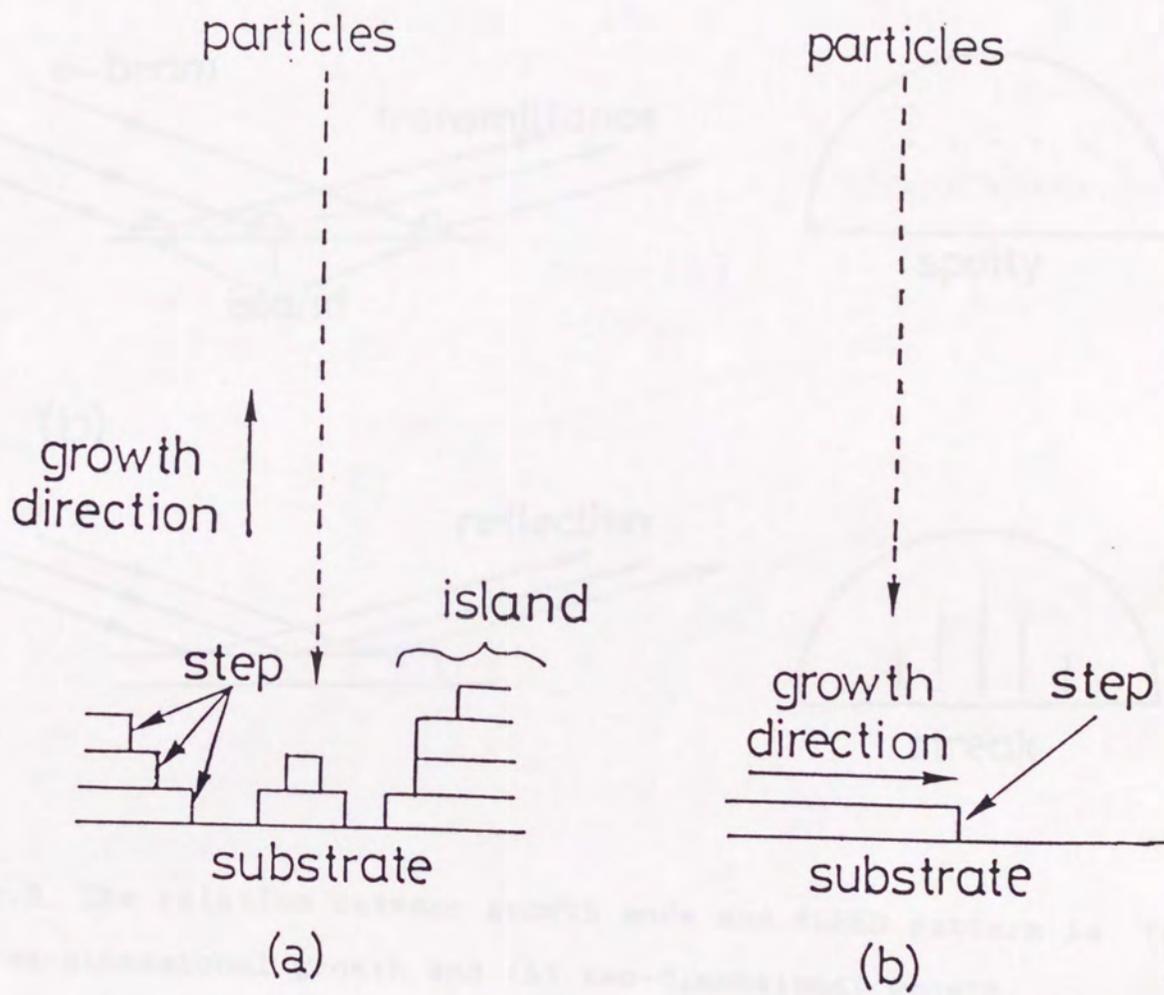
Fig.2 The profiles of growth modes. (a) Three-dimensional island growth and (b) two-dimensional layer growth.
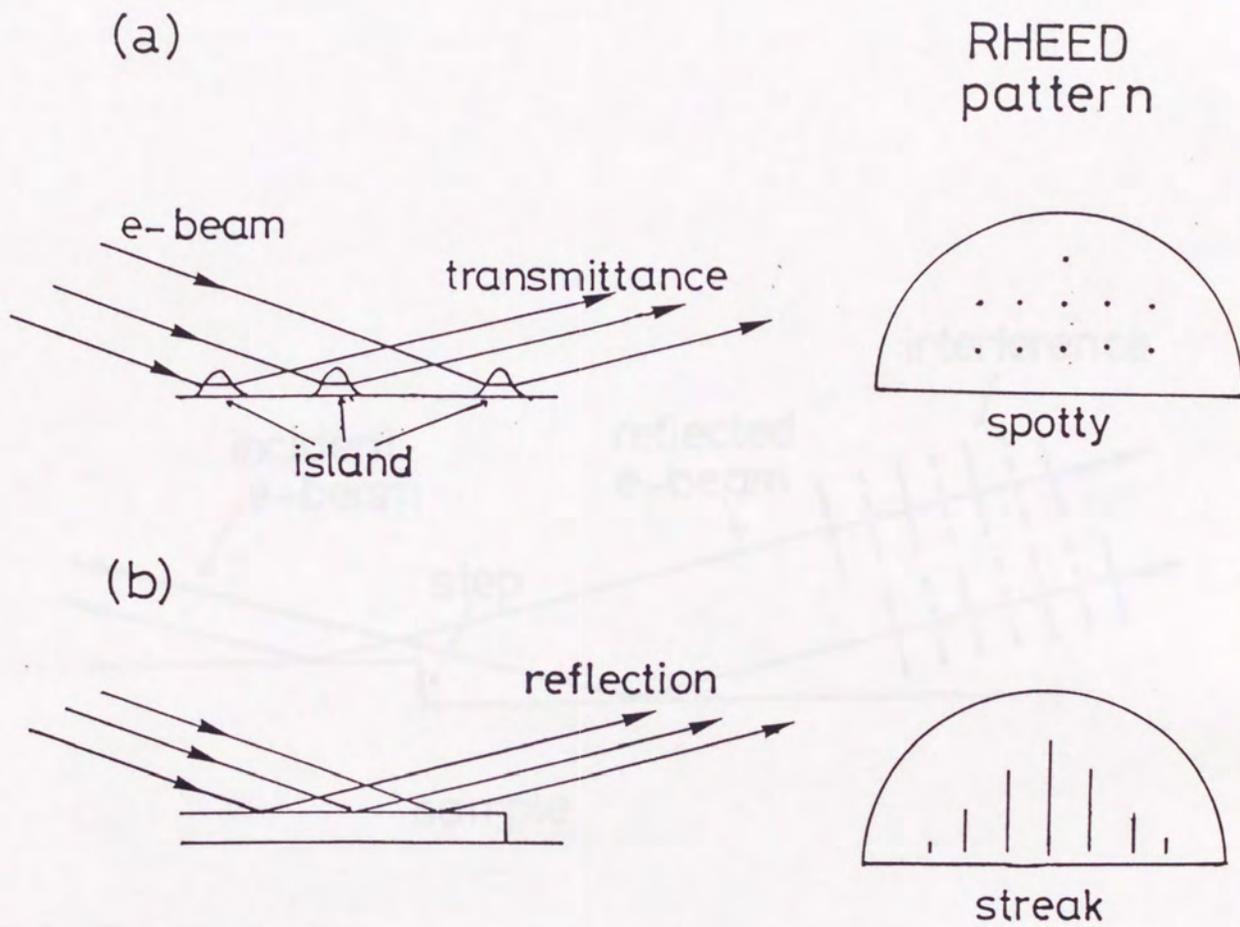
Fig.3 The relation between growth mode and RHEED pattern in (a) three-dimensional growth and (b) two-dimensional growth.
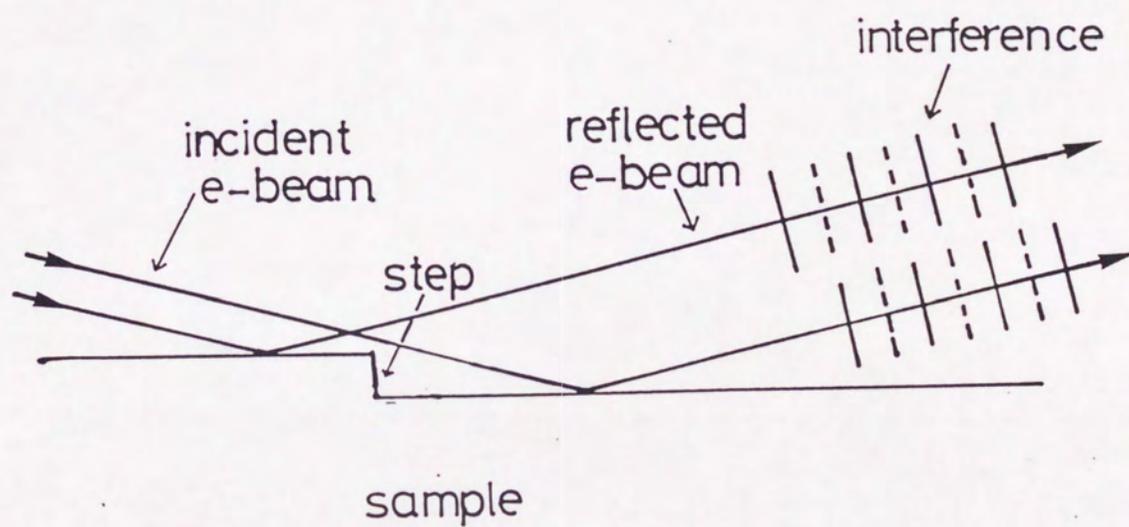
Fig.4 The explanation for oscillation of RHEED intensity by single scattering approximation.